SPATIAL ECOLOGY OF DEEP-SEA BENTHOS FOR MANAGEMENT OF MARINE PROTECTED AREAS

by

Sarah Natasha de Mendonça

Submitted in partial fulfilment of the requirements
for the degree of Doctor of Philosophy

at

Dalhousie University
Halifax, Nova Scotia
March 2024

Dalhousie University is located in Mi'kma'ki, the
ancestral and unceded territory of the Mi'kmaq.
We are all Treaty people.

For my grandparents, parents, and everyone I call family,

Thank you for your love and support.

° ° °

Adventure hangs in the air, just a whisper of a dare.

TABLE OF CONTENTS

LIST OF TABLES

LIST OF FIGURES

ABSTRACT

Deep-water corals, sponges, and other animals play functional roles, such as providing habitat, promoting diversity in seafloor communities in the deep sea. Little is known about the spatial organization of these vulnerable marine ecosystems, limiting our ability to link patterns to ecological processes for effective management. I quantified spatial patterns of invertebrates (> 2 cm) on soft sediments from imagery, focusing on the Laurentian Channel Marine Protected Area in the Canadian Northwest Atlantic. At broad scales (100s m – 100s km), three types of assemblages of varying composition, diversity, and abundance were associated with benthoscape class (environmental mosaic), a potential proxy for different habitats. At fine scales (0 – 100s m), I recorded taxon-specific local aggregations and variation in patchiness. For broad-scale patterns, potential spatial drivers included benthoscape classes [incorporating depth, pockmarks (fluid/gas-created pits), ice scours, and sediment composition)] and food quantity/quality; for fine-scale patterns, drivers likely included bathymetric position index (local changes in depth), pockmarks, and biological relationships. My results illustrate that sampling designs that ignore spatial patterns can result in the misrepresentation of diversity and abundance, impacting follow-up analyses and scientific conclusions. Further, different sampling tools [remotely operated vehicle (ROV), drop camera, and trawl] and designs (e.g. number and spacing of images and transects) had trade-offs and biases. For example, in some instances, the drop camera captured higher abundance and diversity than ROV. Sampling by ROV was advantageous for spatial and species association analyses, because of high spatial resolution, maneuverability, and minimal disturbance. Recommendations for developing deep-sea monitoring frameworks include optimized sampling designs for scales relevant to taxa and processes of interest, and high spatial resolution, replication, and multiple spatial lags to ensure representation of assemblages. My novel application of spatial statistics is applicable to other areas to quantify spatial patterns (abundance or different variables) at various scales e.g. transect, station, regional, or network levels. The thesis advances the field of spatial ecology in deep-sea ecosystems, to better understand changes in species distributions and comparisons at different spatial scales.

LIST OF ABBREVIATIONS USED

Abbreviation	*Definition*
AI.#	Appendix I figure #
AII.#	Appendix II figure #
A1, C1, C2, or TZ2	Deep (> 400 m) benthoscape classes, part of an output from Lacharité et al., (2020).
A2, B1, B2, or TZ1	Shallow (< 400 m) benthoscape classes, part of an output from from Lacharité et al., (2020).
AB, CD, EF, or GH	Two paired parallel transects, e.g. AB = transects "A" and "B" together. Paired transects were ~400 m long at ~10 m spacing.
ANOVA	Analysis of Variance, a statistical method.
AUV	Autonomous Underwater Vehicle
BPI or TPI	Bathymetric Position Index; also called TPI (topographic position index). Examines relative changes in local bathymetry [high (i.e., crests) and low (i.e., troughs)].
BTM	Benthic Terrain Modeler, software.
Campod	A drop camera system operated by Fisheries and Oceans Canada (Bedford Institute of Oceanography, Dartmouth, NS).
C:N	Total organic carbon to total nitrogen ratio.
Chl *a*	Chlorophyll *a*
CTD	Instrument for conductivity (salinity), temperature, and depth.
DFO	Fisheries and Oceans Canada (government department)
FDR	False Discovery Rate correction is used to adjust the significance level for multiple testing and spatial autocorrelation.
*Gi**	Getis-Ord statistic, examines local patterns in spatial association, i.e. hotspots (aggregations) and coldspots.
GIS	Geographic Information System
LC	Laurentian Channel

Abbreviation	*Definition*
LC MPA	Laurentian Channel Marine Protected Area
LH or HL	Local Moran outlier - an observation (i.e. image) and its neighbourhood have dissimilar values, high observation-low neighbourhood (HL) or low observation-high neighbourhood (LH).
LL or HH	Local Moran cluster - an observation and its neighbourhood have similar values, both low (LL) or both high (HH).
MPA	Marine Protected Area
Moran's *I*	Global Moran's *I* is a statistic that summarizes spatial autocorrelation over an entire area, whereas local Moran's *I* examines local changes within an area.
NMDS	Non-metric multi-dimensional scaling, a community analysis.
OFOP	Ocean Floor Observation Protocol, a software for imagery data processing (may also be used during collection and annotation).
PERMANOVA	A permutational multivariate analysis of variance, a statistical method.
ROPOS	Remotely Operated Platform for Ocean Sciences, the specific remotely operated vehicle used in this research.
ROPOS_ACE	Three individual ROV transects, called "A", "C", and "E", assembled into a sampling design. Parallel transects were ~ 400 m long at ~ 200 m spacing; 4 groups of transects, including ROPOS_BDF, ROPOS_CEG, and ROPOS_DFH.
ROPOS_all	Eight individual transects ("A", "B", "C", D", "E", "F," G", and "H") assembled into a sampling design. Transects had alternating spacing of 10 m and 200 m.
ROV	Remotely operated vehicle
SD	Standard deviation
SE	Standard error
SIMPER	A procedure that calculates Similarity Percentages, the contribution of each taxon to the average dissimilarity between stations.

Abbreviation	*Definition*
sp. #	A taxonomic grouping, "[Name] sp. #" e.g. *Pennatula* sp. 2, containing one species/taxon. Some distinguishing characteristics are difficult to see in imagery and prevent identification to the species level.
spp.	A taxonomic grouping, "[Name] spp." e.g. *Kophobelemnon* spp. that likely contains several related species/taxa that are difficult to distinguish in imagery. Initials were used to represent the taxonomic level of identification e.g. Anthozoa (C.) spp., where (C.) = Class. O = Order, F= Family P = Phylum, InfraO. = Infraorder, SF = Subfamily, and SC = Subclass.
TN	Total Nitrogen
TOC	Total Organic Carbon
TOM	Total Organic Matter
USBL	Ultra-short baseline, acoustic positioning system.
WoRMS	World Register of Marine Species, taxonomy resource.

ACKNOWLEDGEMENTS

To my supervisor Anna Metaxas, I am beyond grateful for your mentorship and the opportunity to perform this research. While working towards this lifetime goal over the past years, your confidence and support has meant the world to me. During both the challenges and successes, you always had my back. It has been an invaluable experience to be part of your lab family.

I would like to thank my committee members Marie-Josée Fortin, Craig Brown, and Jon Grant for their guidance and feedback. Further, thanks to my many mentors for their advice and encouragement — Bob Scheibling, Lindsay Beazley, Roxanne Beinart, Nat Beltran, Hannah Carr, Erik Cordes, Andrew Davies, Mackenzie Gerringer, Catherine Johnson, Paul Snelgrove, Ryan Stanley, and others, including those below.

Thank you to everyone who provided their expertise and assistance, contributing to the success of this research. Peter Lawton (Chief Scientist) and the crews and scientists involved on the collaborative CHONe-DFO research cruises on the research vessels CCGS Hudson and CCSG Martha L. Black, with the remotely operated vehicle ROPOS and drop camera Campod. Assistance at sea provided by Vonda Wareham-Hayes and Bárbara de Moura Neves (DFO-NL) [invertebrate expertise, LC MPA boundaries and cruise planning], Callum Mireault (deceased), Beatrice Proudfoot, Tamara Wilson, Marta Miatta, Marion Boulard, and Adam Stoer. Research assistants Kate Arpin [image analysis], Jovana Kornicer [literature search/screening], and Brogan Regier, Adam Stoer, and Alexis Savard-Drouin [data export/search]. In addition to, Craig Brown (DAL), Myriam Lacharité (UTAS), and Vicki Gazzola (DAL) [benthoscape and geomorphic

features], Marie-Josée Fortin (U of T) [advice and workshop on spatial statistics], Rémi Daigle [advice with R data processing], and specific expertise on tools (in Chapter 2) provided by Vincent Auger, Robert Benjamin, Peter Pledge, and Luiz Mello.

This research was funded by the NSERC Canadian Healthy Oceans Network and its partners: Department of Fisheries and Oceans Canada and INREST (representing the Port of Sept-Îles and City of Sept-Îles). In addition to, Natural Sciences and Engineering Research Council of Canada (NSERC) Discovery Grants for Anna Metaxas and graduate research scholarships for myself, including NSERC PGS-D/CGS-D, Nova Scotia Graduate Scholarship, Faculty of Graduate Studies and President's awards at Dalhousie University, and conference support provided by the GeoHab Ron McDowell Student Support Award.

Furthermore, I am immensely grateful for my family, their unwavering love and support, as well as continuous interest and investment in my grandest dreams — Hafiza, Joseph, Samunnesa (deceased), Fazia, Neil, Anil, Michelle, Daniel, Sarah, Joanne, Sandy, Nisa, and my partner Tom. Special thanks to Joey, Arie, Meghan, Mere, Conrad, Em, Kayla, Tani, Jess, and Hanna, for your friendship and laughter that kept me balanced. Finally, thanks to those in the Metaxas lab, Dalhousie Oceanography Student Association, CHONe group, and Department of Oceanography for making this an amazing experience.

CHAPTER 1

INTRODUCTION

1.1 Background

The deep sea (defined as the region of the ocean with depth greater than 200 m), supports high biodiversity and provides biological and mineral resources, yet is one of the least explored ecosystems on the planet (Ramirez-Llodra et al., 2010). Cold-water corals, including sea pens, are an important deep-sea ecosystem which forms biogenic habitat by altering currents, retaining nutrients, and providing nurseries and protection for fish (e.g. DFO 2015; Baillon et al., 2012; Tissot et al., 2006). These are considered vulnerable marine ecosystems, areas that are unique, fragile, structurally complex, functionally significant habitats, or include species with life-history traits that make recovery difficult (ICES, 2010; Kenchington et al., 2010; FAO 2009). Vulnerable marine ecosystems face threats such as fishing, oil-gas or extractive activities, and climate change making them a conservation priority (e.g. DFO, 2012; Ramirez-Llodra et al., 2011). In the northwest Atlantic Ocean, the Laurentian Channel Marine Protected Area (LC MPA) was designated in 2019, encompassing high risk areas for sea pen communities (DFO, 2017a), which have been associated with other epibenthic megafauna (e.g. invertebrates > 2 cm such as cup coral, soft coral, sea anemones, echinoderms, crustaceans) and fish (Baillon et al., 2012, 2014a; De Clippele et al., 2015). Knowledge gaps still exist, therefore further research on abundance, distribution, taxonomy, life histories, and other aspects of deep-

sea ecology is needed for the development of an appropriate monitoring framework for the MPA (e.g. DFO, 2015, 2017a, 2017b; Stanley et al., 2015).

For a monitoring framework to be successful, it must apply the most appropriate tools and spatial-temporal scales for relevant ecological features. Sampling designs must be optimized to ensure meaningful statistical analyses and robust monitoring (Neves et al., 2021). For the LC MPA, Fisheries and Oceans Canada (DFO) have proposed state indicators (i.e. ecological components such as sea pen biomass, abundance, size, diversity, and geospatial measurements such as patch stability, connectivity, or environmental parameters) and stressor indicators (i.e. anthropogenic components like fishing), in addition to monitoring tools, such as ROV, cameras, and trawls (DFO, 2015; Neves et al., 2021). Imagery surveys can be used to sample most of these state indicators, but other tools may be needed for biomass (i.e. trawls) and environmental parameters (e.g. CTD and other instruments).

The field of spatial ecology is based on understanding space and ecological processes on various scales (Fletcher & Fortin, 2018). Several existing hypotheses for the patterns of deep-sea diversity and community structure involve ecological processes such as disturbance, competition, and spatial heterogeneity (e.g. as discussed in Mcclain & Schlacher, 2015; Rex, 1981). Spatial statistics (e.g. global/local Moran's *I* and *Gi**) can be used to identify patterns such as aggregations and patchiness through the interpretation of spatial autocorrelation (Dale & Fortin, 2014) yet are rare in the deep-sea literature (e.g. for deep-water corals see Conti et al., 2019; Price et al., 2021; Watters et al., 2022; and for other megafauna Vad et al., 2020). In particular, benthoscapes (also called landscapes, seascapes, or seafloor habitat maps) classify patches of seabed based on biotic (e.g.

biogenic structures) and abiotic (e.g. sediment and geomorphic features) components (Zajac, 2008) and can be used to interpret spatial patterns. For example, specific benthoscape classes can correspond to areas with unique benthic communities (e.g. Jones & Brewer, 2012; Mortensen et al., 2009; Proudfoot et al., 2020; Swanborn et al., 2023), and thus may have management applications (e.g. scallop fishery, Brown et al., 2012). Spatial analyses provide insight into ecological patterns and processes, on fine and broad scales, relevant for appropriate sampling designs that capture epibenthic megafauna for effective research and monitoring.

1.2 Objectives

This thesis aimed to improve our understanding of best practices for deep-sea sampling designs that ensure accurate representation of spatial patterns and allow for reliable spatial comparisons to help elucidate the ecology of epibenthic megafaunal communities. Furthermore, the outputs on community structure and spatial pattern can provide baseline data for the LC MPA. This thesis fell under the umbrella of the NSERC Canadian Healthy Oceans Network (CHONe II) that aimed to support conservation activities in Canada.

The thesis includes 5 chapters, including this introduction (**Chapter 1**) and a conclusion with recommendations for developing a monitoring framework in the deep sea (**Chapter 5**). **Chapter 2 - 4** were developed as standalone manuscripts to address our research objectives: **Chapter 2 and 4** are published in the peer reviewed journals (de Mendonça & Metaxas, 2021, 2024) and **Chapter 3** is *under review.* I used high resolution transect arrays with multiple spatial lags to collect georeferenced imagery (ROV and drop

camera) in **Chapters 2 - 4** for measures of abundance, diversity, and/or composition for epibenthic megafauna > 2 cm in the largest dimension (excluding highly mobile or pelagic taxa e.g. fish, holothurians, and shrimp, because our sampling methods were not appropriate for their enumeration). Only a subset of the imagery data was used in **Chapter 2** (stations 2 and 5) and **Chapter 4** (only ROV), based on the sampling design requirements for those analyses. I also used biomass data from DFO research trawls (**Chapter 2**) and environmental variables for interpretation [i.e. from the literature or collected during our surveys, such as benthoscape and geomorphic features (provided by Lacharité et al., 2020), food and sediment properties (Miatta & Snelgrove, 2021, 2022), as well as depth and oceanographic properties (e.g. salinity, temperature, oxygen)].

In **Chapter 2**, I compared how ROV and drop camera captured the abundance and diversity of the most common morphotaxa of epibenthic assemblages (based on external morphology/characteristics visible in imagery) and examined differences between 3 tools (ROV, drop camera, and trawl), including in image quality and sampling bias (i.e. catchability and position accuracy). In **Chapter 3**, I quantified broad-scale spatial patterns (100s m – 100s km) in community composition, abundance, and diversity, and discussed the potential drivers that could have generated these patterns. I also investigated how assemblages related to benthoscape classes and highlighted sampling resolution biases. In **Chapter 4**, I quantified fine-scale spatial patterns (0 – 100s of meters) in the distribution of deep-sea epifauna, using global and local spatial statistics at two scales (station ~ 0.256 km^2 and paired transects ~ 0.004 km^2). Therefore, I objectively detected significant changes in abundance, and provided hypotheses for their potential causes. In **Chapter 5**, I integrated all results to provide recommendations for

sampling designs and monitoring of epibenthic megafauna in the deep sea, including some suggestions for future research.

CHAPTER 2

COMPARING THE PERFORMANCE OF A REMOTELY OPERATED VEHICLE, A DROP CAMERA, AND A TRAWL IN CAPTURING DEEP-SEA EPIFAUNAL ABUNDANCE AND DIVERSITY[1]

2.1 Abstract

Deep-sea ecosystems provide services such as food, minerals, and nutrient recycling, yet baseline data on their structure is often lacking. Our limited knowledge of vulnerable deep-sea ecosystems presents a challenge for effective monitoring and mitigation of increasing anthropogenic threats, including destructive fishing and climate change. Using data from two stations differing in total epifaunal abundance and taxonomic composition, we compared the use of imagery collected by two non-invasive tools [remotely operated vehicle (ROV) and drop camera] and data collected with a trawl system, commonly used to quantify epibenthic megafauna in the deep sea. Imagery and trawl data captured different epifaunal patterns, the former being more efficient for capturing epifauna, particularly Pennatulacean recruits. The image-based methods also caused less disturbance, had higher position accuracy, and allow for analyses of spatial structure and species associations; fine-scale distributions could not be elucidated with a trawl. Abundance was greater for some taxa, and diversity accumulated faster with increasing

[1] de Mendonça, S. N., & Metaxas, A. (2021). Comparing the Performance of a Remotely Operated Vehicle, a Drop Camera, and a Trawl in Capturing Deep-Sea Epifaunal Abundance and Diversity. *Front. Mar. Sci., 8*:631354. https://doi.org/10.3389/fmars.2021.631354

Anna Metaxas supervised the development of the study design, analyses, and co-authored the manuscript.

sample size for the drop camera than the ROV at one station. However, there are trade-offs between these tools, including continuous and discrete sampling for the ROV and drop camera, respectively, which can affect follow-up analyses. Our results can be used to inform monitoring frameworks on the use of appropriate sampling tools. We recommend further research into tool sampling biases and biometric relationships to help integrate datasets collected with different tools.

Keywords: sampling tools, imagery, sea pens, monitoring, epifauna, marine protected area, corals, deep sea

2.2 Introduction

Sampling deep-sea ecosystems (at depths > 200 m) is extremely challenging because of the absence of ambient light, the high pressure and the remoteness (Jamieson et al., 2013). Consequently, we have investigated less than 0.0001% of the deep sea (Danovaro et al., 2017). It is now recognized that deep-sea ecosystems provide provisioning services (e.g. fish and minerals), regulating services (e.g. carbon sequestration), cultural services (e.g. aesthetic), and supporting services (e.g. nutrient recycling) (Folkersen et al., 2018). At the same time, these ecosystems are experiencing increasingly greater anthropogenic impacts, including waste disposal, extractive activities that disturb the seafloor (i.e. fishing, cables/pipelines, mining, oil/gas, acoustics), as well as ocean acidification and climate change (Ramirez-Llodra et al., 2011). Vulnerability to these impacts is enhanced by the generally slow growth, extended longevity, and low recruitment of deep-sea species (Danovaro et al., 2017; Neves et al., 2015). In addition,

deep-sea communities exhibit slow recovery (>10-40 years) from disturbance (Baco et al., 2019; Bennecke and Metaxas 2017; Huvenne et al., 2016; Simon-Lledó et al., 2019).

Epifaunal communities in the deep sea have been sampled in part with tools which are lowered to the seafloor and collect physical samples, such as trawls, corers, and epibenthic sleds (Jamieson et al., 2013). A widely used trawl system includes a net towed along the seafloor, adapted from coastal commercial fishing techniques. Trawls are regularly used for commercial fishing (Hall-Spencer et al., 2002), as well as fish stock assessment (Clark 1979). Often, trawl data are used to determine patterns in distribution and biomass of megafaunal communities (Gullage et al., 2017; Kenchington et al., 2011, 2014, 2016a, 2016b; Moritz et al., 2013; Murillo et al., 2020).

However, some megabenthos (e.g. sponges, alcyonarians, and gorgonians) and fish, collected through either targeted sampling or as bycatch, may not be well represented in trawl surveys because of their flexibility, size, or behaviour (Auster et al., 2011, Pacunski et al., 2016; McIntyre et al., 2015; Walsh 1992; Wassenberg et al., 2002). For example, corals and sponges may be light and flexible enough to pass through the net or heavy enough to fall through the net (Auster et al., 2011). Sea pens anchor in the sediment (Williams 1999; Williams and Alderslade 2011) and some species (e.g. *Pennatula rubra, Pennatula aculeata, Virgularia mirabilis*, *Protoptilum carpenteri)* can contract and withdraw into the sediment (Ambroso et al., 2013; Chimienti et al., 2018a; Kenchington et al., 2011; Langton et al., 1990).

Relatively less invasive tools such as remotely operated vehicles (ROVs), autonomous underwater vehicles (AUVs), drop cameras, towed cameras, camera sleds,

rovers, and baited cameras, have been used to collect imagery data. ROVs generally hover above or make minimal contact with the seafloor and can maintain a relatively constant speed and height above the bottom while sampling. ROVs are non-destructive, allow for habitat associations and behaviour analyses, are suitable in complex/high relief habitats, and have high maneuverability (Sward et al., 2019). Recent direct comparisons suggested that ROVs captured a higher abundance of sea pens than trawls (Chimienti et al., 2018b, 2019). Other imaging systems are also less destructive than research trawls. Unlike ROVs, AUVs are not tethered to a ship, and can run imagery transects close to the seafloor, possibly producing less noise and discontinuous lighting than ROVs (Morris et al., 2014). Drop cameras are towed behind a ship and hop along the seafloor capturing still images, only when stationary and in contact with the seafloor. Towed cameras are tethered and towed by a ship, often maintaining a target height above the seafloor without making contact (Drazen et al., 2019). Camera sleds and rovers generally make continuous contact with the seafloor, with sleds being towed by a ship and rovers being autonomous. Baited cameras are deployed as free-falling systems, which rest at a fixed location on the seafloor with an attached bait that attracts fauna (Drazen et al., 2019; Logan et al., 2017). These baited camera systems may capture imagery continuously or at discrete time intervals.

While there is a wealth of literature on individual descriptions and qualitative comparisons of performance for these various deep-sea sampling tools (e.g. Durden et al., 2016; Flannery & Przeslawski, 2015; Jamieson et al., 2013), direct empirical comparisons between the tools and their sampling biases are limited. Some studies have compared quantitatively the performance of tools used to collect megaepifaunal data in

the same study area (e.g. abundance, diversity, biomass, size). For example, several studies have compared fish abundance and composition, as well as abundance of select megafauna (e.g. crustaceans, echinoderms and molluscs) between ROVs or drop cameras and trawls of different sizes (Ayma et al., 2016; Adams et al., 1995; Chimienti et al., 2018b; Kenchington et al., 2011; Pacunski et al., 2016, Nybakken et al., 1998). Other studies have compared abundance and diversity of both megafauna and fish among human-occupied submersibles, camera sleds (analogue), and otter trawls (Uzmann et al., 1977) and among AUV, towed cameras, and trawls (Morris et al., 2014). A few studies have focused on comparing diversity, abundance, and size across imaging systems such as AUVs, towed camera systems, or baited cameras (Logan et al., 2017; Schoening et al., 2020).

In this study, we had the opportunity to directly compare the performance of three commonly used tools in quantifying megaepifauna, a ROV (ROPOS), a drop camera (Campod), and a research trawl (Campelen 1800 shrimp trawl) by sampling at the same 2 locations on the Northwest Atlantic Ocean, in the Laurentian Channel Marine Protected Area (MPA). This opportunity allowed us to: (1) compare the composition of the same benthic assemblages (abundance of the most common morphotaxa and diversity) as quantified using the ROV and the drop camera; and (2) examine differences in image quality and sampling bias, such as catchability, spatial extent, and position accuracy, between the ROV, drop camera, and trawl. We were able to compare tool performance in two locations which differed in megafaunal density, community composition, and environmental characteristics, using a replicated sampling design. Monitoring and research logistics related to operation and maintenance costs, frequency of use, and

technical specifics are outside of the scope of this study, as those factors change rapidly with evolving technology, are highly variable between tools in the same category, as well as dependent on the research objectives, finances, and the specific ecosystem.

Detected differences in species abundance or diversity among tools could imply varying catchabilities. Although many studies have used some of these tools, such empirical (quantitative and qualitative) direct comparisons across all three tools used to characterize the same assemblage have not been made to our knowledge. These types of comparisons can provide insight into the selection of the most appropriate tool(s) for capturing a targeted species or different ecological attributes of interest, thus ensuring high data quality and supporting appropriate data interpretation. Our study can both guide the collection of relevant baseline data and enhance monitoring efforts of deep-sea ecosystems. However, our study also underscores the need for more detailed evaluation of catchability, encompassing other tools, species, ecosystems, and ecological attributes of interest.

2.3 Methods

2.3.1 Study Site

Our sampling areas were in the Laurentian Channel Marine Protected Area (MPA), located in a deep submarine valley off the southwest coast of Newfoundland, Canada (Figure 2.1), is ~ 11,580 km^2 (DFO, 2019a), and ~115-490 m deep (Lacharité et al., 2020). We sampled two stations, LC2 and LC5, to capture a range of taxonomic diversity and abundance. A map of biophysical seafloor features classified station LC2 as part of a benthoscape characterized by intermediate depth (200-400 m) with low relief

(0.5-1°), very abundant pockmarks (>5 km^{-2}), sparse ice scours (<1 km^{-2}), and mixed sediment with some gravel (Lacharité et al., 2020). Station LC5 was classified as deep (> 400 m) with low relief, sparse pockmarks (<1 km^{-2}), abundant ice scours (>2 km^{-2}), and sandy mud with gravel traces. The environmental conditions (bathymetry, pockmarks, ice scours, and slope) were similar within stations as supported by Lacharité et al., (2020) and video observations of the sampled areas. Thus, we assumed that our results could be attributed mostly to how the tools captured the morphotaxa, rather than spatial patterns in environmental variables.

2.3.2 Imagery

We used two different tools to collect and compare imagery from the two stations. In 2017, we performed 8 400-m parallel transects with the remotely operated vehicle Remotely Operated Platform for Ocean Sciences (ROPOS; https://www.ropos.com/). Sampling was based on a systematic cluster design with alternating spatial lags, recommended for capturing spatial patterns in the absence of prior knowledge (Fortin et al., 1989). Transects were spaced at spatial lags of 10 m and groups of 2 were spaced at 200 m (Figure 2.2). This design allowed us to combine large spatial extent with high spatial resolution. We used continuous video collected with a downward-facing Insite Pacific Zeus-Plus HD camera (1920 x 1080 pixels) to capture epibenthic fauna and quantify sampling area. The ROV includes 3 x 400 W HMI and 3 x 350 W LED primary light sources, as well as 8 x 150 W LED lights used to fill in shadows near the vehicle and for additional sampling, e.g. using the manipulator arms and attached equipment. Video was stored as a series of MPEG files for easier processing, resulting in 70 video segments at station LC2 and 68 at LC5. Metadata included a real-time comment log,

voiceover comments on videos, closed-caption encoding (geo-referencing; using Digital Rapids StreamZHD recorders, (Canadian Scientific Submersible Facility, 1995-2020), date, time, latitude, longitude, depth, heading, pitch, roll, forward velocity, starboard velocity, downward velocity, altitude above seafloor, as well as temperature and salinity from a CTD. Specimens, water samples, and sediment samples were collected opportunistically.

In 2018, we collected additional imagery with the drop camera Campod (operated by the Department of Fisheries and Oceans (DFO) – Canada, Bedford Institute of Oceanography). The sampling design was modified from the one used with ROPOS to 3 1-km parallel transects at ~200 m spacing because the passive drifting of Campod makes maneuvering difficult. Still images (JPEG) were captured every 10 s, timed to manual hops of the camera along the seafloor, using a downward facing NIKON D810 camera (7360 x 4912 pixels). This drop camera system had two Quantum Qflash Model T5D-R light sources, which were operated at full power at 150 W. A total of 2886 images at station LC2 and 2202 images at LC5 were captured over the longer transects; however, we only processed images corresponding to a 400-m segment of each transect to make the transect arrays comparable between sampling tools (Figure 2.2). We used a real-time comment log and other metadata (date, time, latitude, longitude, depth, and altitude) were provided by the Campod technical crew after post-processing of the Navnet, CTD, altimeter, and USBL systems.

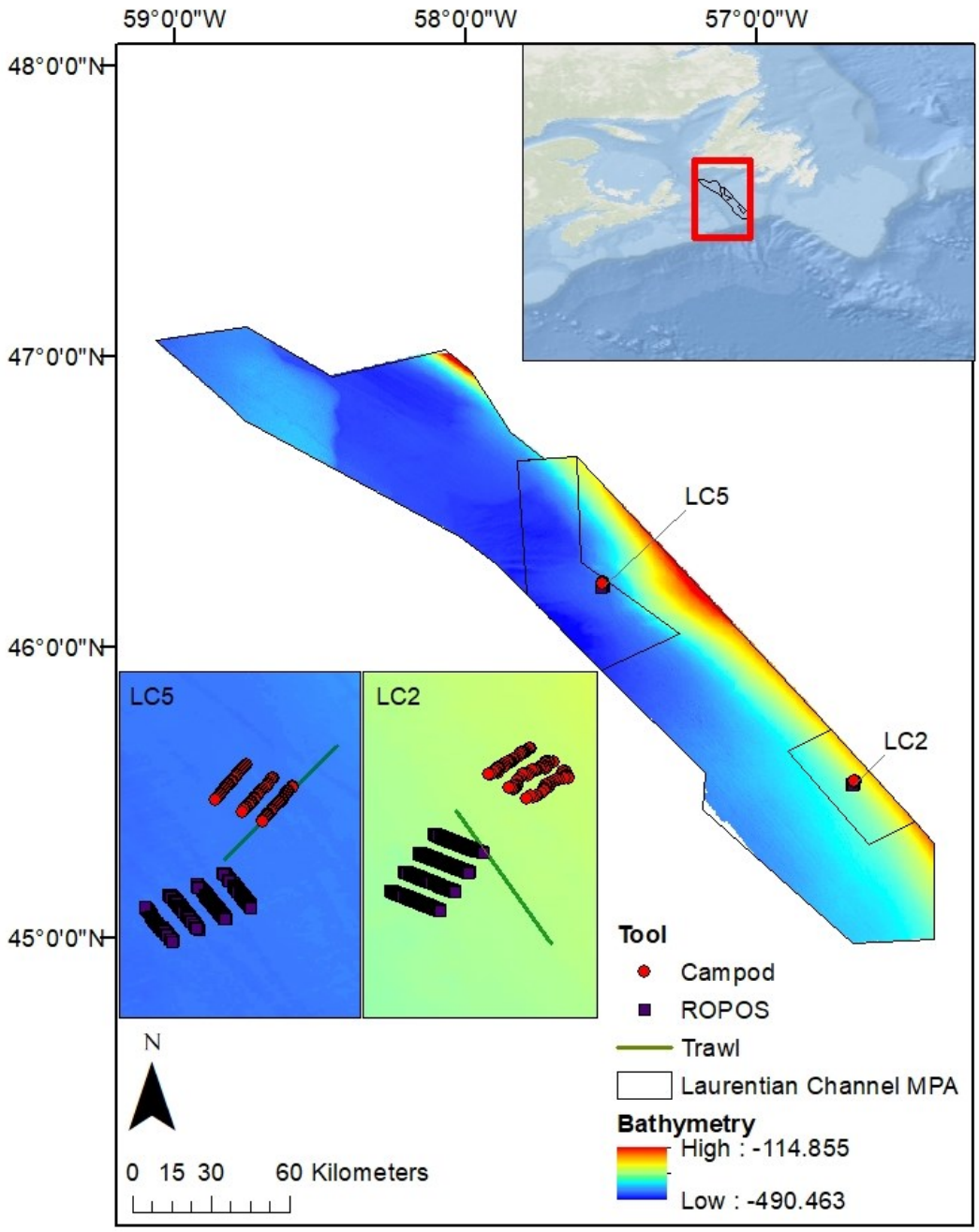

Figure 2.1 Map of the Laurentian Channel MPA (boundary provided by DFO), in Atlantic Canada off the southwest coast of Newfoundland indicating the locations of the two sampling stations (LC2 and LC5). Shown are 8 400-m ROPOS transects, 3 400-m Campod transects, and trawl set at station LC5 (inset i) and LC2 (inset ii) (DFO, 2019a). Esri (2020a.) for World Ocean Base layer, using coordinate system GCS_WGS_1984. Bathymetry data layer is from Lacharité et al., (2020). This MPA is located within a deep submarine valley in the Northwest Atlantic and was designated to protect corals (predominately sea pens), several fish and shark species, as well as leatherback turtles (DFO, 2019a).

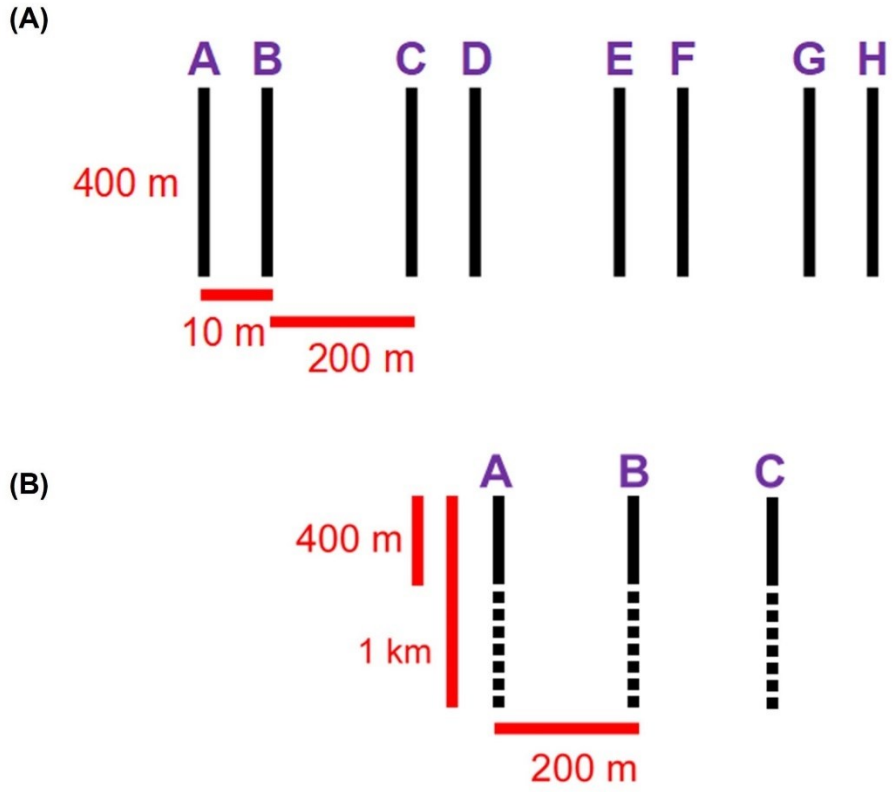

Figure 2.2 (A) ROPOS sampling design: 8 400-m parallel transects, spaced at spatial lags of 10 m and pairs spaced at 200 m. (B) Campod sampling design: 3 1-km parallel transects spaced at 200 m; 400-m segments (solid back lines) were used for comparisons with ROPOS transects.

2.3.3 Trawl

Biomass of all caught coral species (sea pens, gorgonians, soft corals, cup corals) was estimated from DFO (Newfoundland and Labrador Region) trawl surveys performed using a Campelen 1800 Shrimp Cosmos Trawl in the 3Ps NAFO region (which included the Laurentian Channel MPA) in 2010 (McCallum and Walsh 1996). We used data from two tows, 0.9 nautical miles in length (17-18 min at 3 knots), providing catch weights (kg) for 5 unique coral records (*Duva florida, Funiculina quadrangularis, Halipteris finmarchica, Pennatula cf. aculeata*, Sea pen sp.), as well as tow metadata (e.g. date, set, NAFO region, distance, duration, damage, depth, temperature, start/end latitude/longitude, gear type).

The principle of stationarity, that the same ecological processes are assumed to be occurring throughout a given area, can be rendered invalid at increasing distances between points of interest (Dale and Fortin 2014). To avoid non-stationarity, we limited comparisons to data within a 2-km buffer around each starting point of the ROPOS transects. This encompassed the entire ROPOS and Campod tracks, but only 1 full trawl track at each station was within the selected 2-km station radius.

Area swept by each trawl set was calculated as tow distance multiplied by wing spread adjusted for the ship used (area = distance × wing spread). Assuming a depth of ~ 400 m at the Laurentian Channel and using the median value for wing spread of 16.5 m on CCGS A. Needler (Walsh et al., 2009), we estimated the area per trawl as 27502 m^2. We estimated biomass in g m^{-2} by dividing biomass (kg tow^{-1}) by the estimated area

swept by the trawl, after weight conversion to grams (biomass (g m^{-2}) = biomass (kg) × 1000 $area^{-1}$). Similarly, to biomass (kg), the estimated biomass per unit area (g m^{-2}) assumes corals were evenly distributed across the trawled area.

2.3.4 Imagery Analysis

Using the Video & Track Replay feature in the software application Ocean Floor Observation Protocol (OFOP 3.3.8c, Huetten and Greinert, 2008; Scientific Abyss Mapping Services, 2009), position data from ROPOS was synced to video with timestamps, and images were extracted at a target distance interval of 1.5 m. We confirmed the start/end of each transect in ArcGIS (Version 10.5 Esri, 2016) and excluded off-transect or overlapping images. We aimed to analyze every 4th image. Images were included in the analysis if total area was less than 6 m^2 as estimated by the scaling lasers spaced 10 cm apart, and if image clarity permitted an unobstructed view of the seafloor (see Figure 2.3 for example imagery). Obscured sections were cropped out to permit taxonomic identification (i.e. removing suspended particles, pelagic animals near the camera, sediment plumes, or sections of low light). Images were deemed unsuitable if they required > 50% cropping. Overall, this protocol resulted in ~ 6-m spacing between images; when images were deemed unsuitable the next sequentially suitable image at a distance of 1.5-6 m was analyzed instead. We filtered out 50% of the analyzed ROPOS images to reduce sampling size, making it comparable to Campod (which generated fewer images), which resulted in final spacing of ~12 m between images for ROPOS.

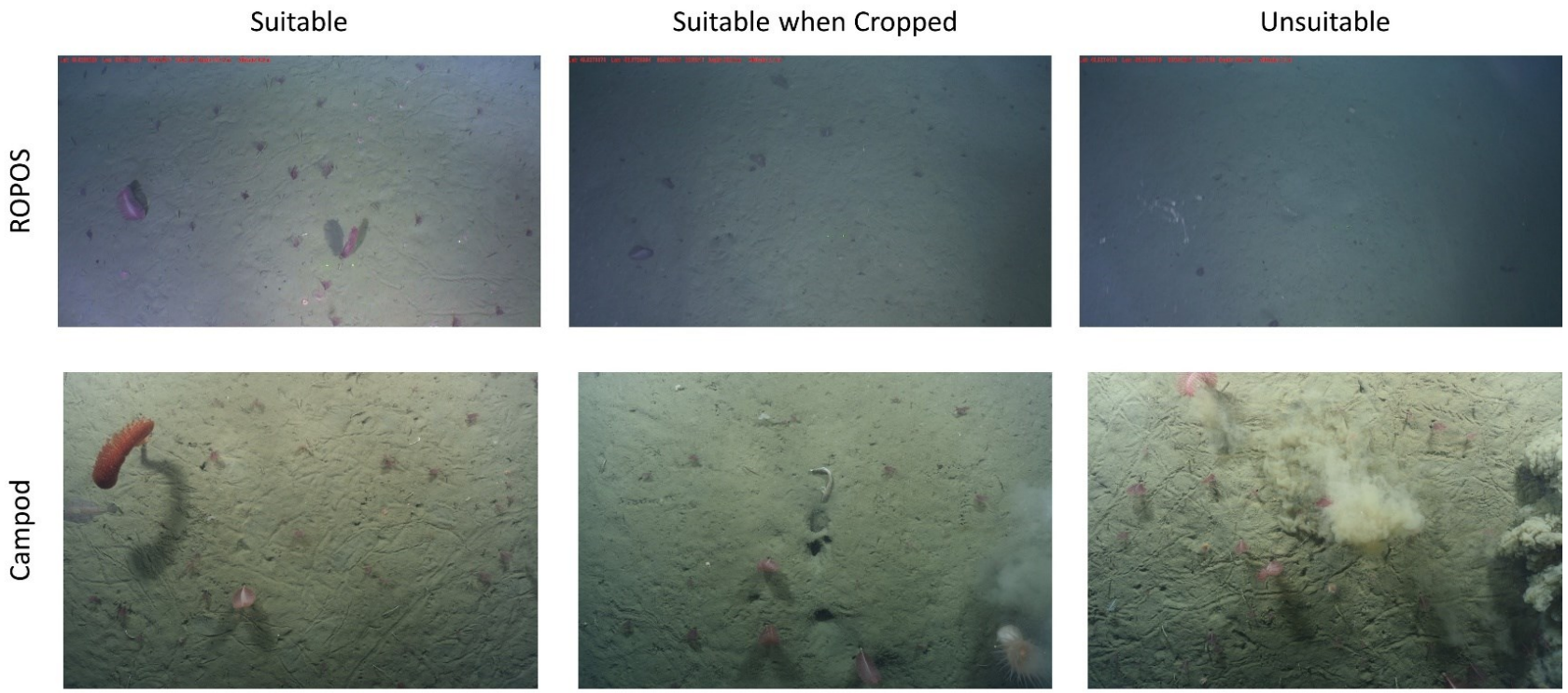

Figure 2.3 Examples of imagery collected by the ROV ROPOS (first row) and the drop camera Campod (second row), deemed suitable (left) or unsuitable (right) for analysis (e.g. poor illumination, blurry edges, sediment plumes). If less than <50% of an image was unsuitable and the scaling lasers were visible (middle), then those images were cropped before enumerating fauna and calculating the area analyzed

Due to the passive drifting of Campod, we used a target time interval of 10 s rather than a target distance between images, which, assuming a speed of 1 knot (0.514 m s^{-1}), corresponds to ~ 5-m spacing. However, this was likely an overestimate of distance due to slower drifting of the camera than expected. To maintain a standard image analysis protocol (using ImageJ software; Abràmoff et al., 2004) consistent to that used for the ROPOS analysis, we analyzed every 4th image for a 400-m section of each transect (spacing ~40 s, ~20 m) using the same protocols as for ROPOS.

All megafauna > 2 cm in the largest dimension were enumerated and identified to morphospecies[2] using a reference guide based on World Register of Marine Species (WoRMS). If morphospecies were too numerous to count or colonial, e.g. holothuroidea and encrusting sponges, they were recorded as percent cover instead of counts. We used the point method to estimate percent cover (209 points for ROPOS and 204 for Campod, respectively, due to differences in image resolution), including only the number of points that fell onto the uncropped area of the image.

2.3.5 Data Analysis

We aimed to avoid spatial overlap of sampling among tools and thus minimizing potential confounding effects. However, some overlap may have occurred between the trawl track and Campod (CON46) at LC5, and ROPOS (2A) at LC2 (Figure 2.1). Since these tools have different levels of position accuracy it was difficult to interpret distances between their tracks, in particular for the trawl, as latitudes and longitudes reflect the

[2] Some morphospecies groupings were renamed in Chapters 3 and 4 (see appendix Table AII.1), but does not alter this chapter.

vessel position rather than having positional equipment directly mounted on the trawl itself.

For each transect of each tool, we evaluated image quality based on a number of criteria: total images captured, number of suitable images selected for analysis, total area covered by images, and total area of images deemed unsuitable for analysis. For analysis, we selected the most abundant taxonomic groups (see Figure 2.4), determined as those recorded on at least 11 of 22 total transects in the study. The less abundant taxa were either aggregated to form groups of higher abundance (e.g. Actiniaria (O.) spp.) or excluded (i.e. too few counts) from the analyses.

To make the sampling design used by ROPOS comparable to that of Campod (which included 3 400-m transects) for statistical analyses, we assembled the 8 individual ROPOS transects (A-H) into 4 groups of 3 400-m transects, ~200 m apart (ROPOS_ACE, ROPOS_BDF, ROPOS_CEG, ROPOS_DFH). We compared the abundance of the most abundant taxa among sampling designs (5 levels: Campod, ROPOS_ACE, ROPOS_BDF, ROPOS_CEG, and ROPOS_DFH) using one-way type 2 ANOVAs (Underwood, 1997). We detected a lack of normality using Shapiro-Wilk tests and normal quantile plots, and heteroscedacity using Levene's tests and residual plots. Although we explored several data transformations (e.g. $\log_e$ and square root versions), none improved heteroscedasticity and normality; therefore, we used the untransformed data (abundance of individuals or colonies m^{-2}) in the ANOVAs. Post-hoc comparisons for significant pairwise differences in treatment means were performed with Tukey HSD tests (Abdi and Williams 2010).

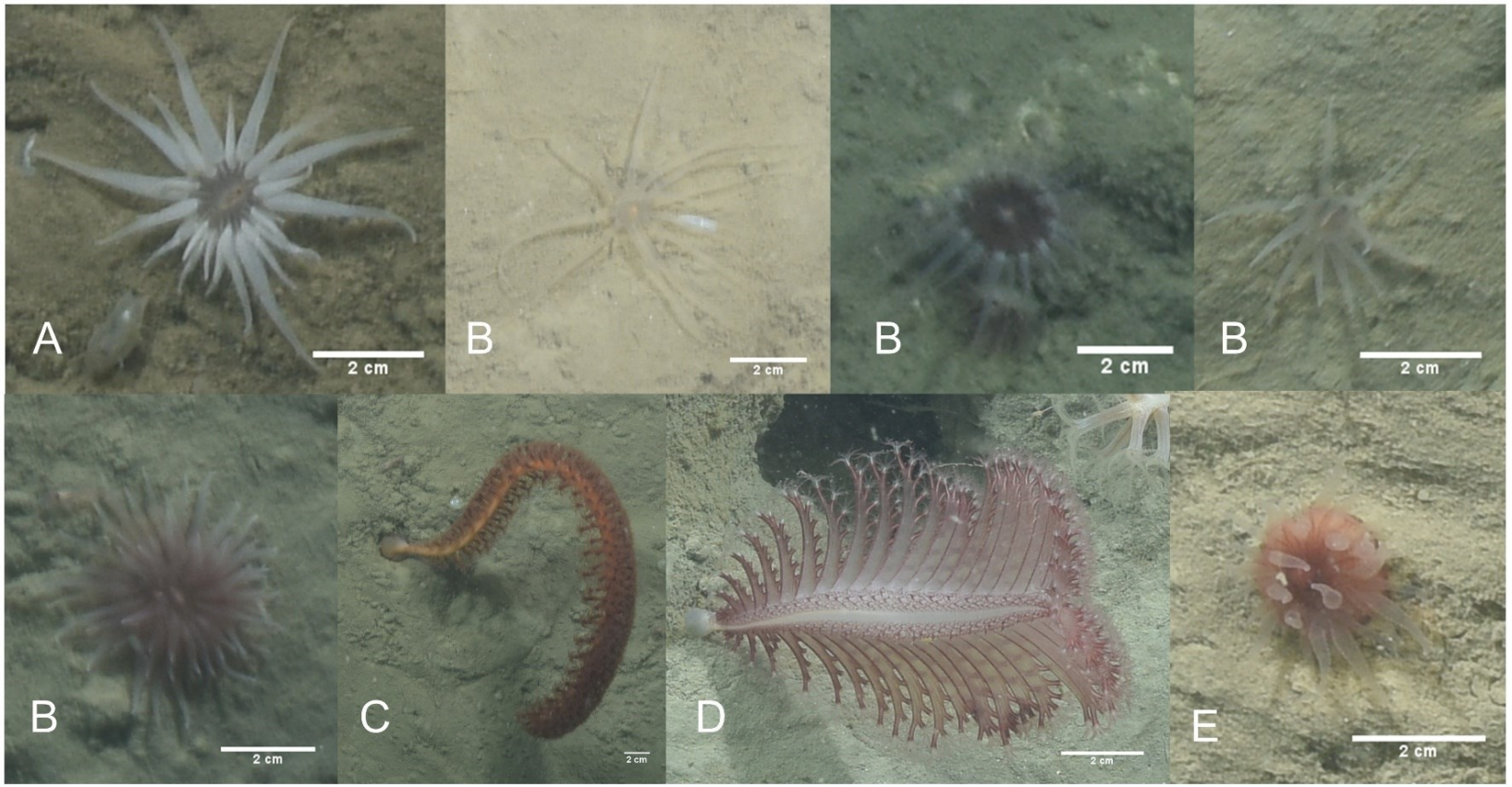

Figure 2.4 Examples of the most abundant taxonomic groups (scale bars are 2 cm). A) Actiniaria (O.) sp. 23, B) Actiniaria (O.) spp., C) *Anthoptilum* spp., D) *Pennatula* sp. 2, and E) Scleractinia (O.) spp.[3]

[3] Some morphospecies groupings were renamed in Chapters 3 and 4 (see appendix Table AII.1).
e.g. Actiniaria (O.) sp. 23 = *Edwardsia* sp. 1, Actiniaria (O.) spp. = Anthozoa (C.) spp., and Scleractinia (O.) spp. = Hexacorallia (SC.) spp.

We used all 8 400-m transects ROPOS transects (ROPOS_all) for some analyses. Including all aggregated taxa, we calculated morphospecies accumulation curves using the random method for each sampling design at each station, with 999 permutations. We used non-metric multi-dimensional scaling (NMDS) to explore similarities in the composition of the assemblages among sampling designs within stations and between stations. Significant patterns were explored using permutational multivariate analysis of variance (PERMANOVA) on the Bray–Curtis dissimilarity matrix with 999 permutations using the "Adonis" function. All statistical analyses were done with R version 3.6.1; packages Tidyverse, Reshape, Vegan, Car, and Agricolae

2.4 Results

Overall, image quality was high for both tools and most transects, except for ROPOS at LC5. For ROPOS, more images per transect were unsuitable at LC5 than at LC2 (Table 2.1). A higher proportion of images collected by Campod than by ROPOS were unsuitable, and only half the images were selected for analysis. However, it was often possible to replace unsuitable images, except for ROPOS at LC5 where fewer images were analyzed. Less area needed be cropped out of images by ROPOS at LC2 than by ROPOS at LC5 and by Campod at both sites (10-40% of the area was cropped out of images with unsuitable sections). Mean (and standard deviation) altitude above the sea floor was consistent across all transects, at ~1-2 m and thus did not affect image quality (Table 2.2).

There were some differences between stations in the detected species composition and some taxa were only found at one station [LC2 only: Pennatulacea (O.) sp. 5,

Pennatulacea (O.) spp., *Protoptilum* sp. 1, Asteroidea (C.) spp., Decapoda (O.) spp., Actiniaria (O.) sp. 19; LC5 only: Actiniaria (O.) sp. 23, Cerianthidae (F.) spp., Gersemia sp. 1; Table 2.3 and 2.4]. The only taxon recorded as percent cover at both stations was Holothuroidea (C.) sp. 1. Average percent cover (± SE) was less at LC2 than at LC5, for ROPOS (all 8 transects; LC2 0.000 ± 0% and LC5 0.005 ± 0.003%) but varied for Campod (all 3 transects; LC2 0.273 ± 0.3% and LC5 0.060 ± 0.003%).

The abundance of taxa varied between tools and stations. Abundance was much greater at LC2 than at LC5, but was dominated by a few species, particularly Pennatula sp. 2. (Figure 2.5). Campod captured significantly higher abundance of Actiniaria (O.) sp. 23 than all ROPOS designs and of *Pennatula* sp. 2 than two of four ROPOS designs, but only at station LC5 (Table 2.5).

Morphospecies accumulation curves were similar for Campod and ROPOS at LC2 (Figure 2.6), but the curve was steeper for Campod than all ROPOS designs at LC5. A plateau of the morphospecies accumulation curves was not reached at either station, except when all ROPOS transects were combined at LC5. Significant differences in species composition existed between the two stations (Figure 2.7A, Table 2.6). Based on the NMDS plots and PERMANOVAs, the imagery tools produced similar assemblages at LC2 (overlapping 95% confidence interval for tools) but not at LC5 (Figure 2.7B-C & Table 2.6).

Table 2.1 Quality of imagery collected by the ROV ROPOS and the drop camera Campod, by 400-m transect at stations LC2 and LC5 in the Laurentian Channel MPA.

Tool	Transect	# Total	# Selected for analysis	# Unsuitable	# Analyzed	# This study	Total area (m^2)	Area cropped out (m^2)	Average percent crop	SD
ROPOS	2A	276	69	8	62	31	71.92	17.32	23.58	9.32
	2B	224	55	5	54	27	60.45	5.43	9.66	6.40
	2C	255	63	2	63	32	63.62	4.05	14.55	10.61
	2D	259	65	14	64	32	63.96	8.98	19.37	15.41
	2E	249	63	0	62*	31	58.61	1.69	12.38	4.43
	2F	258	64	35	58	29	67.46	20.20	25.35	12.94
	2G	251	62	2	62	31	57.36	8.09	13.66	7.32
	2H	257	64	21	61	30	71.63	15.62	17.91	10.21
	5A	250	62	34	55	27	53.44	4.69	19.55	10.04
	5B	251	65	101	40	20	36.27	13.17	25.09	10.39
	5C	259	64	6	63	32	49.31	6.08	16.73	10.63
	5D	257	62	100	44	22	34.63	23.06	38.67	12.97
	5E	257	64	20	62	31	49.91	21.52	27.53	10.86
	5F	266	66	142	38	19	20.50	12.46	37.46	9.47
	5G	261	64	83	46	23	29.51	15.92	34.22	9.47
	5H	238	59	140	32	16	18.28	13.19	41.10	9.21
Campod	LC2A_CON16	118	30	26	29	29	55.80	16.16	22.00	13.81
	LC2B_CON17	129	33	19	32	32	73.39	17.37	26.62	17.68
	LC2C_CON18	141	36	17	36	36	70.33	17.11	27.60	14.25
	LC5A_CON46	125	32	10	31	31	59.93	17.06	21.71	12.35
	LC5B_CON47	121	31	14	31	31	71.64	19.08	20.16	11.42
	LC5C_CON48	109	28	6	28	28	58.21	12.90	20.45	11.94

Note: * One image was inadvertently missed during processing. Unsuitable images were replaced by the next suitable image if possible. To reduce sampling bias, only half of the analyzed ROPOS images were used in statistics for this study. Total suitable image area, unsuitable area cropped out, and average percent of cropped area (± SD) per transect was reported for the subset of images used in this study.

Table 2.2 Summary of imagery transect metadata at stations LC2 and LC5 in the Laurentian Channel MPA. DD: decimal degrees.

Tool	Transect	Date	Mean depth ± SD (m)	Mean altitude ± SD (m)	Images analyzed	Start longitude (DD)	Start latitude (DD)	End longitude (DD)	End latitude (DD)
ROPOS	2A	2017-09-09	348 ± 0.68	1.24 ± 0.31	31	-56.6704	45.53298	-56.666	45.53126
	2B	2017-09-09	349 ± 0.69	1.03 ± 0.24	27	-56.6665	45.53134	-56.6703	45.53281
	2C	2017-09-09	350 ± 0.52	0.93 ± 0.18	32	-56.6672	45.52954	-56.6716	45.53128
	2D	2017-09-09	350 ± 0.55	1.03 ± 0.23	32	-56.6717	45.5312	-56.6674	45.5295
	2E	2017-09-09	351 ± 0.77	0.83 ± 0.05	31	-56.6686	45.52792	-56.6728	45.52957
	2F	2017-09-09	351 ± 0.82	1.20 ± 0.35	29	-56.673	45.52954	-56.6685	45.52782
	2G	2017-09-09	354 ± 0.79	0.89 ± 0.15	31	-56.6699	45.52628	-56.6741	45.52796
	2H	2017-09-09	354 ± 0.93	1.23 ± 0.40	30	-56.6742	45.52788	-56.6699	45.52617
	5A	2017-09-12*	439 ± 0.61	0.94 ± 0.13	27	-57.5277	46.21105	-57.53	46.2138
	5B	2017-09-13	438 ± 0.53	1.27 ± 0.28	20	-57.5302	46.2138	-57.5277	46.21074
	5C	2017-09-13	440 ± 0.21	0.91 ± 0.03	32	-57.5298	46.20974	-57.5324	46.21284
	5D	2017-09-13	440 ± 0.30	1.35 ± 0.29	22	-57.5324	46.21259	-57.53	46.20969
	5E	2017-09-13	440 ± 0.39	1.11 ± 0.32	31	-57.5322	46.20882	-57.5347	46.21186
	5F	2017-09-13	440 ± 0.27	1.08 ± 0.22	19	-57.5349	46.21187	-57.5325	46.20894
	5G	2017-09-13	440 ± 0.24	1.00 ± 0.18	23	-57.5345	46.20781	-57.537	46.21084
	5H	2017-09-13	440 ± 0.29	1.11 ± 0.25	16	-57.5365	46.20997	-57.5346	46.20777
Campod	LC2A_CON16	2018-07-09	340 ± 1.37	1.81 ± 0.58	29	-56.6588	45.53846	-56.6622	45.53608
	LC2B_CON17	2018-07-09	342 ± 1.95	1.72 ± 0.53	32	-56.6598	45.53925	-56.6637	45.53701
	LC2C_CON18	2018-07-10	343 ± 1.39	1.61 ± 0.52	36	-56.6618	45.54047	-56.6655	45.53813
	LC5A_CON46	2018-07-09	440 ± 0.84	1.76 ± 0.40	31	-57.5239	46.22137	-57.5266	46.21836
	LC5B_CON47	2018-07-09	439 ± 1.01	1.63 ± 0.33	31**	-57.5257	46.22215	-57.5284	46.21914
	LC5C_CON48	2018-07-09	441 ± 1.22	1.41 ± 0.30	28	-57.5281	46.22326	-57.5308	46.22028

*Some data also collected on 2017-09-13, **13 images from CON47 were missing measurements of depth and altitude; means and SD are calculated for n=18 images

Table 2.3 Abundance of individuals/colonies m^{-2} (mean ± SE) at station LC2 in the Laurentian Channel MPA averaged across transect and then averaged across each of six sampling designs. Data for Campod, ROPOS_ACE, ROPOS_BDF, ROPOS_CEG, and ROPOS_DFH are averaged across 3 400-m transects. Data for ROPOS_all were averaged across 8 400-m transects.

Taxon	Campod (n=3)	ROPOS_ACE (n=3)	ROPOS_BDF (n=3)	ROPOS_CEG (n=3)	ROPOS_DFH (n=3)	ROPOS_all (n=8)
Arthropoda						
Decapoda (O.) spp.	NA	0.004 ± 4E-03	NA	NA	NA	0.002 ± 2E-03
Lithodes maja	NA	NA	0.004 ± 4E-03	NA	0.004 ± 4E-03	0.001 ± 1E-03
Cnidaria						
Actiniaria (O.) sp. 1	0.005 ± 5E-03	NA	NA	NA	NA	NA
Actiniaria (O.) sp. 19	0.014 ± 1E-02	NA	0.004 ± 4E-03	NA	0.004 ± 4E-03	0.001 ± 1E-03
Actiniaria (O.) spp.	0.016 ± 9E-03	NA	0.007 ± 7E-03	NA	NA	0.003 ± 3E-03
Anthozoa (C.) sp. 4	0.028 ± 2E-02	NA	NA	NA	NA	NA
Flabellum alabastrum	0.007 ± 7E-03	0.016 ± 1E-02	NA	0.018 ± 1E-02	NA	0.008 ± 5E-03
Scleractinia (O.) spp.	0.962 ± 1E-01	0.262 ± 6E-02	0.907 ± 4E-01	0.387 ± 7E-02	0.493 ± 2E-01	0.547 ± 2E-01
Pennatulacea						
Anthoptilum spp.	0.016 ± 1E-02	0.007 ± 7E-03	NA	NA	NA	0.003 ± 3E-03
Kophobelemnon spp.	NA	NA	0.007 ± 7E-03	NA	NA	0.002 ± 2E-03
Pennatula sp. 2	6.629 ± 1E+00	3.722 ± 4E-01	4.032 ± 1E+00	3.825 ± 3E-01	2.408 ± 9E-01	3.457 ± 5E-01
Pennatulacea (O.) sp. 5	NA	0.016 ± 3E-04	NA	0.011 ± 5E-03	NA	0.006 ± 3E-03
Pennatulacea (O.) spp.	0.007 ± 7E-03	NA	0.006 ± 6E-03	NA	NA	0.002 ± 2E-03
Protoptilum sp. 1	NA	NA	0.011 ± 6E-03	NA	0.006 ± 6E-03	0.004 ± 3E-03

Table 2.3 *(Continued)*

Taxon	Campod (n=3)	ROPOS_ACE (n=3)	ROPOS_BDF (n=3)	ROPOS_CEG (n=3)	ROPOS_DFH (n=3)	ROPOS_all (n=8)
Echinodermata						
Asteroidea (C.) sp. 4	0.012 ± 1E-02	0.013 ± 2E-03	0.012 ± 1E-02	0.010 ± 5E-03	0.012 ± 1E-02	0.010 ± 5E-03
Asteroidea (C.) spp.	NA	0.005 ± 5E-03	0.011 ± 5E-03	0.005 ± 5E-03	0.011 ± 5E-03	0.008 ± 3E-03
Ophiuroidea (C.) spp.	0.004 ± 4E-03	NA	NA	NA	NA	NA
Pteraster sp. 1	0.011 ± 1E-02	NA	NA	NA	NA	NA
Other						
Porifera (P.) spp.	NA	0.005 ± 5E-03	NA	0.005 ± 5E-03	NA	0.002 ± 2E-03
Unidentified sp. 216*	NA	0.006 ± 6E-03	0.092 ± 9E-02	0.011 ± 6E-03	NA	0.039 ± 3E-02

* Possibly *Funiculina* sp. but image quality obscured polyps.

Table 2.4 Abundance of individuals/colonies m^{-2} (mean ± SE) at station LC5 in the Laurentian Channel MPA averaged across transect and then averaged across each of six sampling designs. Data for Campod, ROPOS_ACE, ROPOS_BDF, ROPOS_CEG, and ROPOS_DFH are averaged across 3 400-m transects. Data for ROPOS_all were averaged across 8 400-m transects.

Taxon	Campod (n=3)	ROPOS_ACE (n=3)	ROPOS_BDF (n=3)	ROPOS_CEG (n=3)	ROPOS_DFH (n=3)	ROPOS_all (n=8)
Arthropoda						
Lithodes maja	0.005 ± 5E-03	NA	NA	NA	NA	NA
Cnidaria						
Actiniaria (O.) sp. 1	0.065 ± 2E-02	0.006 ± 6E-03	0.029 ± 2E-02	0.018 ± 1E-02	0.008 ± 8E-03	0.017 ± 8E-03
Actiniaria (O.) sp. 23	0.531 ± 3E-02	0.070 ± 2E-02	0.070 ± 2E-02	0.084 ± 2E-02	0.058 ± 1E-02	0.078 ± 1E-02
Actiniaria (O.) spp.	0.033 ± 2E-02	0.060 ± 1E-02	0.087 ± 3E-02	0.090 ± 4E-02	0.089 ± 3E-02	0.083 ± 2E-02
Anthozoa (C.) sp. 4	0.006 ± 6E-03	NA	NA	NA	NA	NA
Cerianthidae (F.) spp.	0.029 ± 1E-02	0.006 ± 6E-03	NA	0.024 ± 2E-02	NA	0.011 ± 9E-03
Flabellum alabastrum	0.018 ± 2E-02	0.007 ± 7E-03	NA	NA	NA	0.003 ± 3E-03
Gersemia sp. 1	0.012 ± 1E-02	0.010 ± 1E-02	0.019 ± 2E-02	0.010 ± 1E-02	0.019 ± 2E-02	0.011 ± 7E-03
Scleractinia (O.) spp.	0.127 ± 6E-02	0.016 ± 9E-03	0.028 ± 2E-02	0.016 ± 9E-03	0.044 ± 9E-03	0.022 ± 8E-03
Pennatulacea						
Anthoptilum spp.	0.037 ± 8E-03	0.044 ± 3E-02	0.016 ± 2E-02	0.053 ± 3E-02	0.036 ± 4E-02	0.048 ± 2E-02
Kophobelemnon spp.	0.030 ± 2E-03	0.012 ± 9E-03	0.035 ± 4E-02	0.012 ± 1E-02	0.035 ± 4E-02	0.021 ± 1E-02
Pennatula sp. 2	0.051 ± 5E-03	0.004 ± 4E-03	0.022 ± 1E-02	0.004 ± 4E-03	0.015 ± 2E-02	0.010 ± 6E-03
Echinodermata						
Asteroidea (C.) sp. 4	0.003 ± 3E-03	NA	NA	NA	NA	NA
Ophiuroidea (C.) spp.	0.013 ± 8E-03	NA	NA	NA	NA	NA
Pteraster sp. 1	0.014 ± 1E-02	NA	NA	NA	NA	NA
Other						
Porifera (P.) spp.	0.006 ± 6E-03	NA	NA	NA	NA	NA
Unidentified sp. 216*	NA	0.008 ± 8E-03	NA	0.008 ± 8E-03	NA	0.003 ± 3E-03

* Possibly *Funiculina* sp. but image quality obscured polyps.

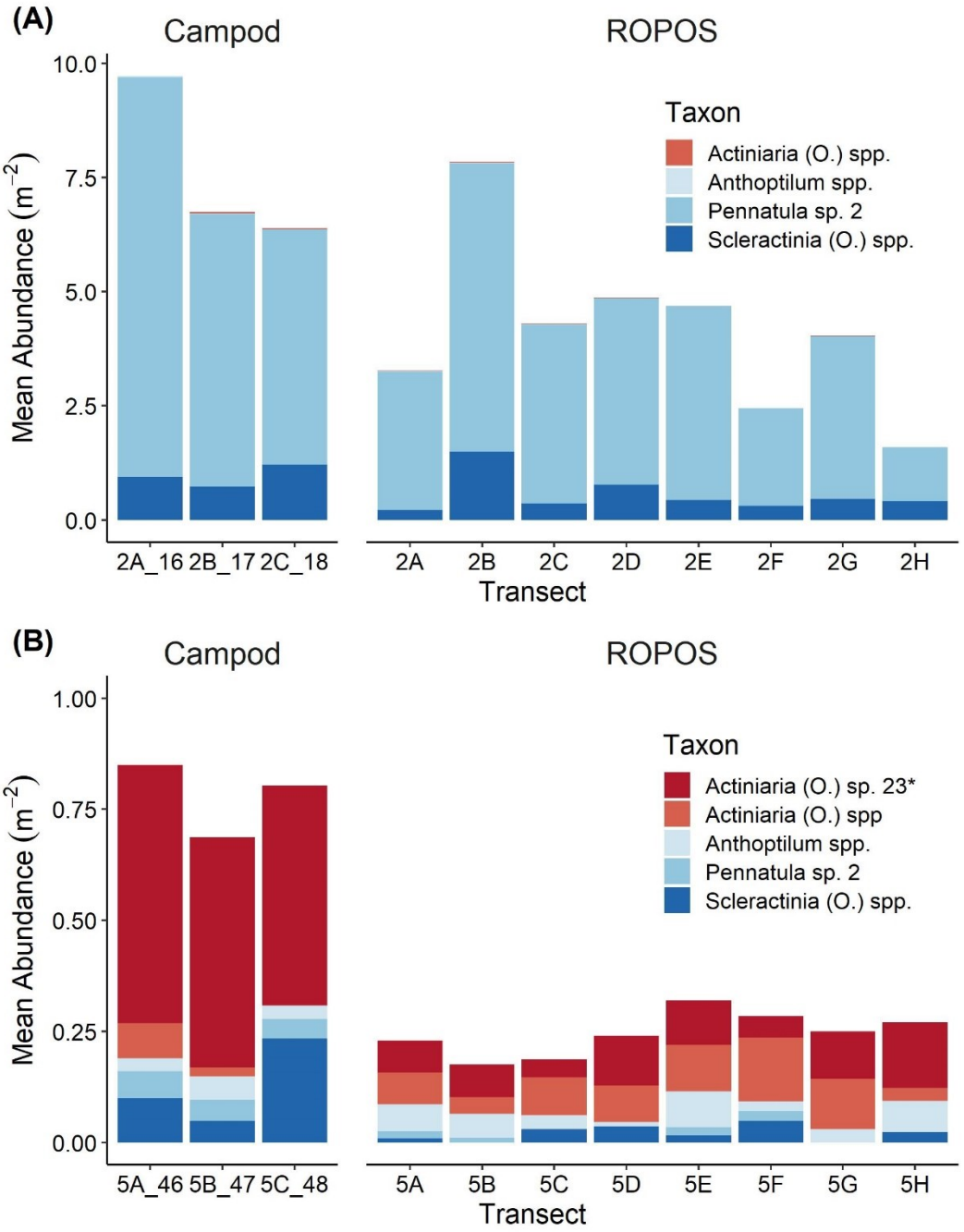

Figure 2.5 Mean abundance of individuals or colonies m^{-2} in each transect for abundant taxa (present in at least 11 of 22 transects) at (A) station LC2 and (B) station LC5 in the Laurentian Channel MPA. Abundance was averaged across images for each transect (n= 16-36), see Table 2.1 for number of images per transect. Note: different scales on y-axis, * denotes taxon that was only found at one of these stations.

Table 2.5 One-way ANOVAs (type 2) on untransformed data, using 5 fixed levels of design: Campod, ROPOS_ACE, ROPOS_BDF, ROPOS_CEG, and ROPOS_DFH (3 400-m transects) for abundant taxa (present in at least 11 of 22 total transects), at stations LC2 and LC5 in the Laurentian Channel MPA.

Station	Taxon	Sum of Squares	F Value	P Value		Tukey HSD
LC2	Actiniaria (O.) spp.	0.001	1.735	0.219		
	Residuals	0.001	-	-		
	Anthoptilum spp.	0.001	1.400	0.302		
	Residuals	0.001	-	-		
	Pennatula sp. 2	28.4	3.457	0.051		
	Residuals	20.6	-	-		
	Scleractinia (O.) spp.	1.19	2.428	0.116		
	Residuals	1.23	-	-		
LC5	Actiniaria (O.) sp. 23	0.510	92.351	<0.001	**	Campod> ROPOS_ACE, Campod> ROPOS_BDF, Campod> ROPOS_CEG, Campod> ROPOS_DFH
	Residuals	0.014	-	-		
	Actiniaria (O.) spp.	0.007	0.775	0.566		
	Residuals	0.024	-	-		
	Anthoptilum spp.	0.004	0.575	0.687		
	Residuals	0.019	-	-		
	Pennatula sp. 2	0.004	3.919	0.036	*	Campod> ROPOS_ACE, Campod> ROPOS_CEG
	Residuals	0.003	-	-		
	Scleractinia (O.) spp.	0.026	3.037	0.070		
	Residuals	0.021	-	-		

Significant Shapiro-Wilk test for all ANOVAs except *Pennatula* sp. 2 at LC2;
Significant Levene's test for LC2 Actiniaria (O.) spp., LC2 *Anthoptilum* spp., and LC5 Scleractinia (O.) spp. * α =0.05, and ** α =0.01. For both stations, df = 4,10. Based on mean abundance data by transect.

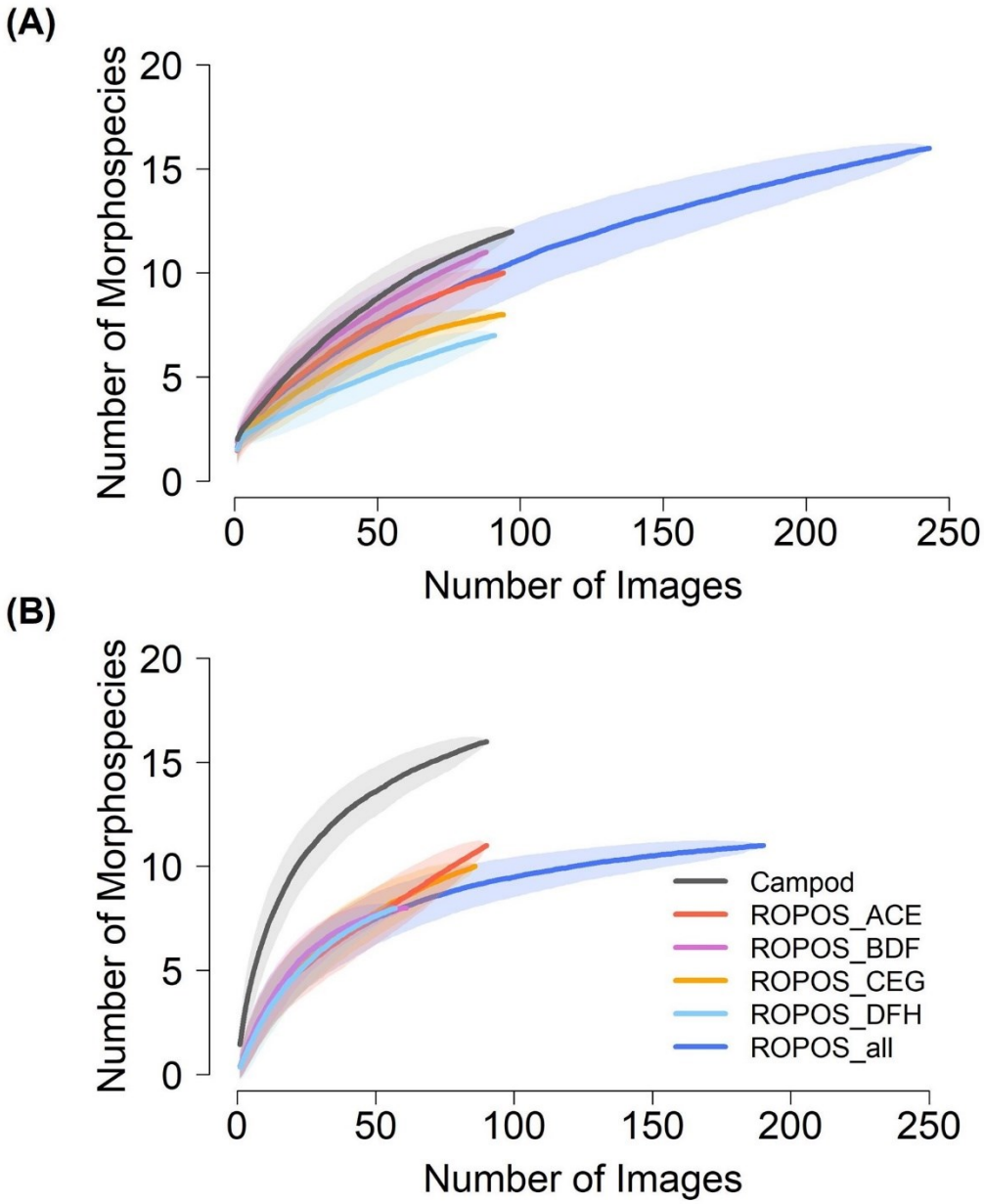

Figure 2.6 Morphospecies accumulation curves at (A) station LC2 and (B) station LC5 in the Laurentian Channel MPA, based on abundance per photo across each of the six sampling designs; Campod, ROPOS_ACE, ROPOS_BDF, ROPOS_CEG, ROPOS_DFH (3 400-m transects), and ROPOS_all (8 400-m transects). Used random method with 999 permutations; shaded confidence intervals are one SD.

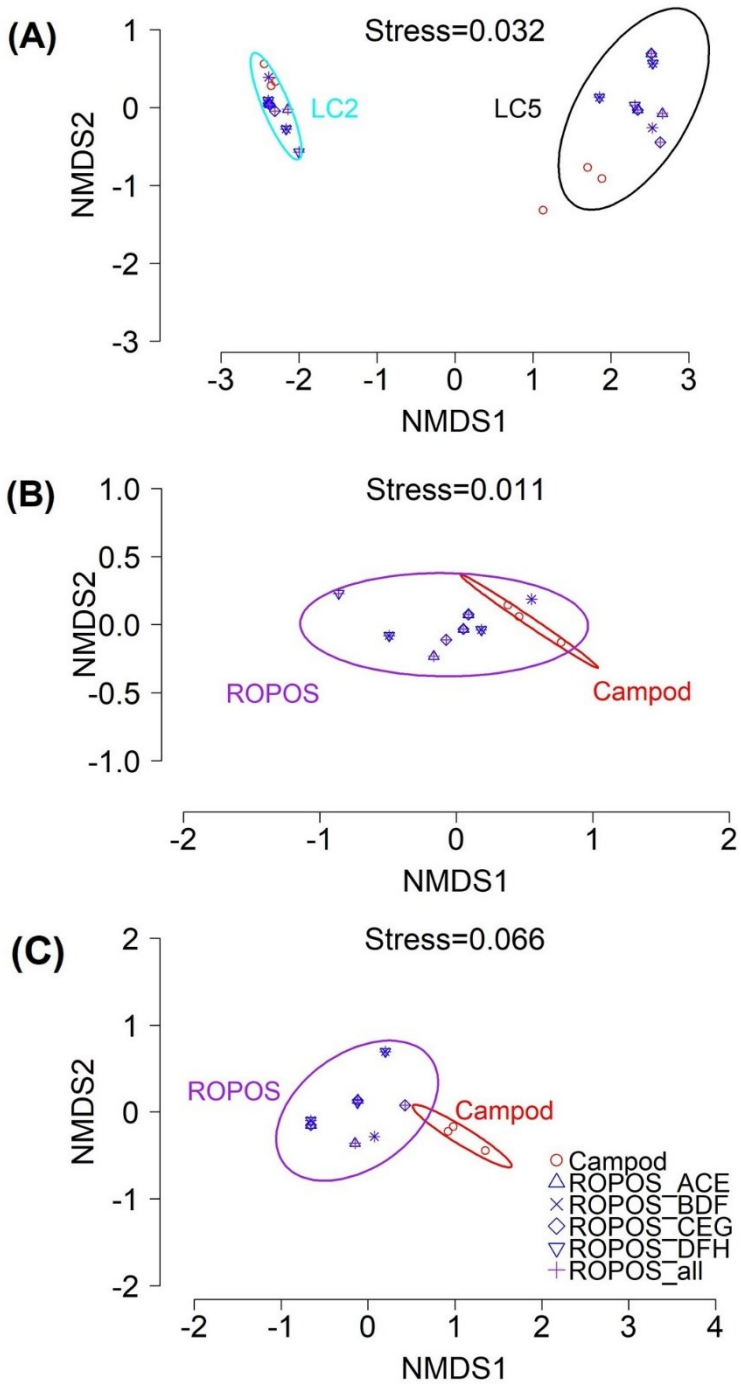

Figure 2.7 Non-metric multi-dimensional scaling (NMDS) plot of the assemblages in the Laurentian Channel MPA (mean abundance m^{-2} per transect for n=23 aggregated taxa) using Bray-Curtis dissimilarity with 95% CI for station and tool groups, at (A) station LC2 and LC5; (B) station LC2 for each sampling design and (C) station LC5.

Table 2.6 Permutational multivariate analysis of variance (PERMANOVA) of distance matrix using Bray–Curtis dissimilarity and 999 permutations examining the effect of sampling designs Campod, ROPOS_ACE, ROPOS_BDF, ROPOS_CEG, ROPOS_DFH (3 400-m transects) and station (LC2 and LC5) in the Laurentian Channel MPA.

Station	Factors	df	Sums Of Squares	Mean Square	*F*	R^2	*P*
LC2 & LC5	Design	5	0.72	0.14	1.67	0.05	0.102
	Station	1	8.66	8.66	100.31	0.66	0.001*
	Design x Station	5	0.79	0.16	1.82	0.06	0.058
	Residuals	34	2.94	0.09	-	0.22	-
	Total	45	13.10	-	-	1.00	-
LC2	Design	5	0.38	0.08	1.61	0.32	0.151
	Residuals	17	0.80	0.05	-	0.68	-
	Total	22	1.18	-	-	1.00	-
LC5	Design	5	1.13	0.23	1.80	0.35	0.036*
	Residuals	17	2.14	0.13	-	0.65	-
	Total	22	3.26	-	-	1.00	-

* Denotes significant p-value using α=0.05. Using 23 taxon in total, some that were found only at one station. Based on mean abundance data by transect.

The trawl only captured a few taxa (Table 2.7) with overall low catch weights, except for sea pens (taxonomically not resolved) at LC5. Biomass normalized to sampled area ranged from <0.01 to 1.45 g m^{-2} for *Pennatula cf. aculeata*, likely the same species as *Pennatula* sp. 2 from the imagery analysis (2.408 ± 0.9 to 6.629 ± 1 m^{-2} at LC2; 0.004 ± 0.004 to 0.051 ± 0.005 m^{-2} at LC5).

Table 2.7 Coral biomass from Fisheries and Oceans Canada (Newfoundland and Labrador Region) multispecies surveys using a Campelen 1800 Shrimp Trawl from one trawl set at station LC2 and LC5.

Site	Date	Mean depth (m)	Taxon	Weight of catch (kg)	Estimated biomass (g m^{-2}) *
LC2	04/14/2010	347	*Funiculina quadrangularis*	1.4	0.05
LC2	04/14/2010	347	*Halipteris finmarchica*	0.14	0.01
LC2	04/14/2010	347	*Pennatula cf. aculeata*	0.1	<0.01
LC5	04/27/2010	429	Sea pen sp.	40	1.45
LC5	04/27/2010	429	*Duva florida*	0.4	0.01

* Estimated biomass (g m^{-2}) for perspective only – not accurate for further fine-scale distribution analyses.

Table 2.8 Qualitative comparisons of three sampling tools [a remotely operated vehicle (ROPOS), a drop camera (Campod), and a trawl (Campelen 1800 Shrimp Trawl)] for capturing different ecological attributes and sampling biases for deep-sea megaepifauna.

Ecological Attribute	Tool		
	ROV	**Drop Camera**	**Trawl**
Demography			
1. Species identification	Based on imagery, possible to morphospecies, sometimes to species. Physical samples, if collected, can resolve verification. Imagery can be re-analyzed by other taxonomic experts if desired.	Based on imagery, possible to morphospecies, sometimes to species. Lack of physical samples for verification. Imagery can be re-analyzed by other taxonomic experts if desired.	To species, but lacks consistency as some sets are grouped to order/common name. Samples are often not stored for further identification.
2. Mean abundance	# individuals m^{-2} by transect	# individuals m^{-2} by transect	N/A
3. Biomass	N/A; may be inferred for some species if reliable size/biomass models are available.	N/A; may be inferred for some species if reliable size/biomass models are available.	# kg $trawl^{-1}$; can standardize tow (i.e. 0.75 nautical miles) [a]
4. Size & recruitment	Sizing possible for objects > 2 cm on same plane as scaling lasers (if present); in absence of appropriate scale, relative sizing (adult vs juveniles) is possible. Caution: erect fauna requires a more appropriate scale.	Sizing possible for objects > 2 cm on same plane as scaling lasers; or in absence of appropriate scale, relative sizing (adult vs juveniles) is possible. It is also easier to see objects <2cm in some imagery. Caution: erect fauna requires a more appropriate scale.	Specimens can be measured (minimum size depends on largest mesh size and catch efficiency). Note: not common practice.

[a] (Walsh et al., 2009)

Table 2.8 *(Continued)*

Ecological Attribute	Tool		
	ROV	**Drop Camera**	**Trawl**
Bias / quality control			
5. Catchability and sampling bias	Mobile animals may be attracted/repelled by continuous presence and lighting of tool; repeat counts possible if individuals reenter the transect at multiple points (i.e. follow the camera).	Disturbance of sediment could cause aversion/retraction maybe preempting capture; repeat counts possible if individuals reenter the transect at multiple points (i.e. follow the camera).	Low efficiency for sea pens [b] (possible retraction may preempt capture), and varying catchability for various fish species [c]. Catchability/spread of the trawl may be affected by obstruction, improper rigging, net damage, depth, amount of warp, stability of the vessel, currents, and bottom type [a].
6. Image quality	Image quality depends on camera resolution, file compression/type chosen, speed of movement, altitude off the seafloor, sufficient lighting, and degraded quality of imagery during extraction of frame grabs.	Tool can disturb sediments which may obscure imagery. Image quality also depends on camera resolution, file compression/type chosen, speed of camera, altitude off the seafloor, sufficient lighting. Note: Video not useable.	N/A
7. Speed over ground for spatial extent/ resolution	≈ 0.75 km h^{-1} with continuous video, target of 0.25 - 0.5 knots.	≈ 0.8 km h^{-1}, depending on current drift; images capture rate depends on flash recharge (i.e. ~10 sec).	≈ 5.6 km h^{-1}; given 0.75 nautical mile for 15 min standard protocol[1].

[a] (Walsh et al., 2009)
[b] (Chimienti et al., 2018b; Kenchington et al., 2011)
[c] (McCallum & Walsh, 1996; Vázquez, 2010; Walsh, 1992; Warren, 1997)

Table 2.8 *(Continued)*

Ecological Attribute	Tool		
	ROV	**Drop Camera**	**Trawl**
8. Real-time quality control	Very flexible (i.e. live video, pause, restart, alter pan/tilt/zoom and lighting)	Limited (i.e. live video, stop, alter capture rate/imagery specifications and lighting).	Not recommended [a]: quality control adjustments during trawl could affect area swept; mostly done before or after tow (i.e. redo tow).
9. Position accuracy	Advanced position accuracy (i.e. using 3 different systems USBL, gyrocompass, DVL) [d]. Real-time positioning adjustments possible (i.e. 0.2% of position depth, ~ ±1m when depth is 500 m).	Good position accuracy (i.e.10s of meters, using USBL but post-processing calculations rely on ship GPS). Passively drifting system, real-time positioning adjustments not possible.	Limited positioning (i.e. system is ship based with accuracy of 10s of meters). May use calculations to estimate trawl position relative to ship or assume same position. Protocol does not allow for real-time adjustments.
Other			
10. Disturbance of the seafloor	Minimal disturbance, slight resuspension of sediment localized to width of ROV (i.e. ~2-m2).	Some disturbance of sediment during bottom contact; hopping of camera on seafloor.	High disturbance of the seafloor; sustained bottom contact.

[a] (Walsh et al., 2009)
[d] (Canadian Scientific Submersible Facility,1995-2020)

Table 2.8 *(Continued)*

Ecological Attribute	Tool		
	ROV	**Drop Camera**	**Trawl**
11. Auxiliary data, sampling, and metadata	Very flexible [i.e. CTD; georeferenced water samples, sediment cores, specimens/plankton. Navigation data (time, date, latitude, longitude, depth, & ROV rotations and altitude)].	Limited to post-processed metadata (i.e. date, time, latitude, longitude, depth, temperature, altimeter, and camera rotations).	Limited [i.e. CTD, SCANMAR/SEATRAWL data on trawl geometry and performance, log sheets (vessel, vessel position, set number, depth, as well as the start/end/speed of tow), and sometimes Roxann is used to collect data on substrate. Specimens usually greater than mesh size.].
12. Processing time (excludes quality control)	High; depending on image resolution, complexity, and observer experience (i.e. ~6.5 min per image).	High; depending on image resolution, complexity, and observer experience (i.e. ~7.5 min per image).	Low to medium (i.e. minutes to hours depending on catch). Processing includes removing specimens from net, on board sorting, identification, weighing. Note: further processing onshore, not included.

2.5 Discussion

We examined differences in the estimation of abundance and diversity, sampling performance and biases among the ROV, drop camera, and trawl when applicable. Image quality was impacted by several factors including resolution (based on camera and file type), speed and mode of movement, elevation above seafloor, sufficiently uniform lighting, and obstruction by plumes of resuspended sediment and animals in the water column. Extracted frame grabs from video of a moving camera (ROV) had reduced quality compared to stills (drop camera), likely related to motion blur (i.e. caused by a moving camera or target) and compression of the video file. It was usually possible to replace unsuitable images with neighboring ones, except for the ROPOS transects at LC5, where significant fish activity created sediment plumes that obstructed many images resulting in a slight sampling bias of fewer images (Table 2.1). This fish behaviour may have been a response to the motion, sound, or constant bright lighting of the ROV in an otherwise low light environment. However, the drop camera produced a yet higher proportion of unsuitable images, as the tool itself caused some sediment disturbance.

Taxon-specific abundance (particularly for *Pennatula* and Actiniaria) was higher and accumulation curves steeper when using the drop camera than the ROV, but only at one station. However, the curves did not reach an asymptote with either tool, suggesting more than 90 images were required to fully capture diversity. These taxon-specific differences suggest the tools had different catchabilities for different morphospecies, possibly because poor image quality compromised the ability to distinguish smaller sized individuals (e.g. *Pennatula* sp. 2 recruits) or taxa with similar colouration to the sediment

(Table 2.8). Another study comparing imagery from towed cameras and an AUV, similarly concluded that higher resolution imagery both leads to detection of higher faunal densities and accounts for smaller fauna (Schoening et al., 2020). Minimizing altitude for higher resolution imagery should also result in higher taxonomic resolution (Schoening et al., 2020). A towed camera produced imagery of lower resolution when sampling from an altitude of ~3 m than ~1 m, resulting in reduced taxonomic identification (Jones et al., 2009).

Sampling adjustments that enhance image quality are needed to optimize data analysis, such as constraining the altitude off the seafloor and speed of the camera movement. In addition, certain video imagery file types during data collection may improve resolution and allow reliable detection of recruits and smaller taxa. In general, differences in catchability between tools may make some tools better suited than others for capturing morphospecies with different magnitudes/patterns of abundance (i.e. very abundant versus rare morphospecies), affecting tool performance. Catchability and sampling biases of all sampling tools need to be compared quantitatively for different species and ecosystems by sampling the same locations and ecological attributes, preferably at the same time. To our knowledge, ours is the first study that compares empirically catchability from a drop camera to that of a ROV and a trawl (with ~16.5 m wing spread) in the peer-reviewed literature.

Trawls are used to assess fish stocks (Trenkel et al., 2004; McIntyre et al., 2015), and sometimes invertebrates, such as octopus, decapods, sea pens, sponges, holothurians, and some gorgonians (*Junceella* sp and alcyonaria) (Adams et al., 1995; Ayma et al., 2016; Chimienti et al., 2018b, 2019; Dinn et al., 2020; Pacunski et al., 2016; Pitcher et

al., 2007; Wassenberg et al., 2002; Zhulay et al., 2019). Otter trawls have a flexible mouth that is better suited for capturing mobile fauna but is less effective for epibenthic fauna (Jamieson et al., 2013). In this study, we showed different patterns in relative abundance for sea pens (Order Pennatulacea) sampled by ROV from those based on biomass data from the trawls. Trawls may have lower capture efficiency for some invertebrates than the drop camera and ROV. Kenchington et al., (2011) suggested ~5.2% sea pen catch efficiency for the Campelen Trawl compared to Campod. Similarly, sea pen density of *Pennatula rubra* was higher based on ROV data than trawl data (Chimienti et al., 2018b).

Trawls are likely more appropriate for assessing some mobile fauna, yet in this study drop camera and ROV appeared to capture sessile fauna and recruits more effectively. Past studies have also found that trawls tend to undersample abundance and diversity compared to imagery returning higher abundance estimates for many but not all species (e.g. Morris et al., 2014; Nybakken et al., 1998; Uzmann et al., 1977). The higher abundance recorded from trawls for some species, such as squid, herring, mackerel, and butterfish, were likely the result of a photonegative response to the lighting on the submersible or camera sled (Uzmann et al., 1977). Logan et al., (2017) recorded overall higher fish abundances and diversity with a baited camera than a towed camera, yet this varied with habitat and functional group, where towed camera recorded higher abundances of species with cryptic or territorial behaviour.

Comparisons of data obtained by imagery tools and trawls are challenging, as the tools appear to have different catchability limitations and capture different epifaunal patterns. In our study, the high catch weights combined with low numerical abundance

captured by the trawl may have been the result of larger sea pen species at one of the stations (LC5), smaller individuals being missed because of net size. Trawls have reduced catchability for small species such as *Kophobelemnon* spp. (Kenchington et al., 2011). Kenchington et al., (2011) also reported varying mean weights for the sea pen species in the Laurentian Channel and our imagery suggested the composition of sea pens may vary by station. Additionally, some sea pens have a withdrawal response (Ambroso et al., 2013; Chimienti et al., 2018b; Langton et al., 1990), which may result in an underestimate of abundance and biomass.

2.5.1 Qualitative Comparison of Tools

Overall, imagery tools appeared to perform better than trawls for most ecological attributes with fewer sampling biases and causing less disturbance, within a smaller footprint (Table 2.8). All 3 tools can be used to identify morphospecies, commonly used for image analyses, which can be verified subsequently with physical samples collected by a ROV or trawl but not a drop camera. However, taxonomic identification using imagery is constrained and efforts on global standardization are underway (Howell et al., 2019). Sizing taxa can allow for examination of population dynamics, such as recruitment events (Bak and Meesters 1998; Chimienti et al., 2018b), although this is not currently common practice for most of the trawl samples in our region. Imagery may be used to estimate size only of non-erect taxa lying on the same plane as the lasers, but in our study, the scaling lasers in both drop camera and ROV imagery were deemed unsuitable to size sea pens.

Tool-specific operational effects likely impacted overall catchability. Lighting, noise, and physical disturbance of sediment may have led to the attraction or aversion of some morphospecies. Fish behavioral reactions to ROVs and trawls have been recorded in previous studies (Adams et al., 1995; Ayma et al., 2016; McIntyre et al., 2015; Trenkel et al., 2004). Other factors including obstruction, improper rigging, net damage, depth, amount of warp, stability of the vessel, currents, and bottom type are known to affect trawl sampling (Walsh et al., 2009). The ROV had the highest real time quality control, which was otherwise limited for the drop camera and trawl systems either due to the passive tow sampling nature or operation protocols (Table 2.8). Positioning accuracy was highest for the ROV at ~ ± 1 m, and estimated as ~ ± 10 of meters for the drop camera and trawl, although the trawl position accuracy has additional limitations as positional equipment is mounted on the vessel rather than on the trawl. Furthermore, wire-out for trawls is often 3 times the depth to the seafloor and the trawl can be 1000s of m below or behind the vessel (Jamieson et al., 2013).

The ROV sampled at a rate of approximately 0.75 km h^{-1}, a slightly smaller distance than the drop camera (0.8 km h^{-1}); the trawl had the most efficient sampling time at ~5.6 km h^{-1} (Table 2.8). Processing time was estimated to be higher for imagery, at ~6.5 min per image for ROPOS and ~7.5 min per image for the drop camera likely due to the higher imagery resolution. Trawl processing time on ship is highly variable, ranging from minutes to hours depending on catch size.

Ultimately, the data collected using different tools may be used in different types of analyses. For example, the more flexible datasets with detailed metadata, such as geo-referenced faunal records collected continuously along video transects, allow for analyses

of spatial structure and species associations (Table 2.8). Further, there are trade-offs between data resolution (complete transect with ROV and snapshots with drop camera) and image quality, as well as sampling/processing time and data quality, which could affect analyses. Overall, real time control of sampling, less disturbance, and higher position accuracy than trawls are desirable features of ROVs.

2.5.2 Future Research and Recommendations

More baseline data are needed to understand the structure and function of deep-sea communities and develop strategies for monitoring and conservation (Aguzzi et al., 2019; Danovaro et al., 2017). However, for this data to be meaningful, appropriate and quantitative tools should be used. It is evident that different tools have different efficiencies in capturing different species, often rendering results incomparable.

Further research is needed into the utility of available sampling tools for different types of analyses. ROVs collect data that may be used to define taxa-specific habitat relationships at more spatially discrete scales, as well as community structure and biogeographic affinities (Zhulay et al., 2019). Key research foci should include size relationships, other biometric relationships, the integration of datasets between tools, ground truthing, and catchability studies. The development of biometric relationships (e.g. inferring biomass from imagery) from trawl catches can help with integration of data from the different tools, allowing the use of historical datasets from trawls as we move toward less destructive monitoring (Chimienti et al., 2019). Research that directly and empirically compares tools should be prioritized, as more than one tool is required to ground truth data and understand catchability. For example, Pacunski et al., (2016)

suggested using both ROV and trawl to assess fish stocks and developing statistical methods to combine data from the two tools. In addition, low detectability of animals due to either their visibility (i.e. cryptic) or observer perception is often ignored in most studies (Katsanevakis et al., 2012). Research into methods for sizing erect taxa is also needed, potentially through 3D photo mosaicking (Bennecke et al., 2016; Gerdes et al, 2019; Kwasnitschka et al., 2013). Lastly, imagery appears to have greater catchability for sessile fauna compared to trawl, yet is a more time-intensive to process. Thus, research into automation of image processing, will also be a great benefit to future deep-sea research (e.g. Lacharité et al., 2015).

2.6 Conclusions

Overall, imagery tools appeared to better capture epibenthic fauna than a trawl and provided more informative datasets that can allow for various follow-up analyses, such as on spatial structure and species associations. We found evidence that drop cameras may be better than ROVs at capturing both abundance (Actiniaria (O.) sp. 23[4] and *Pennatula* sp. 2) and diversity (morphospecies accumulation curves at LC5) of some taxonomic groups, possibly due to its higher imagery resolution and catchability for some species. However, more research is needed to understand the catchability of all these tools, and allow for better interpretation and integration of datasets, to ensure effective sampling in deep-sea environments. Catchability studies are essential to address whether we are effectively and quantitively capturing our target species or ecological attributes, to ensure high data quality and accurate representativity.

[4] Actiniaria (O.) sp. 23 renamed to *Edwardsia* sp. 1 in Chapter 3 and 4 (see appendix Table AII.1).

CHAPTER 3

REGIONAL DIVERSITY AND SPATIAL PATTERNS OF EPIBENTHIC COMMUNITIES IN THE LAURENTIAN CHANNEL MARINE PROTECTED AREA[5]

3.1 Abstract

Megafauna, such as cold-water corals and other invertebrates, can promote diversity through various processes, such as predation, bioturbation, competition, and facilitation as habitat engineers. Further investigation into their ecology and role in epifaunal community structure in the deep sea is needed. Diversity, abundance, and spatial patterns of epibenthic megafauna (≥ 2cm) were quantified in the Laurentian Channel Marine Protected Area, Canada, at regional-scales (100s m – 100s km) using high-resolution imagery from 15 stations. A patchy community structure was significantly associated with station and benthoscape class, which was based on geological factors. Three types of assemblages included: (1) dominated by corals *Pennatula* sp. 2 and/or Hexacorallia (SC.) spp. in shallow eastern benthoscape classes with high abundance and low diversity; (2) a diverse mix of taxa (e.g. sea pens *Anthoptilum* spp. and *Kophobelemnon* spp., sea anemones/cerianthids, etc.) in deeper (> 400 m) western benthoscapes, low abundance and high diversity; and (3) a unique community dominated by sponges. Overall, eight taxa contributed to most dissimilarities between stations, and communities were similar

[5] Manuscript, *under review.*

Anna Metaxas supervised the development of the study design, analyses, and co-authored the manuscript.

within 10 km but could differ at greater distances. Benthoscape classes captured environmental factors (e.g. depth and substrate) that may be responsible for changes in diversity and abundance, as a proxy for different habitats. Additional studies at multiple spatial and temporal resolutions are needed to assess the drivers of spatial patterns. This study advanced our understanding of regional spatial patterns in the abundance, composition, and diversity of epibenthic communities, adding to interpretations of spatial ecology in a previous fine-scale study. Additionally, implications from our study can help inform future monitoring designs to promote representative and meaningful spatial assessments.

Keywords: megafauna, monitoring, distribution, assemblage, ecology, mapping

3.2 Introduction

Taxonomic diversity is the outcome of a combination of long-term evolutionary (e.g. speciation and geographic dispersal) and short-term ecological processes (e.g. competition and predation) (Levin et al., 2001). In the deep sea, megafauna (invertebrates and fish > 1-2 cm) can promote diversity through multiple processes (predation, bioturbation, competition, and facilitation as habitat engineers) although the relative importance of each process is not well understood (Mcclain & Schlacher, 2015). Several hypotheses have been proposed to explain patterns of diversity in the deep sea, including some that integrate different processes on ecological time scales, such as physical or biological disturbance and niche partitioning through competition or spatial heterogeneity (e.g. Mcclain & Schlacher, 2015; Rex, 1981). The dynamic equilibrium hypothesis integrates productivity, competition, predation, and physical disturbance to explain

patterns in diversity (Huston, 1979; Rex, 1981). As depth increases, competitive displacement rates are hypothesized to decrease, with lower diversity on the continental shelf and upper continental slope than the lower slope, as a result of high rates of displacement. In the last few decades, although our knowledge of deep-sea ecosystems and biodiversity has increased substantially, through network initiatives such as iAtlantic (Boteler et al., 2023) and the Census of Marine Life (Snelgrove, 2010) significant gaps still exist, including for cold-water coral communities.

Sea pens are primarily sessile cold-water corals that anchor into soft sediments using a peduncle, although several species have been observed retracting into the sediment. Several species have been estimated to be long lived (2-48 years) with generally slow growth of 1.0 ± 0.09 to 4.9 ± 0.06 cm/year (Greeley, 2022; Murillo et al., 2018; Neves et al., 2015, 2018; Wilson et al., 2002). Sea pens can play an important functional role in soft-sediment environments, possibly providing biogenic vertical habitat structure which alters currents, retains nutrients, and provides nurseries and protection for fish (e.g. Baillon et al., 2012; Tissot et al., 2006). In the Northwest Atlantic, sea pen species have been associated with fish (Baillon et al., 2012; Boulard et al., 2023) and macrofauna (Miatta & Snelgrove, 2022).

Several environmental factors have been identified as important drivers in observed distributions and as predictors in regional species distribution models for deep-water corals. These factors include depth, substrate, temperature, salinity, and surface chlorophyll *a* as important predictors of abundance (e.g. Baker et al., 2012; Greathead et al., 2015; Gullage et al., 2017; Kenchington et al., 2016a; Lacharité & Metaxas, 2017; Murillo et al., 2016). Other geological variables such as pockmarks, pits in the sediment

created by gas or fluid (Fader, 1991), could also play a role in abundance and diversity but have not been thoroughly tested (de Mendonça & Metaxas, 2024; Somoza et al., 2021; Sumida et al., 2004; Webb et al., 2009).

In the deep sea, data on environmental drivers that explain the distribution and diversity of epibenthic megafauna often do not exist in appropriate resolution and proxies are used instead. Benthoscapes are such a proxy, used to identify patches of seabed, based on biophysical sea floor classification of biotic (e.g. biogenic structures) and abiotic (e.g. sediment and geomorphic features) components (e.g. Zajac, 2008). For example, unique epifaunal communities were found in different benthoscape classes in Newfoundland and Labrador, Canada (Proudfoot et al., 2020), fish assemblages on a seamount on the southwest Indian ridge (Swanborn et al., 2023), as well as megafauna in Norway (Mortensen et al., 2009) and the Mauritian continental slope (Jones & Brewer, 2012). The selection of the components is subject to environmental context, relevance of indicators, and data availability.

The Laurentian Channel is a cross-shelf trough, located in Atlantic Canada (southwest of Newfoundland) between the St. Lawerence river and the edge of the continental shelf (Todd, 2016). In 2019, the eastern portion of the channel (11 619 km^2) was designated as the Laurentian Channel Marine Protected Area (LC MPA) with one of the conservation priorities being to protect sea pens from human activities (DFO, 2019b). In the channel, suitable habitats for sea pens have been projected based on regional distribution models using primarily depth, temperature, salinity, slope, chlorophyll *a* and trawl bycatch data as predictors that vary in importance by species (Guijarro et al., 2016; Gullage et al., 2017). Suitable habitat was also projected for cup corals and soft corals

using similar predictors (Gullage et al., 2017). Various other invertebrates have also been observed within the channel in past imagery surveys, for example asteroids and sea anemones (e.g. Lacharité et al., 2020). Fisheries and Ocean Canada are doing extensive work towards characterizing the LC MPA and developing a monitoring plan. However, the spatial patterns of megafauna and ecology in the region are missing, particularly for sea pens.

Estimating the abundance of sea pens is challenging because of their small size, possible retraction behaviour (Kenchington et al., 2011) and flexibility or fragility (Auster et al., 2011). For the Newfoundland region, research trawls have recorded the highest biomass of several sea pen species in the Laurentian Channel, although trawls have low catch efficiency for sea pens (Chimienti et al., 2018b; Kenchington et al., 2011). Sea pen biomass was predicted to be up to 24.27 kg in a small portion of the channel but lower elsewhere (Guijarro et al., 2016). High-resolution imagery can provide more accurate measures, as it has a higher capture efficiency than trawls (e.g. sea pens; Chimienti et al., 2018b), and can provide insights into distribution and ecology that are not possible with trawl catch weights at a coarse resolution. However, small size and avoidance behaviours can also lead to sampling bias with imagery. Thus, optimal sampling methods vary based on the species of interest, their morphology, and behaviours. Imagery appears to capture abundance and diversity of benthic invertebrates (e.g. sea pens) better than trawls (Chimienti et al., 2018b; de Mendonça & Metaxas, 2021), and allow for analyses of spatial patterns through *in situ* observations.

In this study, we investigate the spatial patterns of epibenthic megafaunal assemblages, particularly sea pens, in the Laurentian Channel MPA. Using high

resolution imagery we: 1) quantify regional spatial patterns (100s m - 100s of kms) in community composition, abundance, and diversity; 2) discuss potential drivers of the patterns in diversity and abundance; 3) investigate and interpret how assemblages are related to benthoscape classes; and 4) briefly highlight sampling resolution bias. Our study complements previous studies on fine-scale patterns of megafauna (de Mendonça & Metaxas, 2021, 2024), fish and infauna in the LC MPA (Boulard et al., 2023; Miatta & Snelgrove, 2021, 2022). Estimating broad scale spatial variation can be useful for the management of large MPAs. Additional research at multiple scales will also help establish a times series and better understand the ecological drivers and response in epibenthic megafaunal communities.

3.3 Methods

3.3.1 Study Area

The Laurentian Channel Marine Protected Area (LC MPA) is 11,619 km^2 in area, located in a deep glacial trough to the southwest of Newfoundland, Canada (DFO, 2019b). The broader channel is approximately 700 km long and 80-90 km wide and has a maximum depth of 522 m in the Cabot Strait (Todd, 2016). Within the MPA, depth ranges from 51 to 497 m with predominantly fine to mixed sediments (mud, sand, and gravel) (Lacharité et al., 2020). The area has underlying geomorphic features, including iceberg scours, pockmarks/pits, and varying slope, which have been used to classify the region into different benthoscapes (Figure 3.1; from Lacharité et al., 2020).

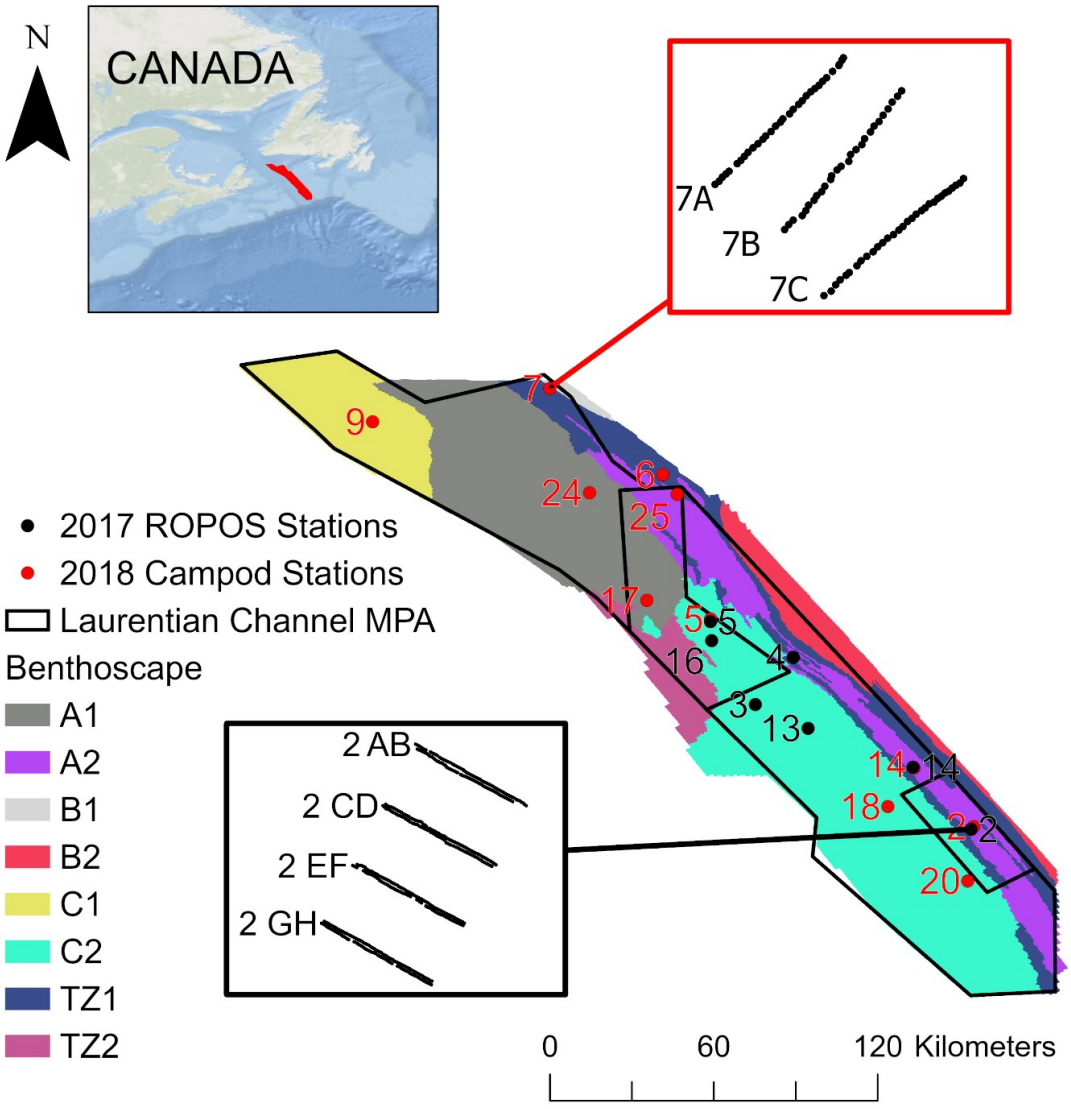

Figure 3.1 Fifteen sampled stations, all, except station 6, located within the boundaries of the Laurentian Channel MPA. Top left inset shows the study region located southwest of Newfoundland, Canada. Black dots and black inset represent the array of 8 transects used to sample with ROPOS in 2017; paired 400-m transects (e.g. 2 AB, 2 CD, 2 EF, and 2 GH) were spaced 10 m apart and 200 m from the next pair. Red dots and red inset box represent the modified transect array used to sample with Campod in 2018; 1-3 transects (e.g. 7A, 7B, and 7C) were spaced 200 m apart. The underlying benthoscape classification[6] layer was based on geological variables including pockmarks, ice scours, slope, depth, and sediment; provided and explained by Lacharité et al. (2020).

[6] For details on the benthoscape classes see Table AI.1. Reprint of Table 41.1 in Lacharité et. al. (2020).

3.3.2 Data Collection

We collected video at 7 stations (2, 3, 4, 5, 13, 14, and 16; Figure 3.1) with a downward-facing Insite Pacific Zeus-Plus HD camera (1,920 × 1,080 pixels) using the remotely operated vehicle ROPOS (www.ropos.com) on 9 -17 September 2017. The array of sampling transects at each station included 8 400-m parallel transects spaced at alternating distances of 10 m and 200 m (i.e., four pairs of transects: AB, CD, EF, GH) (Figure 3.1) for a total of 56 transects; navigation metadata was collected simultaneously (i.e., depth, altitude above seafloor, latitude, longitude).

In 2018, we used the drop camera Campod, a towed system with passive drifting, operated by the Department of Fisheries and Oceans (DFO) [Canada, Bedford Institute of Oceanography] to collect high-resolution still images (JPEG) at 11 stations (2, 5, 6, 7, 9, 14, 17, 18, 20, 24, and 25; Figure 3.1), with station 6 being just outside the boundary of the LC MPA on 8 - 11 July. Images were captured at 10-s intervals, timed to manual hops of the camera along the seafloor, using a downward facing NIKON D810 camera (7,360 × 4,912 pixels). Due to limitations on time and maneuverability, we performed a modified sampling array with 1 to 3 transects at each station, 1-km long and spaced 200 m apart (Figure 3.1) for a total of 26 transects. Navigation metadata (date, time, latitude, longitude, depth, and altitude) were provided for each image after post-processing of the Navnet, CTD, altimeter and USBL systems by the Campod technical crew. Campod had lower position accuracy of 10s of meters, compared to ~± 1 m for ROPOS. Additional specifications for both imagery tools and sampling arrays have been previously published (de Mendonça & Metaxas, 2021).

3.3.3 Image Analysis

Overall, we aimed to avoid spatial overlap between all images included in a combined ROPOS and Campod dataset. For ROPOS, navigation metadata (using the first record per second) and video were synchronized with the Ocean Floor Observation Protocol software (OFOP 3.3.8c , Huetten & Greinert, 2008; Scientific Abyss Mapping Services, 2009). Non-overlapping images were then extracted at 1.5-m target intervals. In general, every 4th image (target interval ~ 6 m) was selected for analysis, if near enough to the seabed (i.e., image area < 6 m^2; scaling lasers spaced 10 cm apart) and image clarity permitted taxonomic identification. However, images were deemed unsuitable if they required > 50% cropping to remove areas that obstructed the view of the seafloor (i.e., suspended particles, pelagic animals near the camera, sediment plumes, or sections of low light), and the next sequentially suitable image ~ 1.5 – 6 m was analyzed instead. This selection protocol resulted in an average of ~ 7 m spacing between analyzed images for ROPOS (grand mean ± SE: 6.94 ± 0.14 m, n=56; range: 6.25 - 10.24 m). For Campod, every 4th image was a target interval of ~ 40 s and resulted in an average of ~ 14 m between analyzed images (grand mean ± SE: 14.25 ± 0.33 m, n=26; range: 11.16 - 18.76 m). Although the sample size was lower for Campod than ROPOS (Table 3.1 & AI.2), the data were standardized per square meter for each 400-m transect to make our analyses comparable. Example imagery were provided in de Mendonça & Metaxas (2021).

Megafauna > 2 cm in the largest dimension were enumerated and identified to morphotaxa, the lowest taxonomic level based on morphology/characteristics visible in imagery, using the World Register of Marine Species (WoRMS). We calculated

taxonomic numerical abundance used in all analyses, including singletons and those morphotaxa with few counts. In addition, we recorded taxa that were too numerous to count or colonial as percent cover (i.e., Elpidiidae (F.) spp., Serpulidae (F.) sp. 1, Porifera (P.) sp. 9, and Porifera (P.) sp. 23), but these were only included in the species accumulation curves that utilized presence/absence data (see Data Analyses). Highly mobile and pelagic invertebrates (e.g., malacostracans, Cephalopoda, Scyphozoa) were excluded from our study because our sampling methods were not appropriate for enumerating them, except for Elpidiidae (F.) spp. because they formed a layer on the seabed, which were included only in the species accumulation curves. To describe spatial patterns, we aggregated taxa to the 10 most abundant taxonomic groups (operational cutoff of total abundance greater than 0.1 m^{-2} at any station for either ROPOS or Campod), in Laurentian Channel MPA, and included an additional unique group that was very abundant at a specific station (Porifera (P.) sp. 21), with all remaining taxa aggregated into an "Other" group (40 unique taxa). We measured the spacing between image locations based on shortest linear distance (range, mean, and standard deviation/error) using ArcGIS Pro (Esri, 2020b). To assess the effect of sampling on species composition, the ROPOS data were subsampled, selecting images spaced at approximately 7, 14, 21, and 28 m (grand mean ± SE: 6.94 ± 0.14, 13.97 ± 0.3, 20.97 ± 0.45, and 27.85 ± 0.58 m, n=56).

3.3.4 Data Analyses

We estimated alpha and beta diversity throughout the LC MPA using count data for 63 unique taxa (e.g. Figure 3.2); for species accumulation curves, we also included 4 additional taxa for which we estimated percent cover. Species accumulation curves were

weighted by the area analyzed of each image for the 18 station-tool combinations, using the "random" method, 999 permutations, and confidence intervals equal to one standard deviation. We calculated Shannon diversity index by station using total abundance (m^{-2}) of each taxon (Pielou, 1966).

To compare spatial patterns of the assemblages among stations and benthoscapes, we calculated Bray-Curtis dissimilarity based on total abundance of each taxon per transect (m^{-2}; based on the summed counts by 63 taxa, divided by summed area per transect). One benthoscape was identified for each station, except for stations 4 and 7 where a second benthoscape was present; however, the primary benthoscape where most images were located was used for analyses. Non-metric multi-dimensional scaling (NMDS) and permutational multivariate analysis of variance (PERMANOVA; 999 permutations) were performed using transects as sites, and 95% confidence intervals for the stations and benthoscapes (Anderson, 2001; Kruskal, 1964). We examined how the different taxa contributed to the NMDS with the *envfit* function (999 permutations). Similarity among transects, was estimated using hierarchical clustering with the complete linkage method (F. B. Baker & Hubert, 1975) (Figure AI.1). We calculated the contribution of each taxon to the average dissimilarity between stations using the Similarity Percentage method proposed in Clarke (1993), the SIMPER procedure. For very abundant taxa for which a high contribution can be an artifact of high variance, permutation tests can be used to confirm contributions (Oksanen et al., 2022). For our study, for each pairwise comparison between stations, we identified the taxa which contributed significantly (using 999 permutations and for $p < 0.05$ to unconfound abundance) by at least 10% of the cumulative percentage difference between stations.

Table 3.1 Summary of station metadata in the Laurentian Channel MPA, including number, area, depth, altitude relative to seafloor or each image (combines 82 transects: 8 transects per ROPOS station A, B, C, D, E, F, G, and H, 1-3 transects per Campod station). Altitude refers to the height of the altimeter attached to the ROV relative to the seabed.

Station	Number of Images Analyzed	Total sum of area analyzed (m^2)	Mean Depth (m)	Standard Deviation of Depth (m)	Mean altitude above seafloor (m)	Standard deviation of altitude above seafloor (m)	Mean analyzed area per image (m^2)	Standard deviation of analyzed area per image (m^2)
ROPOS								
2	486	1033.18	350.81	2.07	1.04	0.31	2.13	0.49
3	499	739.87	445.99	0.59	0.99	0.20	1.48	0.22
4	511	862.53	335.93	2.10	1.13	0.27	1.69	0.45
5	380	592.66	439.68	0.91	1.09	0.30	1.56	0.44
13	443	574.62	432.36	1.30	1.03	0.22	1.30	0.32
14	495	616.94	343.72	1.63	1.14	0.31	1.25	0.41
16	457	464.67	444.88	1.34	1.10	0.27	1.02	0.28
Campod								
2	97	199.52	341.73	1.85	1.70	0.54	2.06	0.93
5	90*	189.78	439.89	1.15	1.60	0.38	2.11	0.65
6	59	166.76	318.72	0.59	1.62	0.29	2.83	0.92
7	90	271.02	221.18	16.35	1.67	0.34	3.01	1.02
9	55	129.66	421.84	1.75	1.53	0.24	2.36	0.69
14	63	127.39	354.40	1.23	1.76	0.42	2.02	0.76
17	29	61.16	467.47	0.82	1.61	0.32	2.11	0.84
18	93	203.83	405.26	0.96	1.58	0.35	2.19	0.70
20	58	153.78	388.21	1.16	2.33	0.86	2.65	0.77
24	96	203.32	453.47	0.85	1.45	0.28	2.12	0.66
25	60	159.82	332.67	1.20	1.57	0.28	2.66	0.86

Note: * Metadata were missing for some images, mean and standard deviation for depth and altitude calculated for N=77 images.

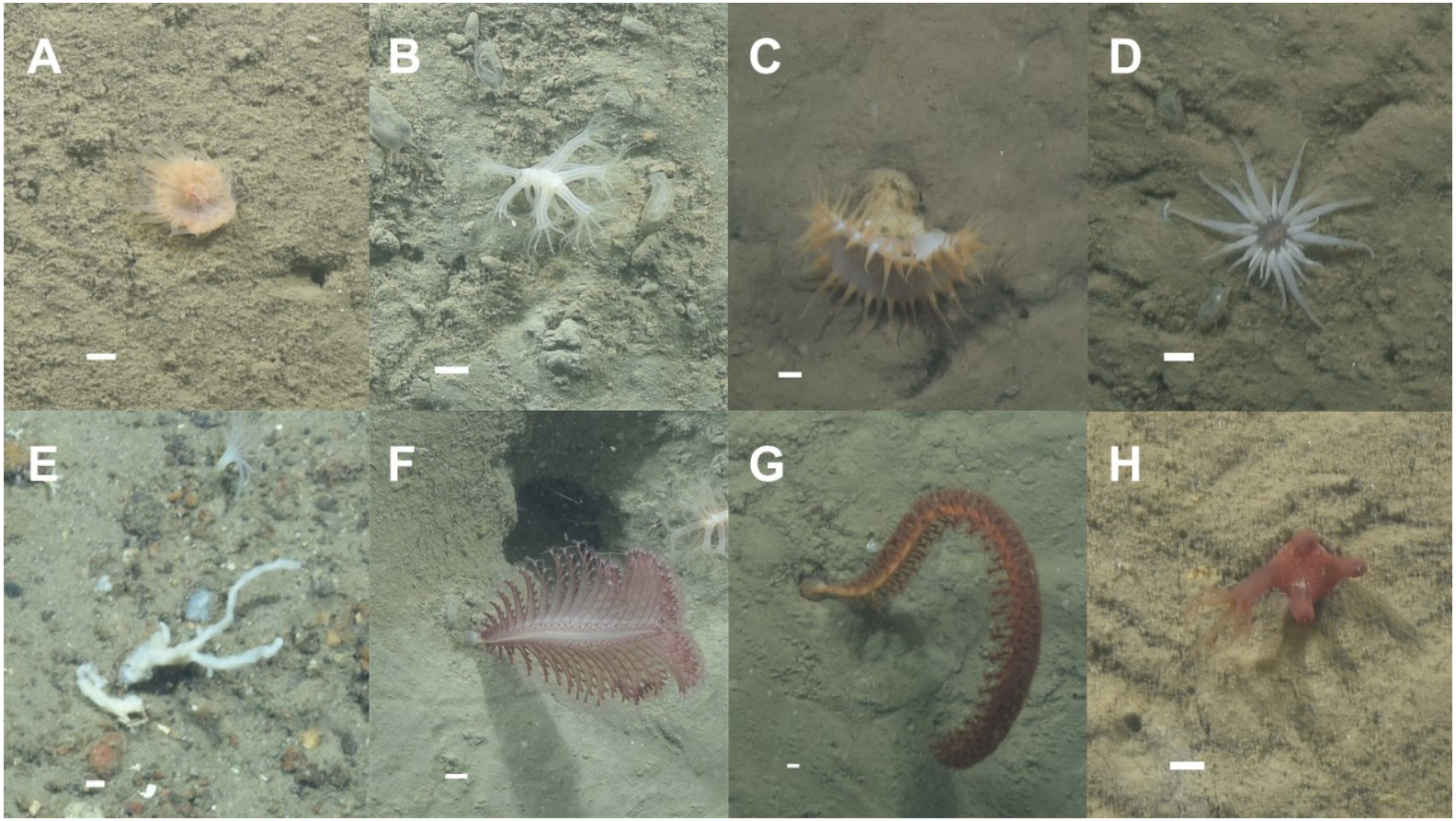

Figure 3.2 Example of taxa in the Laurentian Channel MPA from Campod imagery, including A) Hexacorallia (SC.) spp. (orange to red), B) *Kophobelemnon* spp., (pink or white) C) *Actinauge cristata* (orange or white), D) *Edwardsia* sp. 1 (translucent pink or white), E) Porifera (P.) sp. 21 (amorphous; shape changes sometimes flatter), F) *Pennatula* sp. 2 (white or pink), G) *Anthoptilum* spp., and H) Anthomastinae (SF.) sp. 1. White scale bars are 1 cm, bottom left of each panel. These eight taxa are ordered from high-low contribution to pairwise station comparisons, based on the SIMPER procedure (see Table 3.4). Some of these taxonomic groups contain multiple morphotypes (e.g., colour varies or potentially indistinguishable species).

To examine the spatial pattern of species assemblages, we produced Mantel correlograms, based on an ecological distance matrix with Bray-Curtis dissimilarity calculated using the abundance of each taxon (m^{-2}) by image, and an Euclidean geographic distance matrix with each image location (latitude and longitude). The null hypothesis was that the distance matrices are independent (Dale & Fortin, 2014), if there are no spatial patterns in diversity. Positive Mantel values indicate positive autocorrelation of the distance matrices, where there is a similar diversity index among images at that distance class (Borcard & Legendre, 2012). Negative autocorrelation indicates the diversity index differs between images at that distance class. The spatial range of the pattern is identified at the x-intercept where the values change from positive to negative (Legendre & Fortin, 1989). Alternation of positive and negative values indicates patchiness, with a repeating pattern throughout the study area (Dale & Fortin, 2014; Legendre & Fortin, 1989).

The Mantel correlogram was computed from 999 permutations using the Spearman's *r*, with the cutoff option to limit the distance classes to include all points, and the Holm method for dealing with multiple testing problems. We included 2976 images (combined dataset for ROPOS and Campod but excluding images with zero abundance). We also computed the detrended version of the Mantel correlogram, using the residuals of Brays-Curtis after a linear model. The detrended version removes a linear trend from the species data, potentially caused by broad-scale processes or environmental gradients across the study area, to reveal finer patterns (Legendre & Legendre, 2012). We also computed a correlogram using smaller fixed distance classes of 5000 m, to help identify the spatial range of the pattern.

All statistical analyses were performed with R version 4.1.2; packages *Tidyverse, Reshape, Vegan*, *Dendextend* and *Geosphere*, as well as ArcGIS Pro for spacing of images (R Core Team, 2021; Esri, 2020b). This study is complementary to our previous study on fine-scale spatial patterns in the Laurentian Channel MPA (de Mendonça & Metaxas, 2024).

3.4 Results

The highest overall abundance of visible mega-epibenthic taxa was at Station 2 and was ~ 4 m^{-2} for ROPOS and ~ 7 m^{-2} for Campod (Figure 3.3). The lowest abundances were at station 5 for ROPOS (< 0.5 m^{-2}) and station 9 for Campod (< 1 m^{-2}). In addition, the composition of the community assemblage varied across the LC MPA in 4 different patterns (Figure 3.3), with a large proportion of the total abundance being: for pattern (1), *Pennatula* sp. 2 and/or Hexacorallia (SC.) spp. (at station 2, 4, & 14, with Hexacorallia (SC.) spp. dominant at station 6, 20, & 25); for pattern (2) *Kophobelemnon* spp. (station 3 & 17); for pattern (3) Porifera (P.) sp. 21 (station 7); and for pattern (4) a mix of various taxa (station 5, 9, 13, 16, 18, & 24). The “Other” grouping only had a minor contribution to overall abundance, which was slightly higher at station 7 & 17 than the other stations. Overall, 11 aggregated taxonomic groups, accounting for 23 taxa, contributed to most of the megafaunal abundance in the LC MPA.

We examined spatial patterns in total abundance and taxonomic composition at 4 spatial resolutions (i.e., distances between images): 7, 14, 21, and 28 m, as well as among 8 transects with alternating spacing of 10 m and 200 m (Figure 3.4). At stations where there were a few dominant taxa and high overall abundance, composition remained

mostly consistent across transects and image spacings. This was the case when *Pennatula* sp. 2 and Hexacorallia (SC.) spp. were dominant and overall abundance was often ≥ 2 m^{-2} on each transect (station 2, 4, & 14; e.g., Figure 3.4A). When the number of taxonomic groups present was higher and variation across transects small, the number of transects was important for capturing diversity to avoid missing taxa. This was the case at station 3, 13, and 16, when abundance was 0.5 to 2 m^{-2} per transect (e.g., Figure 3.4B). When overall abundance was low, differences in image spacing led to different estimates of abundance, and some taxa were missed. For example, at station 5, where total abundance was often < 0.5 m^{-2} per transect, composition varied by transect (Figure 3.4C). Therefore, a higher spatial resolution with images closely spaced will likely provide more accurate estimates of abundance and capture taxa with lower abundance.

Species accumulation curves were standardized to image area (m^2), as the area and number of images varied by station (i.e., ROPOS: 380 - 511 images per station with area ranging 0.52 to 4.47 m^2 per image; Campod: 29 - 97 images per station with area ranging 0.75 to 5.40 m^2 per image). The curves using the ROPOS imagery began to approach an asymptote, with station 2 and 3 including a higher number of morphotaxa than the other stations (Figure 3.5). Most curves had a similar slope, except the one for station 3 which had the steepest slope. While no accumulation curves from the stations sampled by Campod approached an asymptote, stations 20 and 24 were nearest to reaching one. Stations 7 and 18 had the steepest slope compared to all other stations (ROPOS and Campod), capturing diversity quickly and including the highest number of species.

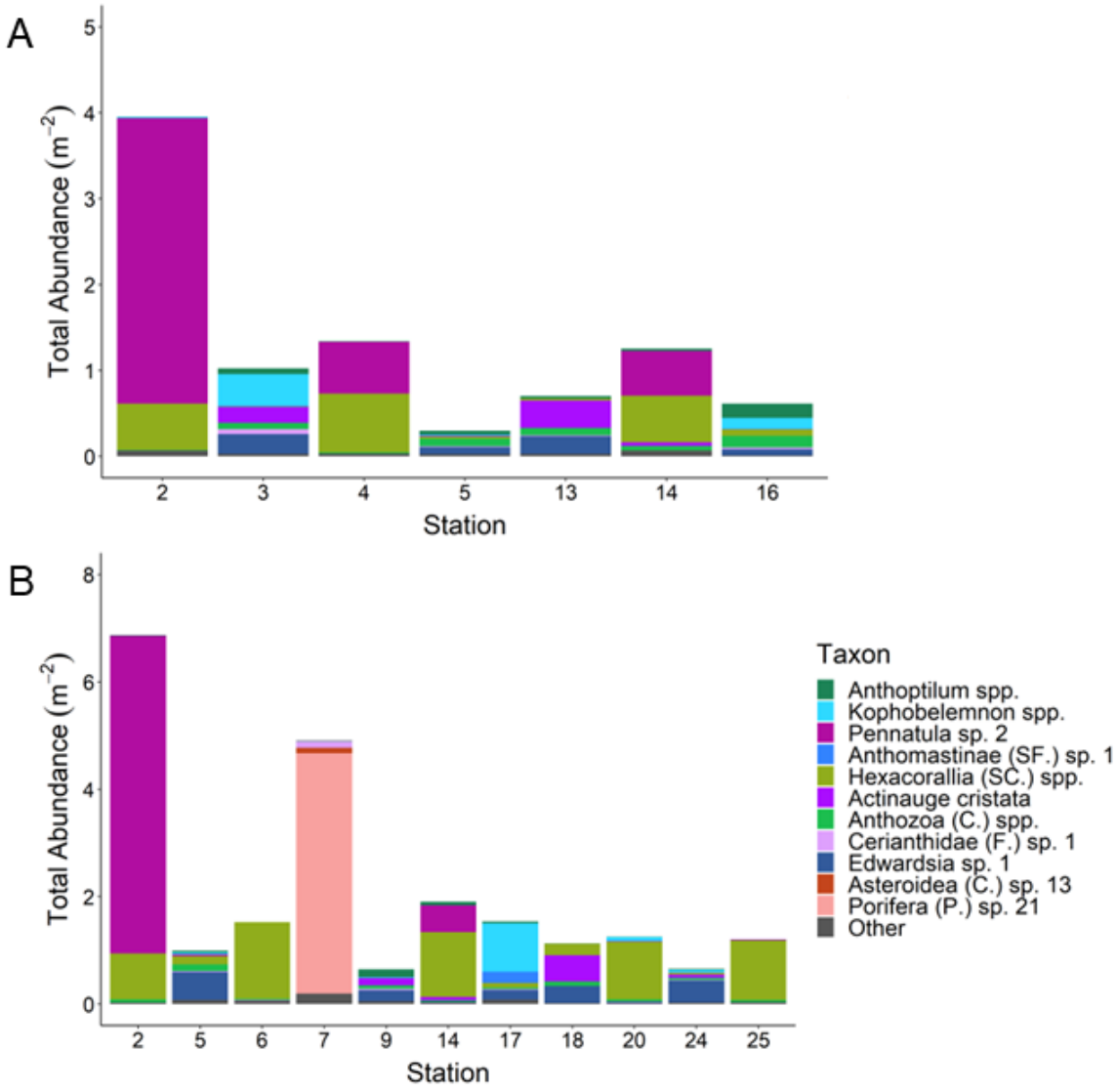

Figure 3.3 Overall abundance and composition of aggregated taxa throughout the 15 Laurentian Channel MPA stations for A) ROPOS and B) Campod. Total abundance calculated for each station as summed taxon counts divided by summed area analyzed.

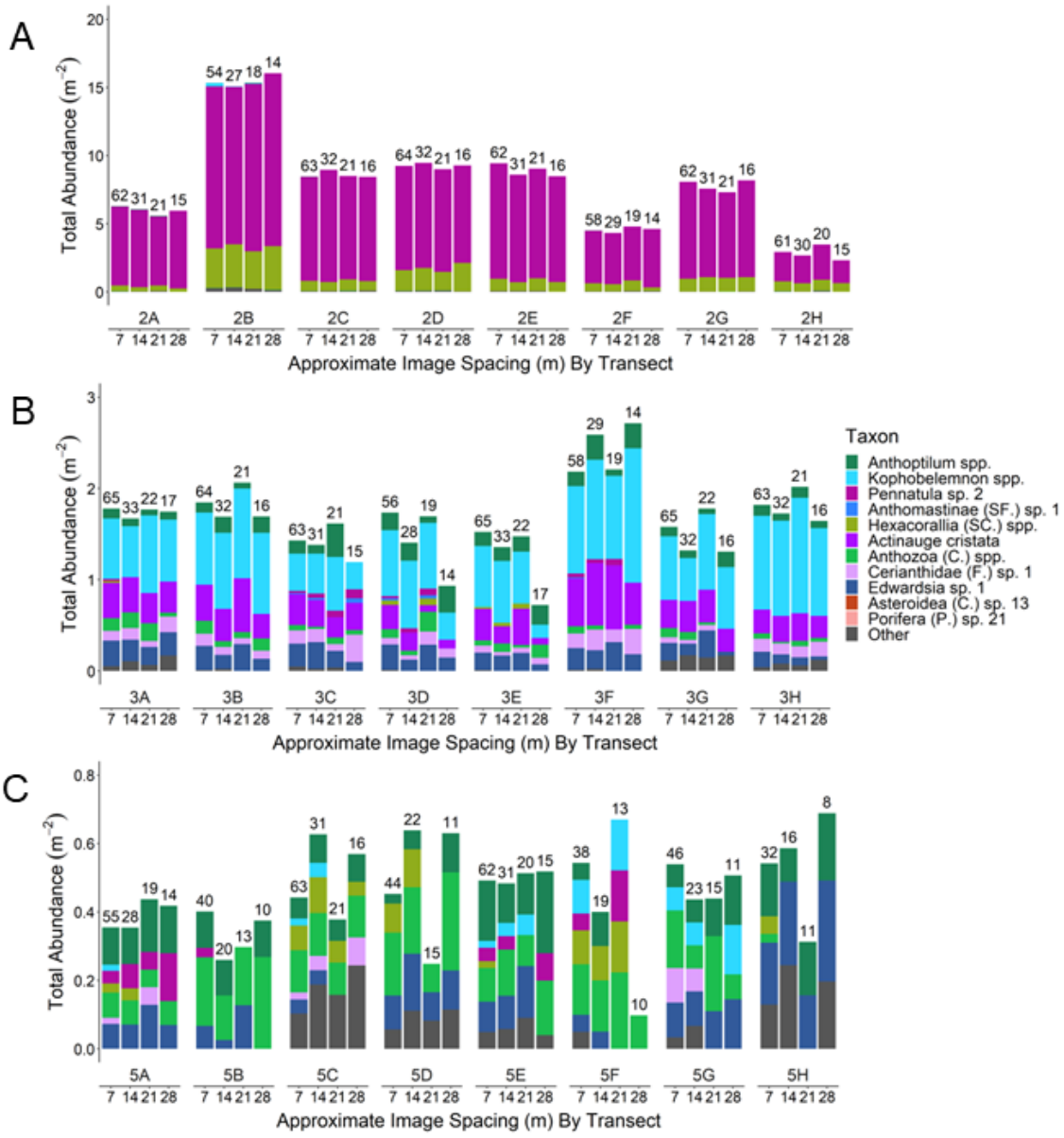

Figure 3.4 Total abundance of different megafaunal taxonomic groups calculated for each transect (A to H) at different spatial resolutions with spacings between images of ~ 7, 14, 21, or 28 m for A) station 2, B) station 3, and C) station 5, using ROPOS imagery. Total abundance calculated for each transect as summed taxon counts divided by summed area analyzed. Number of images are reported above each bar.

Shannon diversity at each station was similar for both ROPOS and Campod (Table 3.2). Station 5 had the highest Shannon diversity, followed by stations 16, 9, and 3. At stations where diversity was high, overall abundance was often low and included relatively high abundance of *Anthoptilum* spp. and/or *Kophobelemnon* spp. (Figure 3.3). The lowest Shannon diversity was found at station 6, followed by station 25 and 7. At stations where diversity was low, overall abundance was high and for a dominant taxon, e.g., Hexacorallia (SC.) spp. at stations 6 and 25, and Porifera (P.) sp. 21 at station 7 (Figure 3.3).

Non-metric multi-dimensional scaling (NMDS) revealed three general groupings in the assemblages of the LC MPA (Figure 3.6). These NMDS groupings were similar to the patterns identified for overall abundance and composition of the numerically dominant taxa (Figure 3.3). Stations 2, 4, 6, 14, 20, and 25 form a related group with the same as pattern (1) (a large proportion of *Pennatula* sp. 2 and/or Hexacorallia (SC.) spp.); and station 7 formed a separate group corresponding to pattern (3) (a large proportion of Porifera (P.) sp. 21). However, patterns (2) (a large proportion of *Kophobelemnon* spp., station 3 & 17) and (4) (a mix of various taxa at stations 5, 9, 13, 16, 18, & 24) fell under a single grouping in the NMDS. Both primary benthoscape and station were highly significant factors affecting the groupings of the assemblages (PERMANOVA; Table 3.3), but primary benthoscape had a close fit to the three ordination groups (Figure 3.6; 95% confidence interval ellipses). Groupings were mostly by benthoscape; benthoscapes A2 and TZ1 (stations 2, 4, 6, 14, and 25; station 20 also included yet an anomaly, as it was in benthoscape C2 but did not group with the others), benthoscape B1 (station 7), and benthoscapes A1, C1, and C2 (stations 3, 5, 9, 13, 16, 17, 18, and 24). Hierarchical

clustering supported these results, but also showed that some transects clustered with different stations at lower branches, albeit still related to their station at upper branches (Figure AI.1). A few taxa drove this pattern, such as Hexacorallia (SC) spp., *Kophobelemnon* spp., *Actinauge cristata, Edwardsia* sp. 1, Porifera (P.) sp. 21, *Pennatula* sp. 2, *Anthoptilum* spp., and Anthomastinae (SF.) sp. 1 (Table 3.4). Overall, 28 of the 63 taxa contributed significantly to the NMDS ($p < 0.05$), with 14 taxa being highly significant ($p = 0.001$).

For the SIMPER analyses, we focused on taxa that significantly contributed 10% or more to the ordered cumulative percentage of differences between pairs of stations. Combinations of eight taxa ranked within the top 4 at pairs, and most were also significant contributors to the NMDS, except for *Kophobelemnon* spp. and Anthomastinae (SF.) sp. 1 (Table 3.4 and Figure 3.2). Most of these key taxa had relatively higher proportions compared to the rest across the LC MPA (Figure 3.3; excluding Anthomastinae (SF.) sp. 1).

Table 3.2 Shannon diversity ranked by station, using total abundance (m^{-2}) as the summed counts of each taxon divided by summed area per station.

Rank	Station	ROPOS Dataset	Campod Dataset	Main Benthoscape	Comments and example taxon
1	5	2.01	1.81	C2	Highest Shannon Diversity; lowest overall abundance; *Anthoptilum* spp., *Edwardsia* sp. 1
2	16	1.94	-	C2	*Anthoptilum* spp., *Kophobelemnon* spp.
3	9	-	1.86	C1	*Anthoptilum* spp., *Actinauge cristata*, *Edwardsia* sp. 1
4	3	1.80	-	C2	*Anthoptilum* spp., *Kophobelemnon* spp., *Actinauge cristata*, *Edwardsia* sp. 1
5	18	-	1.80	C2	*Actinauge cristata*, *Edwardsia* sp. 1
6	13	1.51	-	C2	*Actinauge cristata*, *Edwardsia* sp. 1
7	24	-	1.45	A1	*Edwardsia* sp. 1
8	17	-	1.45	A1	*Kophobelemnon* spp.
9	14	1.35	1.17	A2	*Pennatula* sp. 2, Hexacorallia (SC.) spp.
10	4	0.95	-	A2	*Pennatula* sp. 2, Hexacorallia (SC.) spp.
11	20	-	0.95	C2	Hexacorallia (SC.) spp.
12	2	0.57	0.48	A2	*Pennatula* sp. 2, Hexacorallia (SC.) spp.; highest overall abundance
13	7	-	0.51	B1	Dominated by Porifera sp. 21; shallowest station with coarser sediment
14	25	-	0.50	A2	Hexacorallia (SC.) spp.
15	6	-	0.43	TZ1	Lowest Shannon Diversity; Hexacorallia (SC.) spp.

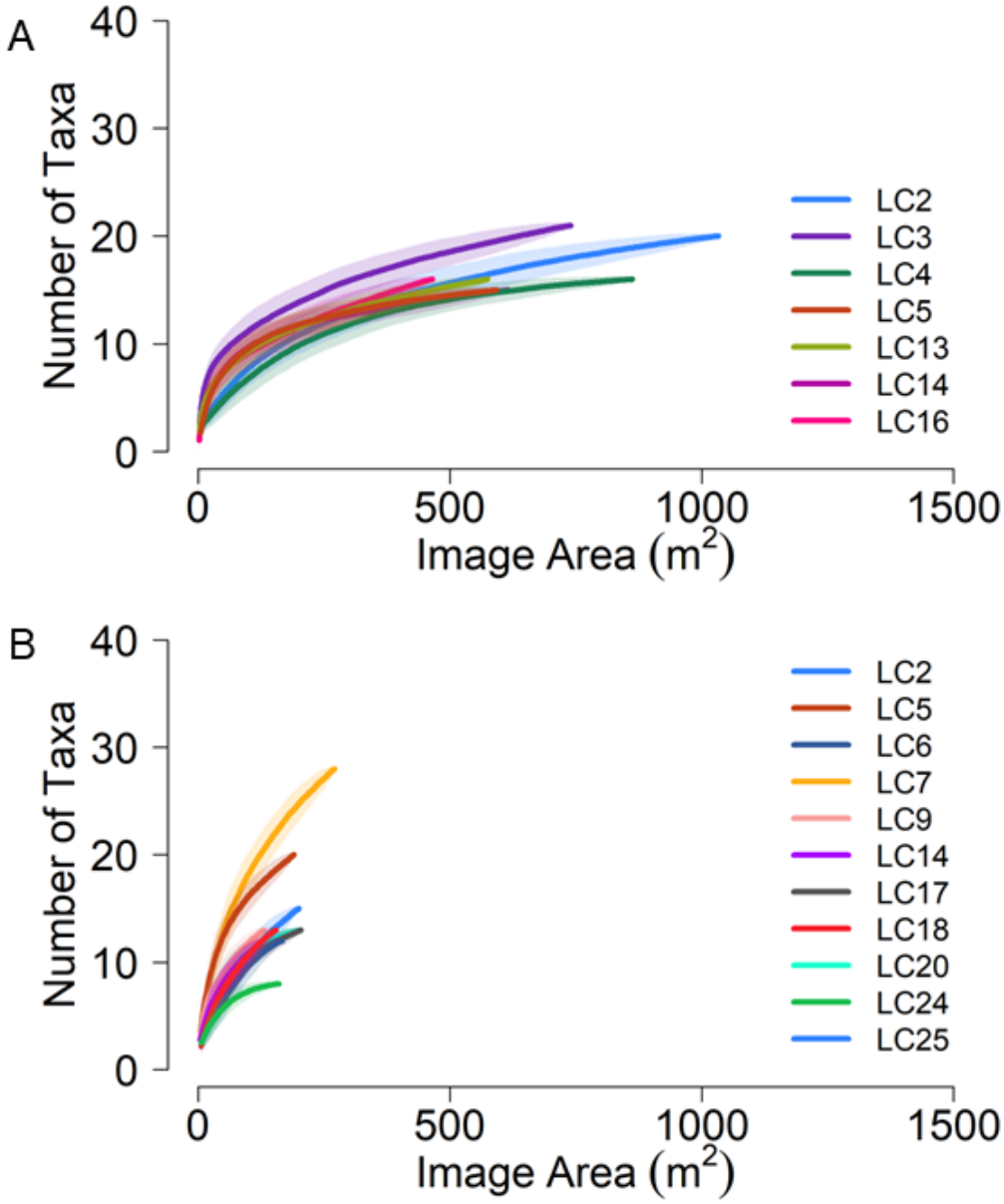

Figure 3.5 Species accumulation curves by image area for each station, A) ROPOS and B) Campod, inclusive of 67 unique taxa across the Laurentian Channel MPA, using the "random" method, 999 permutations, and shaded confidence intervals of one standard deviation.

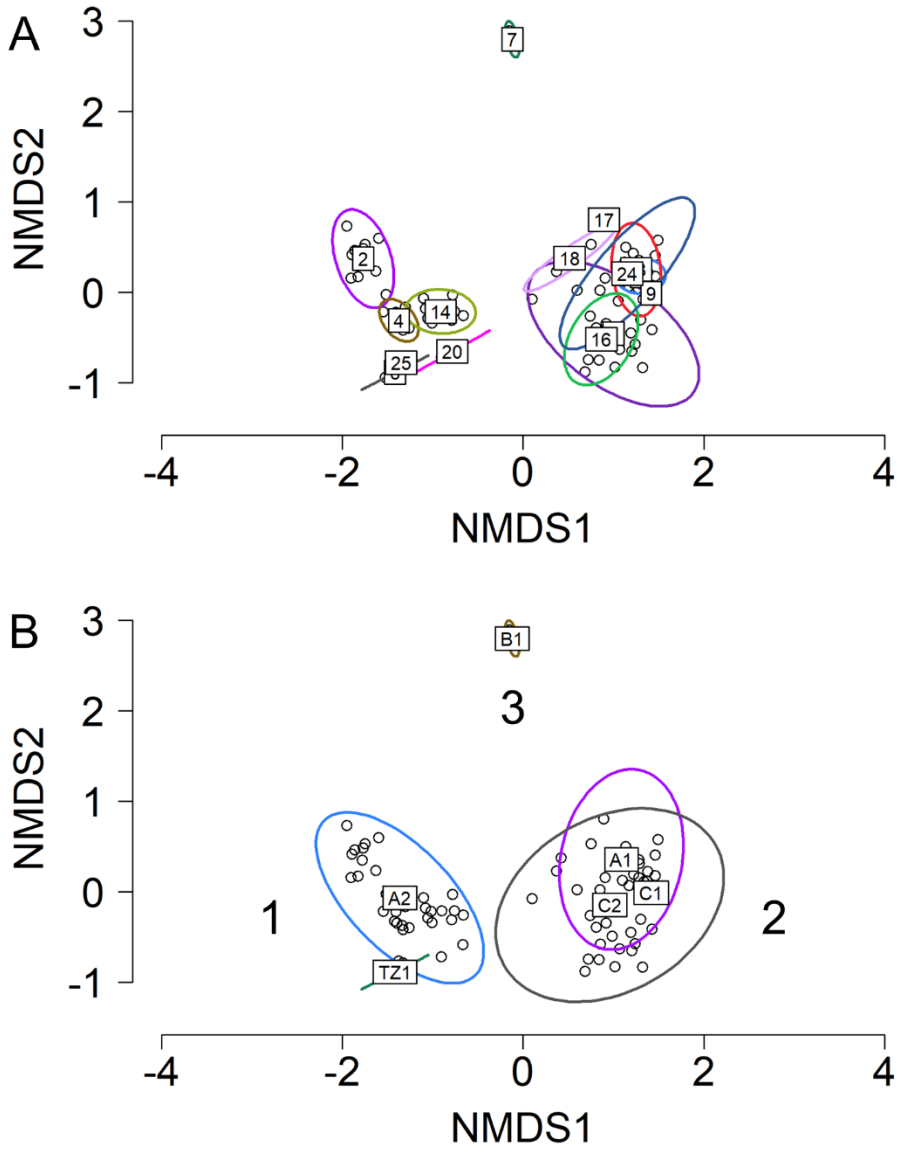

Figure 3.6 Non-metric multi-dimensional scaling (NMDS) with stress of 0.109, Bray-Curtis dissimilarity using total abundance of each taxon (n=63) per transect (m^{-2}; summed counts, divided by summed area per transect). Different coloured ellipses outline the 95% confidence intervals for the groupings based on A) stations and B) primary benthoscapes with labels (1-3) for the three types of assemblages. Each point represents a transect, and the number of images analyzed per transect were 32 - 65 for ROPOS and 25 - 37 for Campod. Note: At least 3 data points are needed to draw ellipses with 95% confidence intervals. For stations 6, 9, 17, 20, and 25 and benthoscape classes C1 and TZ1, there were less than 3 transects, resulting in a warning. While the ordination is valid, "ellipses" appeared as lines for groups with 2 transects or absent for station 17 with 1 transect, and thus not a true 95% confidence intervals.

Table 3.3 Permutational multivariate analysis of variance (PERMANOVA) using Bray–Curtis dissimilarity and 999 permutations, examining the effect of primary benthoscape class and station in the Laurentian Channel MPA.

Factor	df	Sums of squares	Mean Squares	*F*	R^2	*P*
Benthoscape	5	13.18	2.64	52.17	0.53	0.001*
Station	9	8.19	0.91	18.01	0.33	0.001*
Residuals	67	3.39	0.05	-	0.14	-
Total	81	24.76	-	-	1.00	-

Table 3.4 Summary of SIMPER results, including the taxa that contributed at least 10% to the cumulative percentage of the difference in Bray-Curtis dissimilarity between pairs of stations. Shown are number of comparisons for which each taxon contributed to significant difference in paired station comparisons (total number pairwise comparisons: 105). Subsets of the 8 listed taxa ranked within the top 4 in all pairwise station comparisons. *envfit* p value related to the taxonomic fit of the NMDS (Figure 3.6), where * is highly significant at α=0.001.

Taxa	Number of pairwise station comparisons for which taxon contributed to at least 10% of difference	Comments on how taxon contributed to pairwise station comparisons	*envfit* p value (NMDS)
Hexacorallia (SC.) spp.	34	Higher abundances in assemblages in benthoscapes A2 and TZ1(stations 4, 6, 14, or 25; excluding 2) and one in C2 (station 20) than in some combinations with the other stations except at 7.	0.001*
Kophobelemnon spp.	25	Higher abundances at stations 3 and 17 than other stations excluding 7; also, in 16 than 5 and 13, and 17 than 3 and 2.	0.007
Actinauge cristata	22	Higher abundances at stations 18 or 13 than other stations excluding 2, 7, 17; also in 3 than 5 and 16, and 9 than 5.	0.001*
Edwardsia sp. 1	21	Higher abundances at stations 18, 24, or 5 than other stations excluding 2, 3, 7, 17; also in 24 and 3 than 5, 5 than 14, and 13 than 14 and 16.	0.001*
Porifera (P.) sp. 21	14	Higher abundance at station 7 than all other stations.	0.001*
Pennatula sp. 2	12	Higher abundance at station 2 than other stations excluding 7 and 17; no other taxon had within assemblage differences for benthoscapes A2 and TZ1(stations 2, 4, 6, 14, & 25) and one in C2 (station 20).	0.001*
Anthoptilum spp.	10	Higher abundances at stations 16 and 9 than other stations (3, 5,13,18, 20, and 24), excluding assemblages in benthoscapes A2, TZ1, and B1 (stations 2, 4, 6, 7, 14, & 25), and one in A1 (station 17).	0.001*
Anthomastinae (SF.) sp. 1	7	Higher abundance at station 17 than stations 3, 9,13,16,18, and 24 (in benthoscapes A1, C1, and C2), excluding assemblages in benthoscapes A2, TZ1, and B1 (stations 2, 4, 6, 7, 14, & 25) and one in C2 (station 20).	0.176

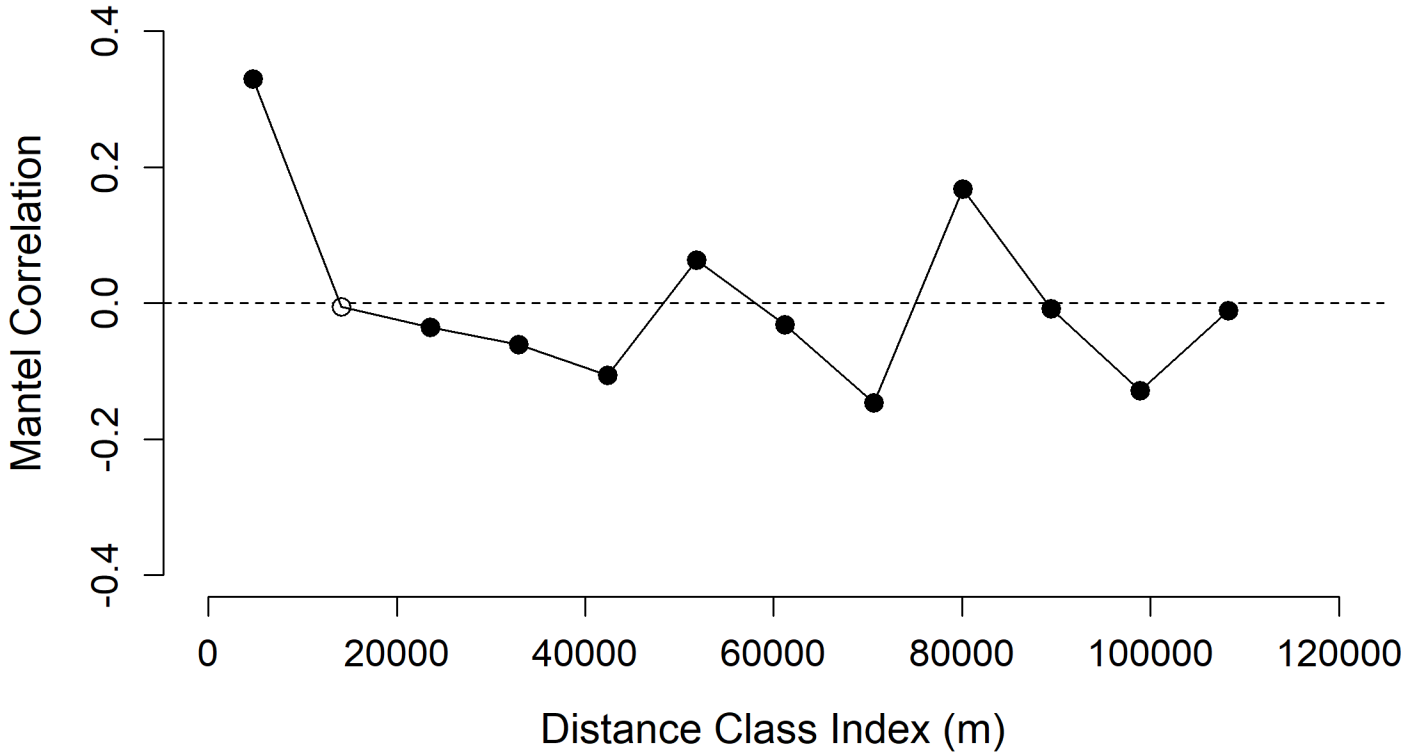

Figure 3.7 Mantel correlogram based on a Brays-Curtis dissimilarity distance matrix and Euclidean distance matrix throughout the Laurentian Channel MPA, calculated from 2976 images (ROPOS and Campod combined but excluding images with zero taxon abundance). Median distance is used to represent each distance class index, which increases in increments of ~9.42 km. See appendix for additional details and the Mantel correlogram performed at 5000-m fixed distances. Spatial range is ~10 km. Black points are significant and white points not significant after the Holm correction, which accounts for multiple testing.

Overall, diversity was similar at distances less than ~10 km (based on Bray-Curtis dissimilarity), but varied at distances > 10 km; thus, diversity was not spatially consistent throughout the LC MPA. The first distance class in the Mantel correlogram showed positive autocorrelation (~ 4.7 km, p = 0.001), but correlation alternated between positive and negative values at the larger distance classes, indicating a repetitive pattern throughout the study area with patches of similar diversity (Figure 3.7 & Table AI.3). The spatial range of this pattern occurred around the second distance class (9.42-18.84 km). A similar pattern was found with the detrended version of the mantel correlogram and fixed distance classes of 5000 m, with the latter narrowing in on the spatial range of the pattern (5-10 km; Figure AI.2).

3.5 Discussion

3.5.1 Assemblages in the LC MPA

We detected 3 types of assemblages in the LC MPA, based on NMDS and composition (overall abundance and diversity), with eight key taxa contributing to most differences. Higher abundances of *Anthoptilum* spp. and *Kophobelemnon* spp. were associated with high diversity, whereas higher abundances of *Pennatula* sp. 2 were associated with overall low diversity. These sea pens have different morphologies, but functional traits of individual species have not been assessed. Sea pens provide biogenic habitat and although known as nurseries for fish and having associated taxa on or in their tissues (Baillon et al., 2012, 2014a), associations with epifaunal invertebrates need to be further investigated. Overall, sea pens were proportionally only dominant at a few stations. Fish were associated with cup corals and soft corals in Alaska (Heifetz, 2002),

and with cerianthids in the Gulf of Maine (Auster et al., 2003). Within the LC MPA, fish density was correlated to abundance of sea pens, cup corals, and a specific sea anemone/cerianthid (our Cerianthidae (F.) sp. 1) (Boulard et al., 2023).

Based on our analyses, one type of assemblage (NMDS; assemblage 1) included few dominant taxa and was detected at six stations (2, 4, 6, 14, 20, and 25), mostly at shallower depths and dispersed along the eastern boundary of the MPA. In all cases, overall diversity was low with *Pennatula* sp. 2 and/or Hexacorallia (SC.) spp. being dominant. While this type of assemblage had a similar range in species richness as the second type below, the Shannon diversity index differed due to variation in evenness. *Pennatula* sp. 2 may be outcompeting other epifauna in areas with suitable conditions, leading to high abundance but low diversity. In addition, *Pennatula aculeata* are likely aperiodic spawners (Eckelbarger et al., 1998), possibly contributing to higher abundances than other species that may spawn less frequently, such as *Anthoptilum grandiflorum* which spawns annually (Baillon et al., 2014b). Although, Couillard et. al (2021) suggest *Pennatula aculeata* may have female biennial spawning. Hexacorallia (SC.) spp. may share a niche with *Pennatula* sp. 2*,* since the two taxa had an inverse trend in overall abundance. Fine-scale spatial patterns also suggest a negative association between these two corals with different local hotspots (de Mendonça & Metaxas, 2024). Abundance of *Pennatula* sp. 2 was particularly high at one station (2), in the southern part of the MPA and towards the mouth of the channel. Lacharité et al., (2020) also found *Pennatula* sp. in the eastern and northern parts of the Laurentian Channel (depths 265-454 m).

The second type of assemblage (NMDS; assemblage 2) included a complex mix of taxa with high overall diversity, and was detected at eight stations (3, 5, 9, 13, 16, 17,

18, and 24) dispersed in the deeper part of the MPA towards the center of the channel, including the station with the highest diversity (5) in the MPA. Within this type of assemblage, patterns varied among taxa and stations. For example, *Kophobelemnon* spp. was very abundant at two stations (3 and 17), and *Anthoptilum* spp. at two different stations (9 and 16). Three additional taxa (*Actinauge cristata*, *Edwardsia* sp. 1, and Anthomastinae (SF.) sp. 1) also accounted for differences within this second type of assemblage and were more abundant in assemblage 2 than assemblage 1 (excluding Anthomastinae (SF.) sp. 1).

The third type of assemblage (NMDS; assemblage 3) occurred at a single station (7), closest to the shallow northeastern point of the MPA, and included several taxa that were not detected in the other assemblages. This assemblage had the second highest overall abundance and low diversity, but higher species richness than the other assemblages (low evenness). Porifera (P.) sp. 21 was the numerically dominant taxon, possibly competing with the other species. Sponges may also play an important functional role, acting as biogenic habitat (Beazley et al., 2013; Maldonado et al., 2016; McClintock et al., 2005).

Sampling designs with high spatial resolution and multiple transects are most appropriate for characterizing assemblages with high diversity. In our study, some taxa in the second assemblage were missed on specific transects and sometimes different image spacings (7, 14, 21, and 28 m) led to different estimates of abundance. Fine-scale patterns (e.g. local hotspots and variation in patch size) likely contributed to this issue (de Mendonça & Metaxas, 2024). We recommend high resolution sampling designs with multiple transects to avoid misrepresenting diversity and abundance of epifauna.

3.5.2 Broad-scale Patterns and Potential Drivers

We detected some spatial structure in epifaunal diversity, reflecting a broader pattern throughout the LC MPA. Similarity in community structure (i.e. composition and diversity) appears to extend past the scale of individual stations, i.e. within ~10 km, with some differences arising at greater distances. Stations that were ~10 km apart had similar overall diversity. For example, two stations (5 and 16) at the center of the MPA had similarly high diversity and two stations (6 and 25) close to the eastern MPA boundary had similarly low diversity. Stations that were separated by greater distances were dissimilar (e.g. Station 6 and 16, spaced at ~ 63 km). The observed spatial structure in Bray-Curtis dissimilarity corresponded to this pattern. Ruiz-Pico et al. (2017) also detected spatial structure in sea pen aggregations in the Bay of Biscay. The mantel correlogram in our study alternated between negative and positive values, suggesting a patchy pattern. Several stations harboured similar assemblage types, despite being >10 km apart, therefore supporting broad scale patchiness in community structure. Since fine-scale spatial patterns can occur (de Mendonça & Metaxas, 2024), our multiple transect design may have partially contributed to the observed patchiness. However, the study area was large enough to have environmental drivers that caused biological differences, as demonstrated by the benthoscape. Overall, broad-scale changes in community structure were apparent across the LC MPA, which was likely the result of varying spatial processes.

3.5.2.1 Benthoscapes

Benthoscapes have been associated with patterns in epifaunal community structure and biodiversity (Proudfoot et al., 2020; Wilson et al., 2021). In our study, benthoscape classes were a significant factor explaining variation in community structure within the LC MPA. The classes appear to reflect preferred conditions or different habitats for assemblages, either directly related to geomorphology or indirectly as a proxy for covarying factors. Assemblage 1 was associated with benthoscapes A2 and TZ1, characterized as mid-depth with low relief, sparse scours, intermediate to very abundant pockmarks, and muddy/gravelly sand to mixed surficial sediment (Lacharité et al., 2020)[7]. Assemblage 2 was associated with deep benthoscapes (C1, C2, and A1) characterized by relatively flat to low relief, sparse to very abundant scours and pockmarks, and various types of surficial sediment (fine sediment, bioturbated mud, & sandy mud with gravel traces) (Lacharité et al., 2020). We did not sample the deep benthoscape TZ2, but Lacharité et al., (2020) suggest that it coincides with the presence of *Anthoptilum grandiflorum*, which was more prominent in deep areas of the Laurentian Channel, consistent with our results. Deep benthoscapes constitute a large portion of the MPA (combined 66% of the layer) and reflect conditions that support high epifaunal diversity (e.g. including assemblages with *Anthoptilum* spp. or *Kophobelemnon* spp). Assemblage 3 was associated with the shallow benthoscape B1, which was very steep, lacked scours, but had sparse pockmarks and coarser sediment (gravel/sandy gravel surficial sediments) (Lacharité et al., 2020). Lacharité et al., (2020) described this region as one with a diverse community (e.g. sponges including *Stylocordyla* sp., crinoids, sand

[7] For details on the benthoscape classes see Table AI.1. Reprint of Table 41.1 in Lacharité et. al. (2020).

dollars, sea cucumbers, coralline algae, and shell debris), in contrast to our findings of overall low diversity.

3.5.2.2 Spatial Drivers

Different environmental factors likely contributed as spatial drivers of the observed assemblage patterns, including depth, geological properties, physical and chemical water properties, and food, some of which were possibly captured by the benthoscape classes. One of the conservation priorities is to protect sea pens in the LC MPA (DFO, 2019b). We recorded lower diversity and higher overall abundance of sea pens in the eastern stations which were < 400 m in depth (assemblage 1 and 3), and higher diversity with lower abundance in western deeper stations > 400 m deep (assemblage 2). Depth is an important driver in sea pen distributions (Ruiz-Pico et al., 2017) and modeling and observations suggest *Pennatula* is often found at shallow depths (Baker et al., 2012; Guijarro et al., 2016; Gullage et al., 2017; Langton et al., 1990). Station 2 had higher mud (silt and clay) than sand (Miatta & Snelgrove, 2022), likely contributing to high abundances of *Pennatula* sp. 2 as mud is a strong predictor of the occurrence of several sea pens (Greathead et al., 2015). Lacharité et al., (2020) suggested higher abundances of sea pen towards the center of the MPA where 5 benthoscapes and thus varying sediment composition occur. In our study, relatively high abundances of *Kophobelemnon* spp. near the center of the MPA may have resulted from recruitment to preferred sediment composition (e.g. mud-sand, Baker et al. 2012) and/or other covarying factors with these benthoscapes. In other studies in the LC MPA, several environmental factors appeared to be similar in all areas where high abundances of *Pennatula* sp. 2 occurred, including the geological properties of slope, pockmarks and ice scour density,

as well as point samples of bottom temperature, oxygen, salinity, and pH (de Mendonça & Metaxas, 2024; Miatta & Snelgrove, 2022). However, differences in oxygen and/or other biochemical properties such as nutrients may arise between the northern and southern parts of the MPA over longer time scales due to ocean circulation. A warm deep (> ~100-150 m, ~ 4-6 °C) water layer flows into the Laurentian channel toward the Gulf of St. Lawrence (El-Sabh, 1977; Hebert et al., 2023; Lauzier & Trites, 1958), with oxygen declining from the mouth of the Laurentian channel towards the Gulf (Gilbert et al., 2005). Chlorophyll *a* can be another strong predictor for sea pens (Gullage et al., 2017), related to phytoplankton, a source of organic matter/food. Of the stations where *Pennatula* sp. 2 was abundant, station 2 had the second highest quantity of food (i.e. high TOM and TOC) and overall higher quality of food (i.e. high Chl *a* & TN, low C:N) (Miatta & Snelgrove, 2022).

Direct (e.g., bycatch) or indirect (e.g., sediment plumes) impacts may have reduced the past and current occurrence of vulnerable sessile species, such as sea pens. Commercial fishing activities outside the eastern and southern boundaries of the MPA and inside the MPA (Muntoni et al., 2019), may possibly impact the abundance of sea pens in nearby areas or reduce diversity. One station within assemblage 1 was located just outside the MPA boundaries (station 6) and had low diversity, suggesting that it may continue to be directly impacted by anthropogenic activities.

3.6 Limitations

Sampling biases in our study could have led to differences in patterns in abundance and diversity arising as a result of unequal sample sizes (images/transects for

ROPOS and Campod), tool-specific bias (de Mendonça & Metaxas, 2021), or small sampling area. Both ROVs and drop cameras are appropriate for community structure; however, an ROV can detect fine-scale patterns more accurately, as in de Mendonça & Metaxas (2024), by continuous sampling leading to higher resolution, and high maneuverability to perform standardized transect arrays. Further, species accumulation curves indicated that an area of > 1000 m^2 is needed to capture the full diversity of each station. Additionally, a lack of spatial and temporal resolution in both environmental and biological data can prevent the detection and explanation of spatial trends related to the assemblages, for example by missing variation at small spatial scales within each station and having fewer distance classes between stations. Further, there are likely transition areas between benthoscape classes, rather than sudden environmental changes/hard boundaries.

3.7 Conclusion

Our study advances the knowledge of spatial patterns in the abundance, composition and diversity of sea pen assemblages and their potential drivers. We found that different assemblages were associated with different benthoscape classes (based on depth and geomorphic features), which in turn may provide a potentially useful proxy for different habitats. Other broad-scale drivers of epifaunal spatial patterns likely include depth or covariates, circulation, sediment properties, and food. However, additional environmental data at multiple spatial and temporal resolutions are needed to assess the importance of these drivers. Overall, adequate characterization of broad-scale patterns,

including diversity and abundance, are needed to address spatial ecology of deep-sea communities, support monitoring efforts, and allow comparisons between areas.

CHAPTER 4

FINE-SCALE SPATIAL PATTERNS OF DEEP-SEA EPIBENTHIC FAUNA IN THE LAURENTIAN CHANNEL MARINE PROTECTED AREA[8]

4.1 Abstract

Ecological processes at local to global scales impact spatial patterns in abundance and distribution of megafauna. Fine-scale patterns have rarely been investigated through explicitly spatial analytical methods in the deep sea and have been assumed random, uniform, or similar to neighbouring areas. We used spatial statistics (Moran's *I*, *Gi**, and local Moran's *I*) to identify significant megafaunal patterns (0–100s of meters; 8 focal taxa) in the Laurentian Channel Marine Protected Area, based on imagery from a remotely operated vehicle, using 8 parallel transects at each of 7 stations. Our results included 2 spatial scales, station level (0.256 km^2) and paired transect level (0.004 km^2). We found local areas with significant aggregations (e.g., *Pennatula* sp. 2 and Hexacorallia (SC.) spp.) and patches extending for ~7–27 m, and in one case for ~155 m. Patchiness also existed between neighbouring images (≤10 m apart). Patterns varied among taxa within stations and for the same taxon among transect pairs. Station-level patterns appear to be related to geological factors, such as BPI (bathymetric position

[8] This article was published in *Deep Sea Research Part I: Oceanographic Research Papers*, *203*, 104195. de Mendonça, S. N., & Metaxas, A. Fine-scale spatial patterns of deep-sea epibenthic fauna in the Laurentian Channel Marine Protected area. Copyright Elsevier (2024). DOI: 10.1016/j.dsr.2023.104195

Anna Metaxas supervised the development of the study design, analyses, and co-authored the manuscript.

index), benthoscape, pockmarks, and slope. We propose that patterns at the transect level were likely caused by biological factors, possibly related to reproduction due to local currents and retention, or community interactions (e.g., competition). Fine-scale patterns should be considered to ensure effective sampling designs when using fine-scale tools (e.g., imagery), and for establishing accurate community metrics (e.g., abundance and diversity). Our study is relevant to future ecological research, linking patterns to processes, as well as monitoring and conservation in deep-sea ecosystems.

Key words: megafauna, spatial pattern, aggregation, distribution, fine-scale, patchiness

4.2 Introduction

Spatial patterns in species abundance and distribution can be a consequence of evolutionary and ecological processes, such as speciation, succession, community evolution, as well as species ranges and persistence (Levin, 1992). Consequently, spatial patterns can provide insight into spatial processes that give rise to these patterns. Some processes act on local scales, e.g., predation and competition, while others act on broader spatial scales with increased variation, such as environmental stress (e.g., temperature), dispersal, or productivity (Menge & Olson, 1990). Additionally, space itself can be a proxy for unknown environmental variables (Levin, 1992; McArthur et al., 2010).

In the deep sea, a wide range of factors may regulate patterns in species distributions, such as depth, substrate, and sediment composition (Hemery et al. 2018; Ruiz-Pico et al., 2017), currents (Downie et al., 2021; Roberts et. al 2009; Tissot et al., 2006), organic matter and nutrients (Miatta & Snelgrove, 2021), other water properties such as flow rate, temperature, and salinity (Greathead et al., 2015), and anthropogenic

stressors such as trawling, although vulnerability varies among species (Downie et al., 2021; Pierdomenico et al., 2018). For example, the BEnthos Sensitivity Index to Trawling Operations (BESITO) highlights how sensitivity to trawling can vary among species such as in their flexibility or ability to burrow (González-Irusta et al., 2018). Additionally, climate change including ocean acidification, warming, productivity changes, and other human-induced threats (e.g., oil and gas activities) also impact deep-sea communities and their spatial distributions (as reviewed in Ramirez-Llodra et al., 2011). Overall, the effects of these factors occur both at regional (e.g., 1000s km^2) and global scales, but their local fluctuations could also impact fine-scale patterns.

In the deep sea, although soft sediments are the dominant substrate type, our knowledge of spatial patterns of epifauna in this habitat is limited and research has mostly focused on broad-scale patterns (kms–1000s km^2). Analyses may be regionally aggregated, despite fine-scale data collection, for example using ROV imagery to determine regional distributions (e.g. Baker et al., 2012; Krigsman et al., 2012; Taylor et al., 2016). Spatial patterns in distribution have been assessed with imagery (e.g., using sampling units of 2–50 m^2 or 1–4 km transects) and acoustics (e.g., 5-m and 50-m resolution multibeam) often linking changes in communities or assemblages with depth (individual studies spanning 100s–1000s m) and substrate (Baker et al., 2012; Grinyó et al., 2018; Neves et al., 2014; Robert et al., 2015). Trawl data (e.g., 1.4–6 km per trawl) have also been used to measure changes in community structure with depth (Gullage et al., 2017; Terribile et al., 2016). Broad scale approaches that involve mapping (e.g. Neves et al., 2014) have provided explicit spatial analyses and interpretations, and a deeper understanding of particular patterns in efforts to address the underlying mechanisms.

Fine-scale patterns (10s–100s of meters) in epifaunal distribution have been more commonly explored using methods that are not explicitly spatial (i.e., analyses do not include x and y co-ordinates for each sampling unit as a factor), such as examining local changes in abundance, diversity, and/or patchiness within imagery transects. For example, high diversity was detected using ROV transects ~1 km in length but analyzed in 10-m segments, resulting from small-scale variation in habitat type (Baker et al., 2012). Images captured 30 s apart from 150–300 m long transects by drop camera showed a patchy distribution of brittle stars with local areas of high abundance (up to 2,800 individuals per image) (Piepenburg & Schmid, 1996). Corals (including *Lophelia pertusa* and *Madrepora oculata*) were often found on local topographic high points (sediment waves) and appeared more frequently on top of a coral mound (based on images taken every 1s from ROV video and multibeam at 0.5-m resolution) (Dolan et al., 2008). Although these studies describe patterns in epifaunal distribution on fine scales, they do not use statistical approaches to quantify the spatial pattern. For example, Meyer et al. (2023) describes patchiness in terms of mean and range but does not statistically quantify local changes.

Spatial statistics provide a tool that can be used to identify how specific communities, species, or individuals interact and perhaps utilize their environment on multiple spatial scales. Since spatial processes can act on various scales (Dale & Fortin, 2014), a multi-scale approach is needed to quantify species patterns, the spatial processes that cause these patterns, and the related consequences to community ecology. Simpler local-scale models nested within more complex larger-scale models can be used to gain a better understanding of these patterns (Menge & Olson, 1990). While used widely in

terrestrial ecology (Getis and other stastistics; Ben-Said, 2021), epidemiology (Getis statistics; Robinson, 2000), and in other fields and environments (modelling spatial processes e.g. Kriging, Markov random fields, etc.; Hjort et al., 1994), similar approaches have only been used in a few deep-sea studies to analyze high-resolution data for megafauna (for deep-water corals see Conti et al., 2019; Price et al., 2021; Watters et al., 2022; and for other megafauna Vad et al., 2020). More studies have examined patterns of macrofauna and fish (e.g., Barnes & Hamylton, 2019; Boulard et al., 2023; Hamylton & Barnes, 2018; Wigand et al., 2013). Fine-scale sampling tools (e.g., remotely operated vehicles, cameras, autonomous underwater vehicles.) are necessary for targeted, high-resolution, georeferenced replicated data, compared to historically exploratory methods that may have lower positional accuracy (e.g., trawl) and cannot elucidate fine-scale pattens (e.g., integrated across one tow) (de Mendonça & Metaxas, 2021). Studies that consider spatial structure help understand ecological processes, as well a generate new ecological hypotheses on underlying mechanisms (Dale & Fortin, 2014).

In this study, our overall goal is to quantitatively explore the spatial patterns (10s of meters) in the distribution of deep-sea epifauna in a soft sedimented habitat using fine-scale spatial statistics to objectively detect significant changes in abundance. We used a novel approach, that includes a high-resolution sampling design combined with analyses of both global and local spatial statistics, to provide insight into epifaunal spatial patterns at two scales (station and transect level) in the Laurentian Channel Marine Protected Area (MPA) and to develop hypotheses for their potential causes. The Laurentian Channel (MPA) was designated partly with the objective to protect sea pen communities (DFO, 2019a), located in soft sediment habitat. In other studies, existing broad-scale patterns in

biomass estimated from trawls were not supported by observed estimates of sea pen abundance from imagery (de Mendonça & Metaxas, 2021). The identification of fine-scale patterns can increase the accuracy of community metrics (e.g., abundance and diversity) and improve sampling designs. Furthermore, monitoring often involves assessing ecosystem changes over time, and should optimize sampling designs to accurately detect and quantify communities with non-random patterns. Thus, our study has application to both ecological research as well as effective monitoring frameworks for conservation.

4.3 Methods

4.3.1 Study Area

The Laurentian Channel Marine Protected Area (LC MPA) is located in a deep glacial trough to the southwest of Newfoundland, Canada (DFO 2019a). The LC MPA is 11,580 km^2 (DFO 2019a), has a depth range of 51 to 497 m, and has predominantly fine to mixed sediments (mud, sand, and gravel) with some underlying geomorphic features, such as iceberg scours and circular depressions, such as pockmarks or iceberg pits (Lacharité et al., 2020, Fader, 1991).

4.3.2 Data Collection and Image Analysis

We collected video at seven stations (2, 3, 4, 5, 13, 14, and 16) in the LC MPA with a downward-facing Insite Pacific Zeus-Plus HD camera (1,920 × 1,080 pixels) mounted on the remotely operated vehicle (ROV) ROPOS (www.ropos.com) on 9–17 September 2017 (Figure 4.1). At each station, we ran 8 400-m parallel transects spaced at

alternating distances of 10 m and 200 m (i.e., four pairs: AB, CD, EF, GH; spatial extent, including area between transects: 0.256 km^2) (Figure 4.1). Based on previously collected data such as biomass from DFO trawls, abundance from imagery, and a benthoscape classification by Lacharite et al. (2020), we selected representative stations. We avoided sampling across benthoscape classes to represent single habitats at each station (except at station 4), as these may have transition zones rather than sharp boundaries (Lacharité et al., 2020). High-definition video and navigation metadata (using the first record per second e.g., depth, altitude above seafloor, latitude, longitude) were synchronized with the software application Ocean Floor Observation Protocol (OFOP 3.3.8c, Huetten & Greinert, 2008; Scientific Abyss Mapping Services, 2009).

Using OFOP, we extracted images every 1.5 m and selected every 4^{th} image with a target image spacing of ~ 6 m. We ensured that image quality allowed an unobstructed view of the seabed and fauna. If areas of the image with low quality (e.g., sediment plumes, blurry sections) covered < 50% of the total area, they were cropped and the image used; otherwise, the next image in sequence was used instead (Table 4.1). Fauna greater than 2 cm in the largest dimension were identified to morphotaxon using a reference guide based on World Register of Marine Species (WoRMS) and enumerated (using laser points separated by 10 cm for scale in ImageJ; Appendix Table AII.1) (Abràmoff et al., 2004). The area of each image was measured and used to calculate abundance (m^{-2}). Mean area per image ranged from 0.73 ± 0.009 m^2 to 2.40 ± 0.63 m^2.

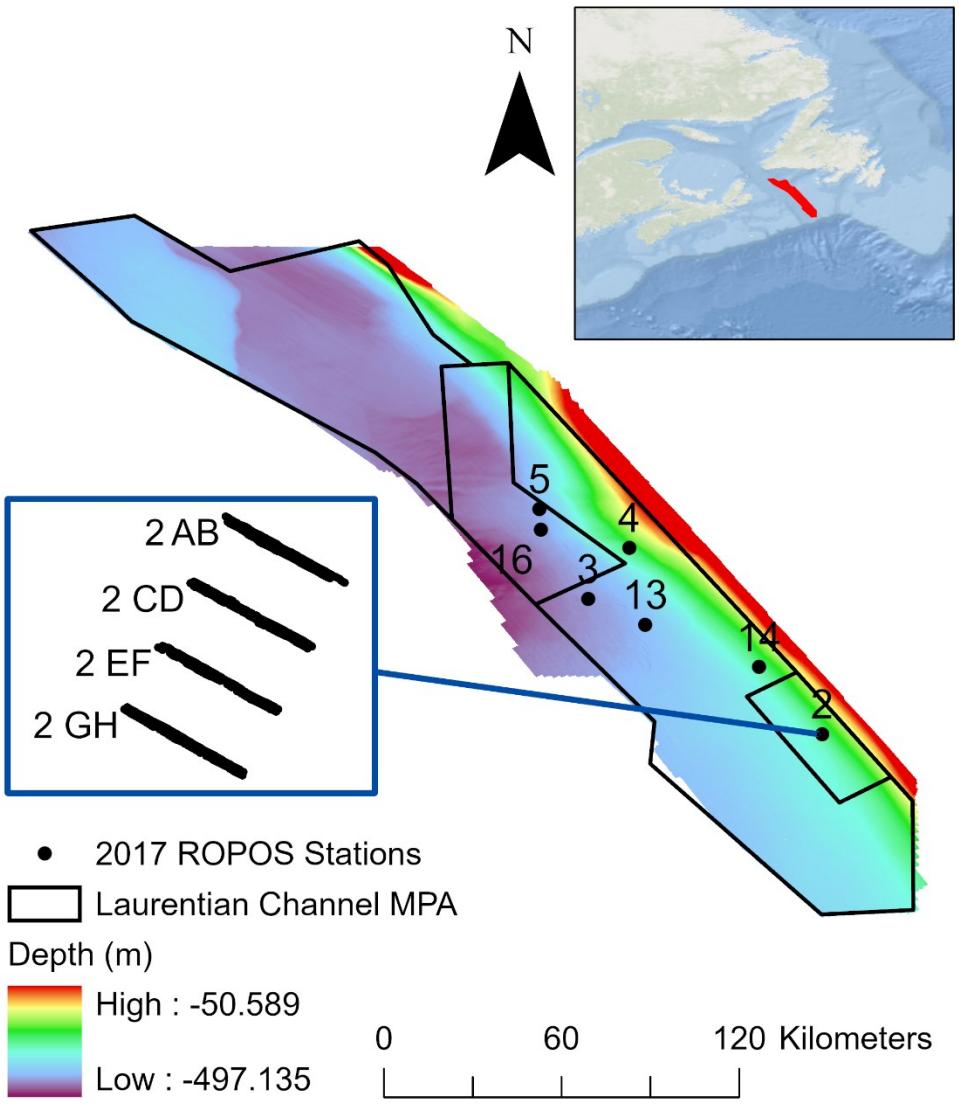

Figure 4.1 Map of stations in the Laurentian Channel MPA. Inset map (top) shows the broader area of the Northwest Atlantic near Canada. Inset map (left) is an example of the four paired transect array (eight transects total) at station 2: 10-m spacing between paired transects (AB, CD, EF, and GH) and transect pairs spaced at 200 m. Transect arrays were similar at other stations but with varying rotation. Depth (20-m resolution grid unpublished) provided by Lacharité et. al., (2020); Word Ocean Base (Esri, Garmin, GEBCO, NOAA, NDGC, and other contributors).

Table 4.1 Summary of transect metadata for the 7 stations in LC MPA, including number of images, area of images, depth, altitude relative to seafloor, start point, end point, distance between images, and total length for each transect (eight transects per station A, B, C, D, E, F, G, and H; for a total of 56 transects). Altitude refers to the height of the altimeter attached to the ROV relative to the seabed. Total length is the sum of distances between individual images, rather than a straight line from the start to end positions.

Transect	# of Images	Total area of images (m^2)	Mean Depth (m)	SD Depth (m)	Mean Altitude (m)	SD Altitude (m)	Start Longitude (DD)	Start Latitude (DD)	End Longitude (DD)	End Latitude (DD)	Mean distance between images (m)	SD of distance between images (m)	Total length (m)
2A	62	141.90	348.15	0.68	1.23	0.33	-56.67042	45.53298	-56.66594	45.53123	6.57	1.28	401.00
2B	54	120.49	348.74	0.70	1.04	0.28	-56.66649	45.53134	-56.67034	45.53284	6.51	0.94	345.27
2C	63	124.87	349.82	0.52	0.92	0.17	-56.66719	45.52954	-56.67163	45.53128	6.42	0.51	398.30
2D	64	132.88	349.79	0.50	1.06	0.25	-56.67175	45.53124	-56.66736	45.52950	6.29	1.50	396.48
2E	62	117.86	351.25	0.75	0.83	0.10	-56.66848	45.52790	-56.67281	45.52957	6.36	0.55	387.67
2F	58	133.72	351.23	0.83	1.20	0.36	-56.67298	45.52954	-56.66854	45.52782	6.98	3.69	397.74
2G	62	114.94	353.58	0.76	0.88	0.13	-56.66980	45.52625	-56.67415	45.52796	6.38	0.53	389.21
2H	61	146.52	353.77	0.95	1.22	0.38	-56.67426	45.52791	-56.66982	45.52615	6.65	2.54	398.84
3A	65	93.31	445.92	0.35	0.99	0.16	-57.37146	45.94323	-57.36749	45.94554	6.29	0.60	402.31
3B	64	91.01	445.78	0.35	0.94	0.13	-57.36737	45.94548	-57.37137	45.94314	6.44	1.67	405.46
3C	63	83.22	445.80	0.83	1.07	0.31	-57.36950	45.94191	-57.36556	45.94421	6.45	0.98	399.73
3D	56	83.01	445.84	0.79	1.00	0.29	-57.36550	45.94412	-57.36943	45.94183	7.23	5.41	397.59
3E	65	104.36	445.87	0.42	1.04	0.20	-57.36767	45.94066	-57.36371	45.94294	6.28	0.80	401.65
3F	58	87.91	446.09	0.42	0.90	0.09	-57.36378	45.94281	-57.36759	45.94060	6.77	2.08	386.14
3G	65	97.56	446.29	0.51	1.00	0.16	-57.36586	45.93942	-57.36183	45.94169	6.31	0.36	404.15
3H	63	99.49	446.35	0.56	0.97	0.15	-57.36181	45.94158	-57.36573	45.93933	6.36	1.06	394.21
4A	64	114.31	333.00	0.68	1.15	0.20	-57.24532	46.09556	-57.24032	46.09642	6.33	0.20	398.56
4B	60	85.64	333.09	0.74	1.16	0.24	-57.24038	46.09634	-57.24540	46.09548	6.78	2.91	400.25
4C	65	115.34	335.66	0.81	1.10	0.23	-57.24472	46.09372	-57.23965	46.09460	6.33	0.41	405.13

Table 4.1 *(Continued)*

Transect	# of Images	Total area of images (m^2)	Mean Depth (m)	SD Depth (m)	Mean Altitude (m)	SD Altitude (m)	Start Longitude (DD)	Start Latitude (DD)	End Longitude (DD)	End Latitude (DD)	Mean distance between images (m)	SD of distance between images (m)	Total length (m)
4D	64	117.80	335.85	1.04	0.96	0.13	-57.23962	46.09453	-57.24472	46.09366	6.47	1.14	407.41
4E	63	75.12	337.10	1.43	1.19	0.34	-57.24401	46.09189	-57.23896	46.09279	6.53	1.19	404.61
4F	65	87.58	337.18	1.52	1.17	0.30	-57.23889	46.09270	-57.24398	46.09180	6.38	0.65	408.03
4G	65	135.63	337.67	1.20	1.19	0.28	-57.24332	46.09007	-57.23826	46.09094	6.33	0.23	405.31
4H	65	131.11	337.66	1.21	1.10	0.29	-57.23823	46.09085	-57.24329	46.09000	6.35	0.71	406.23
5A	55	109.94	438.52	0.63	0.93	0.10	-57.52767	46.21098	-57.53005	46.21384	6.83	3.68	368.56
5B	40	74.74	438.08	0.56	1.34	0.40	-57.53016	46.21380	-57.52765	46.21069	10.19	11.57	397.31
5C	63	97.18	440.47	0.22	0.91	0.02	-57.52980	46.20974	-57.53241	46.21284	6.43	1.24	398.63
5D	44	70.66	440.37	0.37	1.36	0.35	-57.53240	46.21263	-57.52996	46.20969	8.80	11.07	378.37
5E	62	101.60	439.78	0.41	1.13	0.34	-57.53216	46.20877	-57.53468	46.21186	6.51	2.43	397.03
5F	38	40.49	440.24	0.22	1.07	0.22	-57.53492	46.21189	-57.53246	46.20894	10.24	8.48	378.88
5G	46	59.31	440.03	0.23	1.00	0.18	-57.53446	46.20778	-57.53702	46.21084	8.75	17.39	393.88
5H	32	38.74	439.83	0.32	1.14	0.27	-57.53648	46.20998	-57.53464	46.20777	9.21	7.14	285.39
13A	63	87.86	433.64	0.64	1.12	0.24	-57.20464	45.86164	-57.20946	45.86288	6.49	2.56	402.59
13B	63	91.18	433.80	0.77	1.19	0.28	-57.20943	45.86296	-57.20461	45.86173	6.45	1.51	399.62
13C	61	76.80	433.23	0.81	0.97	0.23	-57.20366	45.86334	-57.20842	45.86462	6.62	3.02	397.02
13D	64	55.23	432.59	0.72	1.00	0.15	-57.20839	45.86472	-57.20366	45.86345	6.26	0.87	394.57
13E	64	90.54	431.19	0.38	0.96	0.13	-57.20262	45.86504	-57.20744	45.86627	6.35	0.86	399.94
13F	39	56.26	431.39	0.27	0.98	0.19	-57.20746	45.86639	-57.20309	45.86527	9.52	20.20	361.90
13G	33	45.03	430.92	0.35	0.89	0.02	-57.20325	45.86719	-57.20609	45.86789	7.31	5.52	234.05
13H	56	71.72	430.94	0.42	1.01	0.21	-57.20649	45.86808	-57.20167	45.86687	7.24	4.32	398.42
14A	65	60.78	343.18	1.60	0.98	0.18	-56.85260	45.73767	-56.84814	45.73952	6.33	0.23	405.17

Table 4.1 *(Continued)*

Transect	# of Images	Total area of images (m^2)	Mean Depth (m)	SD Depth (m)	Mean Altitude (m)	SD Altitude (m)	Start Longitude (DD)	Start Latitude (DD)	End Longitude (DD)	End Latitude (DD)	Mean distance between images (m)	SD of distance between images (m)	Total length (m)
14B	63	65.38	342.95	1.51	1.03	0.20	-56.84811	45.73941	-56.85237	45.73765	6.25	0.51	387.52
14C	64	71.84	343.34	1.77	1.24	0.34	-56.85119	45.73603	-56.84671	45.73790	6.47	1.58	407.73
14D	65	99.25	343.35	1.65	1.22	0.35	-56.84662	45.73781	-56.85112	45.73595	6.37	0.44	407.68
14E	62	70.21	343.96	1.52	1.24	0.31	-56.84999	45.73446	-56.84569	45.73629	6.42	0.98	391.75
14F	60	59.02	344.35	1.47	1.12	0.29	-56.84565	45.73619	-56.84986	45.73438	6.53	1.32	385.14
14G	54	90.52	344.32	1.41	1.36	0.36	-56.84874	45.73287	-56.84440	45.73473	7.47	4.01	396.16
14H	62	99.94	344.51	1.30	0.97	0.18	-56.84443	45.73462	-56.84864	45.73281	6.31	0.64	384.88
16A	63	87.30	444.26	1.09	1.03	0.21	-57.51709	46.14507	-57.51707	46.14150	6.41	2.07	397.52
16B	61	85.63	444.36	1.10	1.03	0.17	-57.51721	46.14165	-57.51719	46.14506	6.36	1.45	381.48
16C	48	42.89	444.58	0.67	1.12	0.24	-57.51976	46.14507	-57.51979	46.14146	8.56	8.19	402.35
16D	61	55.17	444.53	0.65	0.99	0.15	-57.51994	46.14146	-57.51992	46.14504	6.64	1.70	398.45
16E	46	47.94	444.41	0.90	1.41	0.32	-57.52253	46.14507	-57.52252	46.14146	8.92	6.42	401.28
16F	62	45.28	444.95	1.00	0.97	0.08	-57.52267	46.14147	-57.52267	46.14507	6.55	1.31	399.65
16G	58	52.18	445.77	1.71	1.41	0.29	-57.52525	46.14505	-57.52526	46.14148	6.97	3.48	397.18
16H	58	48.28	446.13	1.66	0.96	0.13	-57.52538	46.14146	-57.52539	46.14504	6.99	3.10	398.44

In total, we measured numerical abundance (counts) for 63 taxa and percent cover for 4 taxa. The less abundant taxa (i.e., present on < 4 transects at any one station) were either aggregated to form groups of higher abundance (e.g., Anthozoa (C.) spp.) or excluded (i.e., too few counts) from the analyses. We also excluded highly mobile or pelagic invertebrates (e.g., Elpidiidae (F.) spp., some malacostracans, Cephalopoda, Scyphozoa), because our sampling methods were not appropriate for their enumeration.

We used physical and geological environmental data to provide context for the interpretation of faunal spatial patterns. From the ROV mounted instruments, water properties included temperature, salinity (conductivity), oxygen and pH collected every 0.25 s with a CTD (Sea-Bird SBE 19plus V2), and depth measured with a sensor [Paroscientific Digiquartz (8B7000-I), accuracy of 0.01%]. For CTD data, we averaged at intervals of seconds, and then related to each image by date and time stamp, to provide a range in values for each station (Appendix Table AII.2). We also used previously collected/analyzed data on geomorphic features such as benthoscapes, pockmark density, iceberg scour density, and bathymetry from the Laurentian Channel (Lacharité et al., 2020). Lacharité et al. (2020) classified the region into different benthoscapes at a 50-m grid resolution, derived from object-based image analysis using multibeam echosounder data from 2010–2013 (i.e., bathymetry, slope, and density (km^{-2}; surrounding each grid cell) of iceberg scours and pockmarks/iceberg pits (see Table 41.1 in Lacharité et al., 2020). However, we also obtained 20-m bathymetry from Lacharité et al., (2020) and calculated slope in ArcGIS at a finer scale.

Table 4.2 Summary data for the 20 taxon-station combinations selected for the analyses, based on being present in more than 10% of images on at least one transect pair. Mean abundance and standard deviation are calculated across all images on that transect pair. The shown statistics are calculated only from the transect pairs with the largest percentage of images with presence, although the taxa were present on all eight transects (except Pennatuloidea (SF.) sp. 9 which was present on only five transects at station 2). Neighbourhood distances were used in station-level *Gi** and Local Moran *I* (including all eight transects), based either on incremental spatial autocorrelation or *k*-neighbour averaging [for # neighbours]; * indicates significant station-level patterns.

Station	Transect Pair	Taxon	# of images	# images with presence	% images with presence	Mean abundance (m^{-2})	Standard deviation of abundance	Neighbourhood distances (m), were applicable [for # neighbours]	Relevant Figures
2	CD	*Pennatula* sp. 2	127	124	98	4.00	2.06	27 *	4.2, 4.5, AII.14
2	AB	Pennatuloidea (SF.) sp. 9	116	18	16	0.12	0.32	15 *	AII.3, AII.11
2	AB	Hexacorallia (SC.) spp.	116	69	59	0.81	1.04	39 *	4.3, AII.1, AII.10
3	AB	*Edwardsia* sp. 1	128	40	31	0.05	0.17	44	AII.9
3	AB	Anthozoa (C.) spp.	128	16	13	0.18	0.34	44 [for 24]	-
3	EF	*Actinauge cristata*	119	34	29	0.14	0.32	44 [for 24]	-
3	EF	*Anthoptilum* spp.	119	15	13	0.09	0.28	44 *	AII.4
3	GH	*Kophobelemnon spp.*	128	60	47	0.43	0.55	44 [for 24]	-
4	GH	*Pennatula* sp. 2	130	86	66	0.59	0.62	46 [for 25] *	4.5, 4.6, AII.2, AII.12
4	GH	Hexacorallia (SC.) spp.	130	89	68	0.69	0.64	46 [for 25]	-
5	AB	*Edwardsia* sp. 1	95	12	13	0.07	0.20	47 [for 19] *	AII.5
5	EF	Anthozoa (C.) spp.	100	15	15	0.12	0.30	23 *	4.4
13	AB	*Edwardsia* sp. 1	126	26	21	0.18	0.39	46 [for 22]	-
13	AB	Anthozoa (C.) spp.	126	17	13	0.11	0.28	46 [for 22]	-
13	AB	*Actinauge cristata*	126	46	37	0.35	0.57	46 [for 22]	-
14	CD	*Pennatula* sp. 2	129	70	54	0.57	0.65	45 [for 24]	-
14	CD	Hexacorallia (SC.) spp.	129	68	53	0.61	0.76	45 [for 24]	-
16	AB	Anthozoa (C.) spp.	124	15	12	0.11	0.31	27 *	AII.6
16	AB	*Anthoptilum* spp.	124	33	27	0.21	0.37	38 *	AII.7
16	AB	*Kophobelemnon spp.*	124	17	14	0.11	0.28	16 *	AII.8

Table 4.3 Main objectives of the spatial statistics at the two scales of spatial analysis.

Scale of Analysis	Definition of neighbourhood		Distance band for neighbourhood (m)		Spatial pattern tested relative to the null hypothesis of complete spatial randomness (CSR)		
	Global Moran *I*	Local Moran *I* and *Gi**	Global Moran *I*	Local Moran *I* and *Gi**	Global Moran *I*	Local Moran *I*	*Gi**
Station-level	At least 1 neighbouring image	Peak incremental autocorrelation OR if not found, *k*-neighbour averaging for 19–25 neighbours	8–15	15–58	Overall spatial autocorrelation [a] ***entire station***	Local changes in spatial autocorrelation [b] **image compared to its neighbours *across the station***	Local changes [c] **sum of neighbourhood compared to sum of *station***
Transect-level	Equally spaced distance bins	Fixed distance of approximate spacing of images	10-m distance class/lag	10	Overall spatial autocorrelation [a] ***each transect pair***	Local changes in spatial autocorrelation [b] **image compared to its neighbours *across each transect pair***	Local changes [c] **sum of neighbourhood compared to sum of *each transect pair***

Notes:

[a] Overall spatial autocorrelation similarity (+) or dissimilarity (-) in neighbouring abundance values, incorporates mean.

[b] Local changes in spatial autocorrelation similarity (HH or LL) or dissimilarity (HL or LH outliers) in neighbouring abundance values (per image).

[c] Local changes in aggregation of like abundance values.

4.3.3 Data Analysis

We recorded 18 different taxa at the 7 stations, for a total of 89 taxon-station combinations. Among these, we retained only those combinations for which the taxon was present in at least 10% of all images analyzed in at least one transect pair in that station, resulting in a total of 20 combinations (Table 4.2). For each taxon-station combination, we performed spatial statistics at two different scales, station level and transect level (Table 4.3).

We used several different statistics to quantify spatial patterns. Local and global Moran's *I* are related statistics, and both examine spatial autocorrelation and deviations from the mean value (i.e., abundance) over the entire sampled area (Anselin, 1995; Dale & Fortin, 2014; Esri, 2022a). For local Moran's *I*, each observation is compared to, but not included in its neighbourhood. The deviation of the observation from mean abundance is used to assess local changes in spatial autocorrelation (see details and equations in Anselin, 1995). Positive values of the statistic result from an observation and its neighbours being similarly larger or similarly smaller than the mean abundance for the station (or transect pair). This defines local Moran clusters of similar abundance values: value of observation high and value of the neighbourhood also high (High-High; HH) or low observation-low neighbourhood (Low-Low; LL). Negative values of the statistic identify situations where an observation and its neighbourhood have dissimilar abundances relative to the mean, one being larger and the other smaller, resulting in local Moran outliers. The calculation of global Moran incorporates the sum of all local Moran's *I*, aggregating spatial autocorrelation over the entire sampled area into a single value and can miss local changes (Anselin, 1995; Dale & Fortin, 2014; Esri, 2022a).

The Getis-Ord statistic (*Gi**) also describes local patterns in spatial association; however, in contrast to local Moran's *I*, *Gi** includes the value (i.e., abundance) of each observation in the sum of its neighbourhood, which is then compared to the global sum of all observations in the sampled area (Esri, 2022b&c; Getis & Ord, 1992; Ord & Getis, 1995). Therefore, an image with zero or low abundance may be included in a hotspot if there are observations of high abundance in its neighbourhood. Overall, *Gi** detects the local pockets of similar abundance values, with hotspots for high values and coldspots for low values.

These statistics describe different spatial patterns. Local Moran's *I* detects whether an observation is similar or dissimilar to its neighbourhood allowing the identification of clusters and outliers. *Gi** describes whether the moving local mean is different from the global mean allowing the identification of hotspots and coldspots. Neither statistic can differentiate between cases where there is an absence of spatial structure and where the local average equals the global average (Dale & Fortin, 2014) (i.e., not significantly different from random or "random locations" in our study).

For the station-level analysis, we calculated Global Moran's *I* across all eight transects at each station using ArcGIS Pro (Esri, 2020b). Firstly, for each taxon retained for that station, a fixed neighbourhood distance was selected, ranging from ~8 to 15 m, to ensure at least one neighbour for each image (Esri, 2022d). For the transect-level analysis, we calculated Global Moran's *I* at 10-m distance bins (as spatial lags) and generated spatial correlograms for each pair of transects separately, using the *ncf* R package (R Core Team, 2021, Bjornstad, 2020, Wickham et al., 2019; *tidyverse*). The first 10-m distance bin reflects the approximate distance between images. To resolve the

challenges with multiple testing, we truncated spatial correlograms to include the first 2/3 of the maximum distance between the farthest images at each station, and calculated the Bonferroni progressive correction for each distance lag, where $\alpha = 0.05$/distance class (e.g., for distance class 2, $\alpha = 0.05/2 = 0.025$) (Fletcher & Fortin, 2018).

We investigated local spatial patterns, by calculating *Gi** and local Moran's *I* both at the station level and the transect level in ArcGIS Pro. To examine station-level patterns, we calculated these statistics across all eight transects at each station. Using the optimized hotspot tool (Esri, 2022e), the software first assessed the validity of each image, ensured there was variation in the dataset, and removed locational outliers (determined by their large distance from other images). The most appropriate neighborhood distance was selected by first determining the highest peak in incremental spatial autocorrelation, which corresponds to the scale of the prominent spatial pattern. This distance may be species-specific, limiting interpretation to individual taxa. The statistic is calculated based on the selected neighbourhood distance. Subsequently, FDR (False Discovery Rate) correction is used to adjust the significance for multiple testing and dependence in the data due to spatial autocorrelation (Esri, 2022e). The FDR procedure involves ranking all probability values to select an adjusted critical value based on the estimated proportion of incorrectly rejected null hypotheses (false significance). The FDR critical value is generally less than the unadjusted value (e.g., $\alpha=0.05$) but greater than the overly strict Bonferroni adjusted value (for details and equations see Benjamini & Hochberg, 1995; Caldas de Castro & Singer, 2006). When the neighborhood size could not be determined using incremental spatial autocorrelation, the software selected a fixed distance based on *K*-neighbour averaging. To examine transect-

level patterns, we calculated *Gi** and local Moran's *I* on each transect pair, spaced at 10 m, after reassessment of valid images and locational outliers, and FDR correction.

In addition to the benthoscape layer, we used layers of geological data to interpret significant station-level patterns (output of *Gi**), including pockmark/pit density, ice scour density, and slope. We extracted the geological data at each image location using ArcGIS Pro and R and we explored the patterns in environmental variables with *Gi** hotspot/coldspot classification (includes all *Gi** hotspots and all coldspots 90%+ significance level). Additionally, to examine fine-scale benthic features, we identified local areas of high (i.e., crests) and low (i.e., troughs) topographic points using a bathymetric position index (BPI) layer calculated using the 20-m bathymetry raster in Benthic Terrain Modeler (BTM) 3.0. BTM performed a comparison across the bathymetry layer, using a neighbourhood with an inner radius of 1 raster grid cell (20 m) and outer radius 25 cells (scalefactor 500 m = 25 outer radius cells x bathymetry resolution 20 m) to calculate the BPI for each 20-m grid cell (Lundblad et al., 2006; Walbridge et al., 2018) [similar to Topographic Position Index (TPI) in other studies].

4.4 Results

4.4.1 Spatial Structure at the Level of Station (0.256 km^2)

Of the 20 most prominent taxon-station combinations (present in more than 10% of images on any transect pair), 10 exhibited station-level patterns including significant *Gi** hotspots and sometimes significant local Moran clusters and outliers (Table 4.2 and Figures 4.2A&C, 4.3A&C, 4A for examples). Many of these taxon-station combinations also showed significant positive spatial autocorrelation at the station level (Global

Moran's *I* of 0.07 to 0.88 for ~8–15 m neighbourhood distance; Appendix Figure AII.1–AII.8 & Table AII.3), indicating spatial structure at this scale. In some cases, the global statistic did not detect spatial autocorrelation, and local spatial statistics were required to detect spatial structure. Ten taxon-station combinations did not show a structure significantly different from random at the station level (Table 4.2 and Appendix Figure AII.9). Overall, the presence of fine-scale spatial structure at the station level implies that summary statistics (i.e., overall mean abundance) may not be representative due to significant taxon aggregations in some areas; thus, local changes in spatial patterns should be considered.

4.4.2 Spatial Structure at the Level of Transect (0.004 km^2)

Overall, the outcomes of the analyses at the transect level were variable and, generally, there was little spatial structure at this scale (e.g., Figures 4.2B&D, 4.3B&D, 4.4B&D). Hotspots were sporadic and smaller than at the station-level, but there were some local Moran outliers on certain transects. Pennatuloidea (SF.) sp. 9 at station 2 had a unique transect-level pattern, with hotspots of abundance only on a single transect pair, yet limited presence elsewhere (Appendix Figure AII.3). Therefore, it was uncommon to find transect-level areas of significantly higher abundance than the mean (hotspots), and those that were present covered a small area along a transect pair. Local Moran outliers (HL or LH) indicated patchiness at the image scale (area per image was up to ~3 m^2), where abundance differed significantly between neighbouring images at ~10 m; those images with higher abundance were present throughout a transect pair. The relatively little spatial structure at the transect level compared to the station level, implies that

transect-level summary statistics (e.g., mean abundance by transect pair) are reasonably representative.

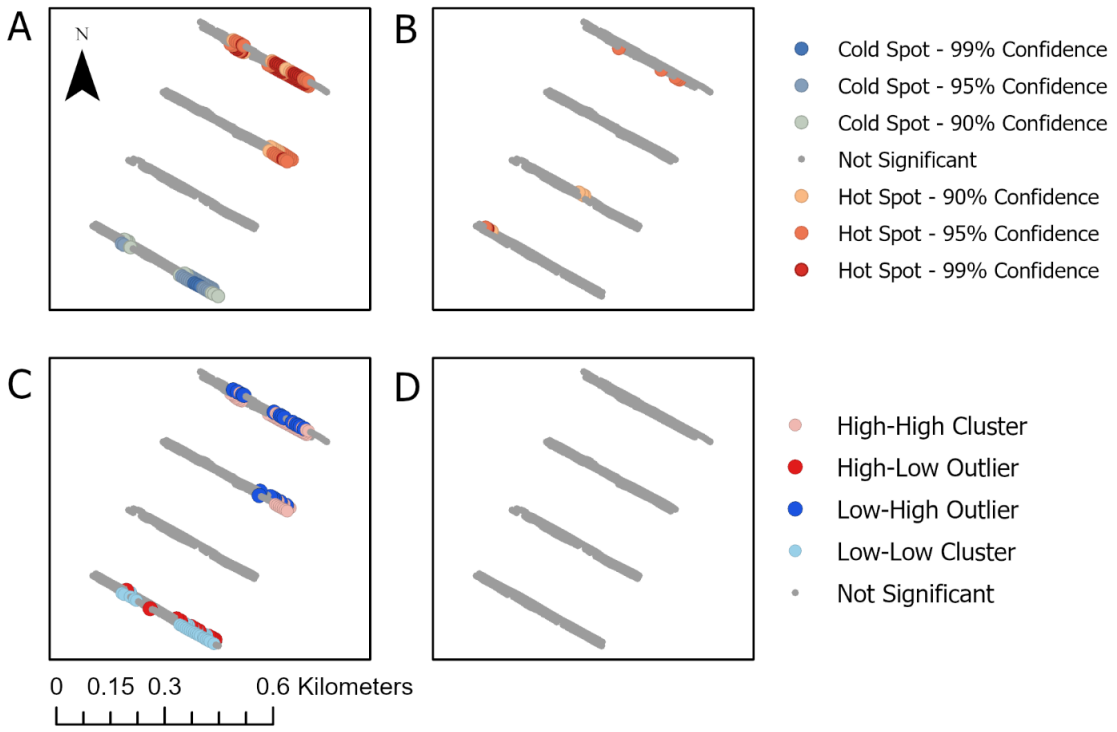

Figure 4.2 Local spatial statistical output for *Pennatula* sp. 2 at Station 2 in the LC MPA; A&C: station-level patterns using neighbourhood of ~27 m including all 8 transects in calculations; B&D: transect-level patterns using 10-m neighbourhood distance for each transect pair (AB, CD, EF, GH) separately. A&B are results from *Gi** hotspot analysis using upper legend; C&D are results from local Moran's *I* analysis using lower legend. *Gi** hotspots and coldspots are shown based on significance level (after FDR correction the critical value may be $\alpha \leq 0.1$ for 90%, $\alpha \leq 0.05$ for 95%, $\alpha \leq 0.01$ for 99%). For local Moran's *I*, a positive statistic results in clusters of similar abundance values: value of observation high and value of the neighbourhood also high (High-High; HH) or low observation-low neighbourhood (Low-Low; LL), whereas negative values of the statistic result from an observation and its neighbourhood having dissimilar abundances, thus outliers, high observation-low neighbourhood (High-Low; HL) or low observation-high neighbourhood (Low-High; LH).

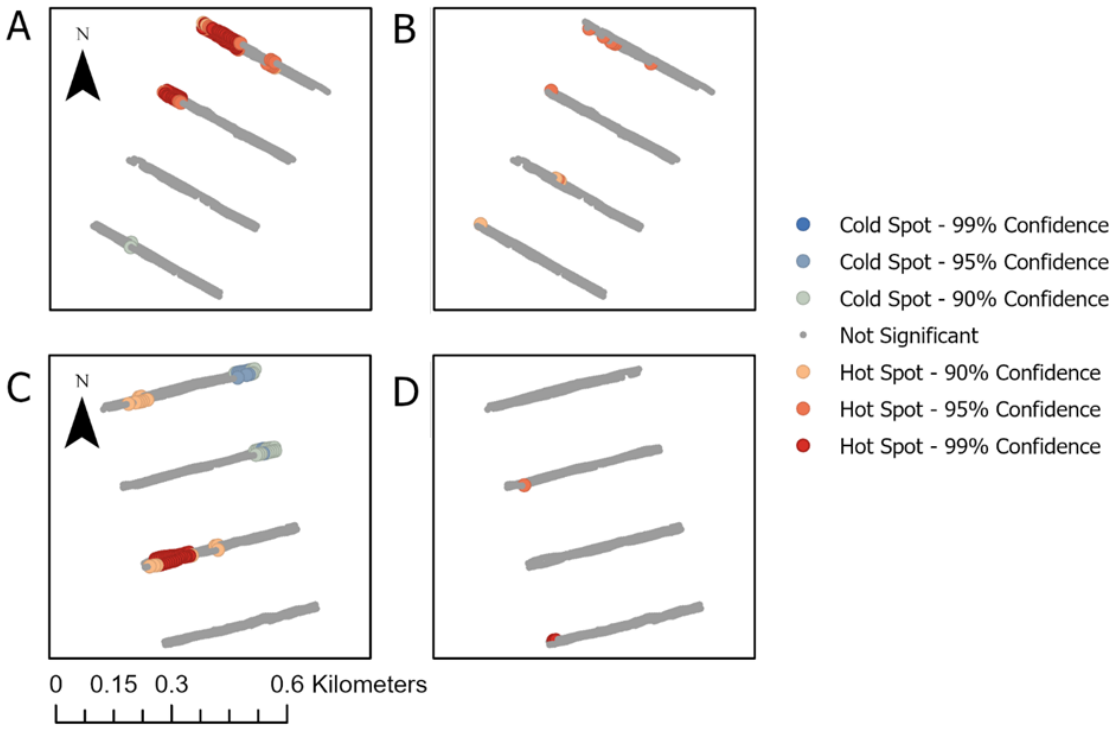

Figure 4.3 *Gi** hotspot analysis in the LC MPA; A&B Hexacorallia (SC.) spp. at Station 2, C&D *Pennatula* sp. 2 at Station 4. A) Station-level at ~39 m neighbourhood distance and C) Station-level at ~46 m neighbourhood distance with 25 neighbours, including all 8 transects in calculations; B&D Transect-level 10 m neighbourhood distance for each transect pair (AB, CD, EF, GH) separately (see explanation of legend in Figure 4.2 caption).

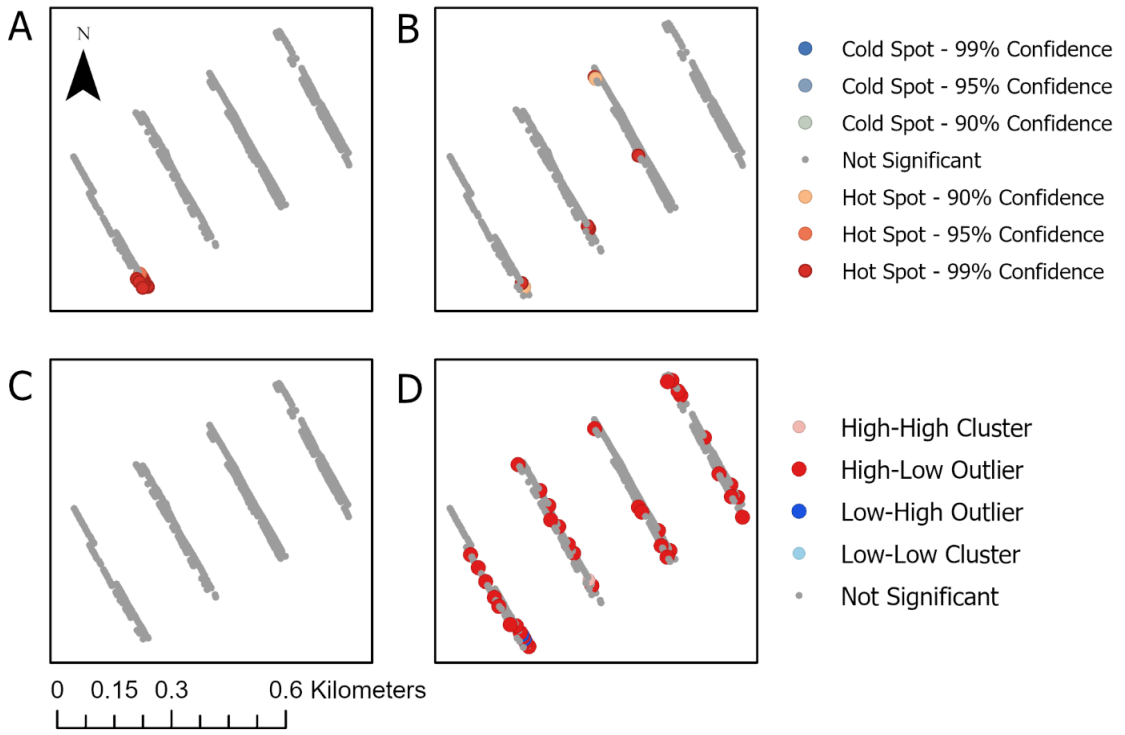

Figure 4.4 Local spatial statistical output for Anthozoa (C.) spp. at Station 5 in the LC MPA; A&C: station-level patterns using neighbourhood of ~23 m including all 8 transects in calculations; B&D: transect-level patterns using 10 m neighbourhood distance for each transect pair (AB, CD, EF, GH) separately. A&B are results from *Gi** hotspot analysis using upper legend; C&D are results from local Moran's *I* analysis using lower legend (see explanation of legend in Figure 4.2 caption).

4.4.3 Significant Taxonomic Aggregations: Hotspots

Three taxon-station combinations showed significant aggregations over large areas at the station level (large *Gi** hotspots at different neighbourhood distances 27–47 m), but also areas of significantly lower abundance (*Gi** coldspots) (Figures 4.2, 4.3, Table 4.2, and Appendix Figure AII.1–AII.2). *Pennatula* sp. 2 and Hexacorallia (SC.) spp. at station 2 exhibited hotspots/clustering on transects in the northern section of the

station (transects AB & CD) and a coldspot in the southern section (GH), although at opposite ends of the transects (Figures 4.2A & 4.3A). *Pennatula* sp. 2 at station 4 showed higher abundance in the western section of the station (AB and EF hotspots; HH cluster at EF) and lower abundance in the northeast part (AB and CD coldspots and LL clusters) (Figure 4.3C).

4.4.4 Size and Location of Hotspots

Overall, our results indicated that hotspots (areas of significantly higher abundance than the mean) varied in size and location for the different taxon-station combinations. Of the 10 taxon-station combinations with station-level patterns, three taxon-station showed large hotspots with some coldspots (Figures 4.2A, 4.3A&C), while seven others showed smaller hotspots without significant coldspots (neighbourhood distances ranged from ~15–47m) (Table 4.2). There was variation in the size and location of hotspots for *Pennatula* sp. 2, Hexacorallia (SC.) spp., and Pennatuloidea (SF.) sp. 9 at station 2 (Figures 4.2A, 4.3A, and Appendix Figure AII.1 and AII.3).

There was minimal overlap among taxa in the location of hotspots and coldspots. For example, at station 2, overlapping hotspots were detected for 3 taxa (Hexacorallia (SC.) spp. at 39 m, *Pennatula* sp. 2 at 27 m, and Pennatuloidea (SF.) sp. 9 at 15 m); all 3 taxa overlapped for 3 image locations and 2 taxa for 32 locations. However, most hotspot and coldspot areas did not overlap (90 hotspot and 41 out of 42 coldspot locations). At station 16, 2 of the 3 taxa (Anthozoa (C.) spp. at 27 m, *Anthoptilum* spp. at 38 m, and *Kophobelemnon* spp. at 16 m) overlapped in 4 image locations. There were no overlapping hotspot/coldspot areas at stations 3, 4 and 5.

4.4.5 Relationship of Environmental Variables and Spatial Structure

Most environmental variables (depth, oxygen, salinity, temperature, and pH) varied little within each station (Appendix Table AII.2). However, some geological variables showed variation within a station that may be ecologically meaningful, such as pockmark density, ice scour density, and slope. At station 2, hotspots of *Pennatula* sp. 2 occurred in steeper areas with slightly more pockmarks than at the coldspots (Figure 4.5A), while those of Hexacorallia (SC.) spp. were in flatter areas than the coldspots with similar pockmark density (see Appendix Figure AII.10–AII.11 for other examples).

Overall, larger hotspots were detected at station 2 and 4 than the other stations. Based on the benthoscape classification, one benthoscape class (A2) was present throughout station 2, but there were two benthoscapes (A2 and TZ1) at station 4 (Appendix Figure AII.12). The A2 benthoscape was associated with an overall higher mean pockmark density (> 5 km^{-2}) than TZ1 (1–2 km^{-2}) (Table 41.1 in Lacharité et al., 2020). Based on overlay of the benthoscape layer, most hotspots of *Pennatula* sp. 2 at station 4 occurred in A2 and coldspots in TZ1; however, local pockmark density was lower (~2.5 km^{-2}) in the A2 than in TZ1 (~5 km^{-2}; Figure 4.5B). Despite occurring in the same benthoscape (A2) at station 2, *Pennatula* sp. 2 hotspot areas had higher pockmark density (over 6 km^{-2}) than the coldspot areas (~5 km^{-2}). Hotspots for most taxon-station combinations were not related to bathymetry position index (BPI), possibly because of the orientation of transects, except for *Pennatula* sp. 2 at station 4, where hotspots were in areas of high points/crests compared to the coldspots (Figure 4.6).

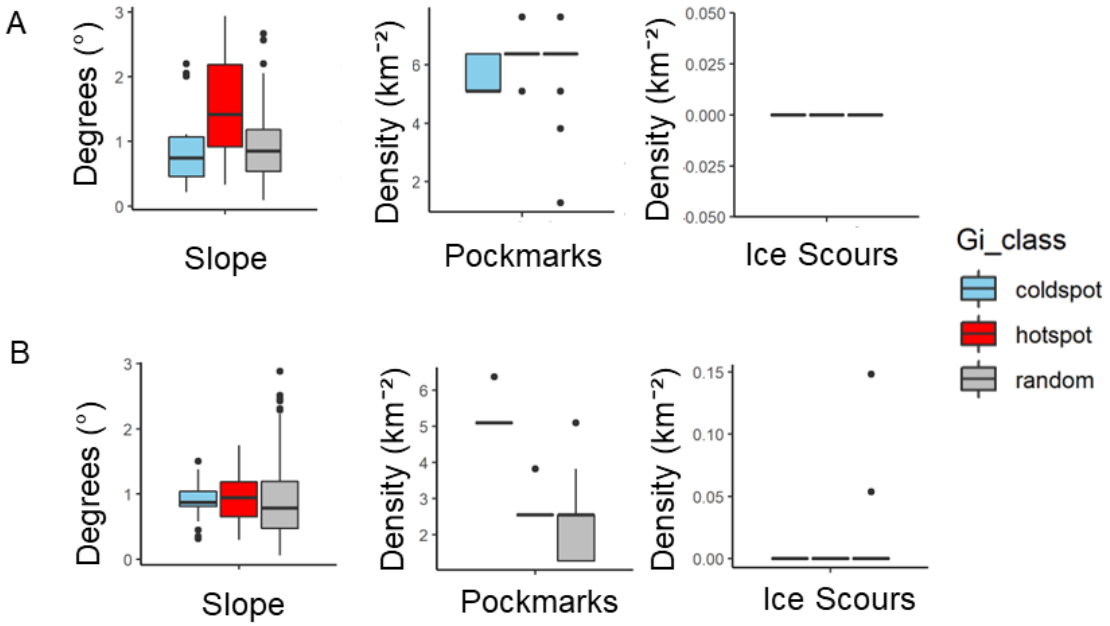

Figure 4.5 Boxplots showing environmental variables (slope based on 20 m bathymetry, pockmark and ice scour density) at each of station-level *Gi** hotspots, coldspots, and random locations for *Pennatula* sp. 2 at A) station 2 and B) station 4. Median with inter-quartile range (25th–75Th percentile), whiskers show the smallest and largest values within 1.5 times the inter-quartile range). For station 2 neighbourhood distance was ~27 m with n=74 images in hotspots, n=41 in coldspots, n=371 in random locations. For station 4, neighbourhood distance was 46 m (*K*-neighbour averaging for 25 neighbours) with n=44 images in hotspots (including 11 with zero-abundance), n=32 in coldspots, n= 435 in random.

4.4.6 Patterns of Patch Size Among Taxa and Transect Pairs

We determined patch size for some taxon-station combinations, when the first 10-m distance class of the spatial correlograms was significantly positive at the transect level (Table 4.4, and Appendix Figure AII.13 & Table AII.4 for example spatial correlogram) and patch size varied by taxon and transect pair. For example, patch size for *Pennatula* sp. 2 at station 2 was ~16–19 m on some transects (AB and CD), but ~7 m on others (EF and GH), whereas at station 4 patch size was ~7 m (EF) or ~10 m (GH) (Table 4.4). For

Hexacorallia (SC.) spp. at station 2, patch size of ~19 m (AB) and 155 m (CD) were identified. We could not determine patch size when the first distance was not significantly autocorrelated or was negatively autocorrelated, as this may result from an insufficient image size or sampling design to detect the pattern. Alternatively, significant negative autocorrelation at 10 m (e.g., Pennatuloidea (SF.) sp. 9 at station 2, transect pair EF) was uncommon in our study but could also imply spatial heterogeneity/dispersion (Appendix Table AII.4 & AII.5).

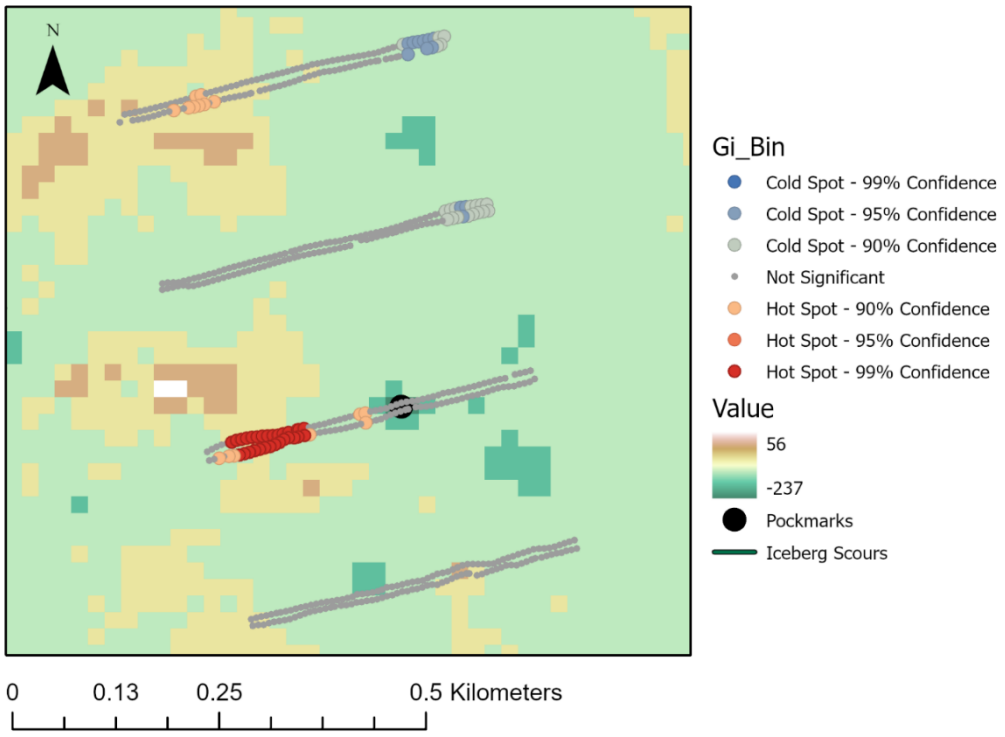

Figure 4.6 Bathymetry position index showing fine-scale features, with inner radius 1 cells and outer radius 25, scale factor 500 m, at station 4 with *Pennatula* sp. 2 station-level hotspots and coldspots overlaid (46 m fixed distance for 25 neighbours), with pockmark/pit center location (unknown size) and absence of ice scours. Based on geomorphic features and 20 m bathymetry from Lacharité et al., (2020).

Table 4.4 Summary results from spatial correlograms performed separately for each taxon-station combination and transect pair. Only showing those with significant positive spatial autocorrelation for the first distance class (mean distance presented in meters), associated Global Moran *I* and probability values using α=0.05. Patch size, also known as spatial range, is the distance of the interpolated *x*-intercept from the spatial correlograms using the *ncf* r package.

Station	Transect Pair	Taxon	Mean of Distance Class (m)	Global Moran *I*	Probability value	Patch Size* (m)
3	EF	*Edwardsia* sp. 1	6.93	0.16	0.01	24.53
5	EF	*Edwardsia* sp. 1	6.52	0.19	0.03	7.62
13	AB	Anthozoa (C.) spp.	6.97	0.19	0.03	8.63
16	CD	Anthozoa (C.) spp.	6.36	0.23	0.02	7.61
3	GH	*Actinauge cristata*	6.90	0.20	0.01	20.13
2	AB	*Pennatula* sp. 2	6.50	0.44	0.01	18.77
2	CD	*Pennatula* sp. 2	6.80	0.32	0.01	16.43
2	EF	*Pennatula* sp. 2	6.74	0.38	0.01	7.17
2	GH	*Pennatula* sp. 2	6.46	0.50	0.01	6.68
3	EF	*Pennatula* sp. 2	6.93	0.37	0.01	7.15
4	GH	*Pennatula* sp. 2	7.28	0.15	0.03	9.84
2	AB	Hexacorallia (SC.) spp.	6.50	0.44	0.01	18.93
2	CD	Hexacorallia (SC.) spp.	6.80	0.26	0.01	155.05

Note: * Patch size ~10 m, can be interpreted as a patch that includes immediate neighbouring images; if > 10 m, patch extends farther.

4.5 Discussion

We examined fine-scale spatial changes in abundance for 8 focal benthic taxa at 7 stations across the LC MPA, at the broader scale of station and the finer scale of paired transects. At the scale of station (spatial extent, including area between transects: 0.256 km^2), 6 taxon-station combinations showed significant positive autocorrelation at neighbourhood distances of meters to 10s of meters. In some cases, local spatial statistics were required to detect spatial structure and reveal significantly higher abundance than

the mean abundance for the area (aggregations) or higher than the local neighbourhood (spatial outliers). For each taxon-station, these aggregations may correspond to important spatial processes that have occurred at the selected optimal scale of analysis. At the scale of paired transects (spatial extent, including area between transects: 0.004 km^2), we only identified a few small aggregations with patchiness between some neighbouring images occurring at 1–10 m distances. Some patches of benthic taxa extended ~7–27 m, and in one case ~155 m, but patch sizes were variable among taxa within stations and for the same taxon among transect pairs. Overall, there was significant fine-scale spatial structure for several but not all benthic taxa in the LC MPA, and these different patterns were likely caused by underlying spatial processes. Significant station-level hotspots and coldspots had overall little overlap among taxa. In addition, patterns were not directly comparable between taxa due to different neighbourhood distances.

Using the local Moran *I* and *Gi** statistics, we identified significant local spatial patterns in deep-water coral communities, based on changes in abundance and fine-scale aggregations (0–10s of meters), at multiple sampling stations across a large region of the LC MPA (1000s of km^2). Hotspots and coldspots have also been identified for sponges and live deep-water corals, mainly *L. pertusa* and *M. oculata* using the *Gi** statistic, on a coral mound in the Porcupine Seabight, NE Atlantic (~ 40 × 60 m spatial extent) at a similar scale as ours (0–10s of meters) (Conti et al., 2019). On the same coral mound, point pattern analysis revealed non-random distributions for corals (Price et al., 2021). Off the continental shelf of California, *Gi** hotspots and coldspots were identified for some sea pens and other deep-water corals, at much larger neighbourhood distances of 1000s of meters and over a larger spatial extent, a depth range of 24–863 m (Watters et

al., 2022). Additionally, contagious (aggregated) sea pen distributions have been identified for *Pennatula aculeata* in the Gulf of Maine, for image sizes of 7, 3, and 1.24 m^2 (Langton et al., 1990). However, local spatial patterns may be species-specific or vary by location and depth.

4.5.1 Potential Causes for Spatial Structure

The local hotspots and coldspots of different sizes may be attributable to differences in suitable habitat for a particular taxon. For example, Hexacorallia (SC.) spp. and *Pennatula* sp. 2 were present throughout station 2 with hotspots concentrated in the northern part and coldspots in the southern part of the station, and on opposite ends of the transect pairs. Therefore, we inferred that spatial processes likely varied throughout the station. A combination of environmental, biological, and anthropogenic factors may have caused these patterns.

4.5.1.1 Environmental Factors

Although environmental data for the LC MPA were scarce, there was some evidence that geological factors, such as BPI, benthoscape, pockmarks and slope, were related to the ecological spatial patterns. We propose that the faunal spatial patterns we observed at the station level (0.256 km^2) were likely caused by environmental factors. At station 4, the coldspots of *Pennatula* sp. 2 appeared associated with lower BPI (scalefactor 500 m) and higher pockmark density (km^{-2}). In contrast, on the Scottish west coast, distributions of three species of sea pen were not related to BPI (unspecified scalefactor, > 200 m due to resolution) (Greathead et al. 2015). However, in Alaska, the presence of the sea pen *Ptilosarcus gurneyi* was related to greater TPI (scalefactor

unknown, > 100 m due to bathymetry) (Sigler et al., 2023). BPI/TPI was retained as an important variable in model distributions of sea pens in Norway (unknown scalefactor; Ross et al., 2021), and various corals in Northeast Pacific region of Canada (1000 m, 5000 m, 10000 m, and 20000 m; Chu et al., 2019). The occurrence of other corals and megafauna have also been correlated with BPI/TPI at different scales in other deep-sea environments, suggesting that local processes and geology may lead to different scale-dependant patterns (e.g. Georgian et al., 2021; Pearman et al., 2022). More research on BPI at various scales is needed to understand its potential influence on spatial patterns.

In our study, most stations included a single benthoscape class and thus similar geological characteristics throughout. However, at station 4 there were two benthoscape classes that may explain the spatial patterns of *Pennatula* sp. 2, possibly because of fine-scale geological variations in pockmark density, slope, or other unknown factors. Pockmarks are craters created by gas/fluid currently or historically escaping from the sediments, they can act as sediment traps (Fader, 1991; Lacharité et al., 2020; Ramos et al., 2020; Webb et al., 2009) and have been associated with epibenthic megafauna, such as sea pens, cerianthids, annelids (Somoza et al., 2021; Sumida et al., 2004; Webb et al., 2009).

Other features that occur at the center of pockmarks (coarser sediment, presence of carbonate precipitates, and possibly altered currents) may provide a refuge for benthic taxa from predators and fishing gear (Webb et al., 2009). For example, at station 2, hotspots of *Pennatula* sp. 2 appeared to be located near the center of two pockmarks/pits (which can be difficult to distinguish), but there were no pockmark/pit centers in the immediate area of the hotspots of Hexacorallia (SC.) spp. The distributions of other deep-

water corals on the continental slope off Nova Scotia (Bryan & Metaxas, 2006) were related to slope. In our study, despite the small range in slope, it appeared to impact *Pennatula* sp. 2 at station 2. Lastly, ice scours varied at some stations, but their effect in the LC MPA is uncertain. Increased epifaunal density has been associated with coarse sediment at the edges of ice scour features (Jones et al., 2007). Other environmental variables not accounted for in this study may also contribute to the spatial patterns we observed in the LC MPA, but environmental data on similarly fine scales are not available to our knowledge.

In our study, substrate might explain the observed spatial patterns for Hexacorallia (SC.) spp. and *Pennatula* sp. 2 at station 2. In Hudson canyon (NW Atlantic), sponges, zoanthids and cup corals were associated with coarse-grained sediments, and sea pens with deep muddy areas (Pierdomenico et al., 2017). Sea pen presence in the LCA MPA was associated with enhanced ammonium efflux likely the result of bioturbation, with stations 14, 13, and 2 having the highest quantities of food (total organic matter/carbon) (Miatta & Snelgrove, 2021, 2022).

4.5.1.2 Biological Factors

Biological factors, such as those related to reproduction (spawning, settlement, and self-recruitment), may have also caused some of the observed spatial patterns, such as the hotspots and coldspots for *Pennatula* sp. 2 at stations 2 and 4. It is possible that the local hotspots for some coral taxa in the LC MPA are a consequence of gregarious settlement. Aggregations of *P. aculeata* may reflect optimal spacing to combine non-competitive feeding based on local currents, density required for effective spawning and

fertilization in the water column, and optimal hydrodynamic and sediment characteristics for settlement (Langton et al., 1990). In turn, coldspots could be the result of competition among benthic taxa for food resources, possibly explaining the spatial pattern of the hotspots and coldspots of Hexacorallia (SC.) spp. and *Pennatula* sp. 2 at station 2. We propose that the patterns we observed at the transect level were likely caused by biological factors, but due to the nested scales, biological factors could have also impacted patterns at the station level.

4.5.1.3 Implications for Monitoring

Our study identified sources of small-scale variability that should be considered during monitoring of biodiversity. Spatial heterogeneity is likely to increase with the size of the area to be monitored, underpinned by different local ecological processes occurring on fine scales. Collection of baseline data and monitoring should ensure that those local scale processes can be captured. For example, positive and negative impacts of protection in different regions of an MPA can lead to an averaged net effect of zero change and misrepresent the conservation outcome.

To effectively capture spatial patterns, processes, and species of interest on most spatial scales, a standardized sampling design is necessary. For example, we showed that several parallel transects were required to detect local hotspots. In addition, a larger number of images with different spatial lags (~ 6-m spacing target with transects 10 or 200 m apart) allowed us to determine patch size for some taxa-stations, but not all. Therefore, fine-scale case studies are useful to refine a sampling design appropriate for a particular species of interest.

4.5.2 Limitations

Sampling design, including sample size (number of images), sampling unit size (image dimensions), and their arrangement throughout the study area, can impact the power of spatial statistics and the detection of significant spatial patterns (Dale & Fortin, 2014). Therefore, a rejected null hypothesis (e.g., Global Moran's *I* being not significantly different from random) could result from a sampling design that is inappropriate for detecting the underlying pattern, rather than actually representing a random pattern. Since the space between images and transects was not analyzed, we assumed that the neighbouring area had a similar pattern (i.e., hotspots likely extend between images), which was reasonable given the small distance interval of ~10 m. In addition, these spatial statistics were not directly comparable across taxa within or between stations, as they were computed with different fixed distances. However, these neighbourhood distances were selected as they reflect prominent spatial processes for specific taxon, providing some insight into their ecology. Our results lacked significant Moran's *I* values at multiple spatial lags, therefore prevented further interpretation of patterns using the shape of the correlograms, such as gradients and repetition in patches (Dale & Fortin, 2014). Overall, limitations were a result of challenges with sampling and performing analyses across a large study area, due to the trade-off between a large spatial extent and high spatial resolution. In addition, the environmental data provided a single snapshot in time and while adequate for providing context, a monthly-sampled long-term time series would be more representative of the conditions and fluctuations relevant to ecological processes (e.g., seasonal changes in food sources).

4.5.3 Conclusion and Significance

Using global and local spatial statistics, we quantify significant fine-scale spatial patterns for benthic taxa in the Laurentian Channel MPA at different resolutions. To our knowledge, ours is one of the first objective assessments of fine scale epifaunal patterns in the deep sea. Few studies performed similar fine-scale spatial analyses of epifauna (Conti et al., 2019; Price et al., 2021; Watters et al., 2022), limiting our ability to interpret and generalize patterns attributed to the processes that occur at fine-scales. While presence and summary statistics (e.g., relative or mean abundance) are valuable, our approach assessed significant clustering and changes in abundance using statistical inference and estimating confidence levels. Additional environmental data, at similarly fine scales, could allow for further interpretation and insight into the ecology and biology of these taxa.

Our research has implications for developing appropriate sampling designs for deep-sea ecology and conservation research at similarly fine scales. Broader scale analyses (e.g., using trawl data) assume uniform or random fine-scale distribution patterns and are thus biased, leading to inaccuracies in abundance (e.g. Chimienti et. al 2018b; de Mendonça & Metaxas, 2021). Misinterpretation of fine-scale patterns can result in ineffective sampling, failure to detect the species of interest, and inability to establish accurate metrics for assessing temporal changes in deep-sea communities. Fine-scale spatial analyses can reveal the ecological processes, such as species associations, predation, and competition that give rise to observed spatial patterns. Studies such as ours illustrate the need for further research at different scales of analysis and spatial extents to expand our understanding of deep-sea communities.

CHAPTER 5

CONCLUSIONS AND RECOMMENDATIONS FOR DEVELOPING A MONITORING FRAMEWORK IN THE DEEP SEA

Our understanding of ecology in the deep sea, including community structure, spatial patterns, and environmental factors for epibenthic megafauna (invertebrates > 2 cm) is generally lacking. This thesis contributed towards: understanding sampling bias for different sampling tools (ROV, drop camera, and trawl); the impact of spatial scale and resolution on ecological indicators (i.e. diversity, numerical abundance, and environmental drivers); applying methods for quantifying patch size and other spatial patterns at large and fine scales; and a discussion of spatial drivers (environmental or biological factors) that may have generated these patterns. Overall, I characterized and interpreted the ecology of macro-epibenthic assemblages in the Laurentian Channel Marine Protected Area, with implications on effective sampling designs to support research and monitoring in deep-sea ecosystems.

Appropriate sampling tools and resolution are needed for accurate measures of abundance and diversity, and reliable spatial comparisons. I compared three commonly used tools (ROV, drop camera and trawl) for sampling epibenthic megafauna and highlighted their benefits (e.g. efficiency to capture megafauna) and trade-offs (e.g. sampling time) (**Chapter 2**). The ROV had the least disturbance, highest positioning accuracy, and continuous sampling that is ideal for quantifying spatial structure and for species association analyses. However, taxon-specific bias occurred at one station (LC5),

where the drop-camera captured higher abundance for two taxa (*Edwardsia* sp. 1 and *Pennatula* sp. 2) and higher diversity with lower sampling effort than the ROV. I quantified community structure and large-scale spatial patterns using imagery from an ROV and a drop camera (**Chapter 3**), which were more efficient at capturing invertebrates than trawls (**Chapter 2**). I found that increased sampling effort (i.e. over 1000 m^2) is needed to fully estimate diversity (**Chapter 3**). A standardized high resolution transect array, obtained with the highly maneuverable ROV, enabled me to examine 3 nested spatial scales [levels: station (~ 0.256 km^2), paired transects (~ 0.004 km^2), and image (mean area of 0.73 ± 0.009 m^2 to 2.40 ± 0.63 m^2)] to quantify fine-scale aggregations and patchiness with local and global spatial statistics (i.e. global/local Moran *I* and *Gi**) (**Chapter 4**). I also assessed sampling resolution bias using ROV data with adjusted spacing between images (7, 14, 21, and 28 m) (**Chapter 3**). I revealed changes in composition (i.e. species richness and abundance) with different sampling resolutions, which were particularly important for diverse assemblages with overall lower abundance. Therefore, sampling designs with higher spatial resolution (e.g. multiple transects and images closer together) are better for representing diverse assemblages.

To gain insight into ecological processes, I quantified spatial patterns in diversity and abundance on large (100s m – 100s km) and fine (0 –100s m) scales. Imagery and trawl captured counter-intuitive epifaunal patterns (i.e. opposed the assumption that higher biomass equates to higher numerical abundance), where one station (LC2) had high numerical abundance and low biomass of sea pens, while the other (LC5) had low numerical abundance and high biomass (**Chapter 2**). Large-scale spatial analyses (100s m – 100s km) revealed a patchy community structure in the LC MPA, exhibiting

similarities within 10 km but potential differences at greater distances (**Chapter 3**). Three types of assemblages were documented: (1) dominated by the corals *Pennatula* sp. 2 and/or Hexacorallia (SC.) spp. in shallow eastern benthoscape classes (A2 and TZ1) with high abundance and low diversity; (2) a diverse mix of taxa (e.g. sea pens and sea anemones/cerianthids) in deeper (> 400 m) western benthoscapes (A1, C1, and C2), with low abundance and high diversity; and (3) a unique sponge dominated assemblage (benthoscape class B1). At fine-scales (0–100s m), local station-level hotspots/aggregations occurred (e.g., *Pennatula* sp. 2 and Hexacorallia (SC.) spp.) with variable patch sizes at the transect level (~7–27 m, and in one case ~155 m), and for some taxa at the image level (<10 m) (**Chapter 4**). Overall, fine-scale patterns were taxon-specific and sometimes varied for the same taxon on different transects. Therefore, sampling designs should consider spatial patterns to ensure that species of interest are captured.

Environmental and biological factors provided ecological context for megafaunal spatial patterns. In **Chapter 2**, differences in epifaunal patterns (biomass and numerical abundance) were likely related to biological factors such as size and morphology of individuals/taxa. For example, small sizes were underestimated with trawls and larger sea pen species showing high biomass despite low abundance. Spatial scales of potentially important drivers were identified for assemblage patterns at the regional level (10 km; **Chapter 3**) and taxon-specific patterns at the station level (neighborhood sizes 15–58 m; **Chapter 4**). Overall, regional community structure included three main types of assemblages associated with benthoscape classes (**Chapter 3**), a potential proxy for geological features (i.e. pockmarks and ice scours) and/or covariates (i.e. depth, slope,

circulation, sediment composition, food, or other factors). Eight taxa contributed to differences between and within each type of assemblage (Top 3: Hexacorallia (SC.) spp., *Kophobelemnon* spp., and *Actinauge cristata*), and thus are potential indicator taxa. These included several sea pens that likely have a functional role, and specific sea pens (i.e. *Anthoptilum* spp. and *Kophobelemnon* spp.) were associated with more diverse communities than others (i.e. *Pennatula* sp. 2). Future research on species associations may help gain insight into the taxonomic relationships at different stations. Some environmental (e.g. BPI, benthoscape, slope, and pockmarks) and biological factors (e.g. reproduction and species associations) likely contributed to local hotspots/coldspots, with biological factors likely important for patchiness at the transect and image scales (**Chapter 4**). To further investigate spatial drivers, environmental and biological data are needed at the scales relevant to significant spatial patterns.

In this thesis, I demonstrated a novel approach to spatial analysis in deep-sea ecosystems. Significant spatial structure was quantified at large (100s m – 100s km) and fine (0 – 100s m) scales from high resolution imagery. Spatial patterns and associated environmental or biological drivers gave insight into ecology, including baseline distributions and community structure, relevant to assessing the effectiveness of MPAs. I found that community measures of abundance and diversity were sensitive to tool-specific bias and sampling resolution (i.e. sample size, number of transects, and spacing). Appropriate sampling designs that consider spatial patterns will lead to improved representation of deep-sea epibenthic megafauna (e.g. composition, diversity, and abundance), facilitating comparisons over time and between regions. From this thesis,

several recommendations have emerged for sampling designs in deep-sea ecosystems, supporting ecological research and future monitoring efforts.

5.1 Recommendations

Due to spatial structure at different scales (0 – 100s m and 100s m –100s km), sampling designs should consider sampling bias, representativity, and replication for accurate community measurements and robust statistics. For the LC MPA specifically, Fisheries and Oceans Canada (DFO) have proposed several different tools and ecological indicators for monitoring (DFO, 2015; Neves et al., 2021). However, sampling bias and protocols need to be assessed before a particular tool or indicator is applied (e.g. Neves et al., 2023 and in this thesis). Sensitivity analyses must be performed for each tool due to tool-specific bias. For example, trawls are a routinely used tool for monitoring but can have substantial sampling bias, counter-intuitive patterns, and are highly destructive, possibly negatively impacting populations and confounding results. ROVs and drop cameras are both recommended for characterizing epibenthic megafauna, capturing multiple parameters, such as abundance, species richness, diversity, relative size, species associations, and patch size/spatial distribution patterns. However, offsetting sampling areas within a station/zone when sampling in consecutive years would help avoid bias caused by any tool (i.e. destruction). Size-frequency distributions and biomass can help assess population dynamics and recovery potential, but are challenging to obtain from imagery, due to taxon behaviours (contraction, retraction, and orientation) and lack of an appropriate 3D scale. However, studies on biometric relationships (e.g. counting polyp leaves; Chimienti et al., 2019) and 3D reconstructions (e.g. photogrammetry; de Oliveira

et al., 2021) may resolve part of this issue and aid in the assessment of size and recruitment. Standardized designs with high positional accuracy and georeferencing can be performed with highly maneuverable and continuous sampling tools (e.g. ROV videos compared to discrete sampling with Campod images), enabling high quality data (e.g. sample replacement while maintaining high resolution) and analyses on fine-scale spatial patterns and species associations.

To be representative of taxa and assemblages, sampling designs should ensure adequate sample size and effort (e.g. number of stations, transects, and images), stratified by habitats and scaled by area (i.e. more stations for larger habitats were assemblage patterns likely have spatial variations). Depth-stratified designs may not be representative, as deeper assemblages (> 400 m) have variable community structure, while shallow assemblages have variable abundance. Benthoscape classes could be useful for planning future sampling locations, as a proxy for different habitat types/co-variates, to ensure that the full diversity of habitats and assemblages are monitored. When using reference sites outside an MPA, comparable areas (e.g. similar benthoscape/habitat) are needed for each type of assemblage. In addition, due to taxon-specific patterns, some spatial analyses (e.g. patchiness and community structure) may need to be performed for individual taxa to be meaningful, rather than for entire functional groups (e.g. all sea pens or all corals).

I used a high-resolution, systematic, cluster design with multiple spatial lags, which is recommended to detect unknown spatial patterns and processes at different scales (Legendre & Fortin, 1989). For macro-epifaunal assemblages in the LC MPA specifically, I recommend spacing between images be ~ 7 m with station and transect

replicates per habitat, i.e. a few stations with > 2 transects spaced at 400 m, which would likely detect local aggregations. In addition, sample sizes of more than 1000 m^2 (per site/station) are suggested to capture abundance and diversity of megafauna. Due to spatial structure, stations should be spaced at least 10 km apart to capture the range of assemblages, but replicates (i.e. multiple transects) <10 km apart are required to avoid skewing estimates of abundance, diversity, and patchiness. Monitoring in subsequent years, should also be < 10 km from the targeted assemblage. Overall, sampling resolution and spatial lags should capture all targeted indicators/parameters and allow for sample replacement or subsampling. Further, designs with multiple spatial lags can be utilized for a wide range of analyses, for example some lags can be applied for spatial analyses that require spatial autocorrelation and subsampled for statistics that require independence.

Monitoring recovery or changes in epibenthic megafauna may take a long time (e.g. > 5-10 years for sea pens) (DFO, 2017b; Neves et al., 2015). However, preliminary/interim studies (e.g. statistical power analysis and spatial statistics) should be used to optimize monitoring sampling designs (i.e. tool, resolution, sample size, replicates, and spatial extent) that are appropriate to perform the desired analyses, and thus assess conservation objectives with confidence. The spatial statistics applied in this thesis may be performed with variables other than abundance and at various scales including the MPA network-level. Monitoring frameworks for individual MPAs could aim to incorporate multi-scale sampling designs and comprehensive data collection (i.e. a range of indicators) that may be scaled-up (e.g. by benthoscapes) to help design/assess the anticipated MPA networks.

REFERENCES

Abdi, H., and Williams, L. J. (2010). Tukey 's Honestly Signiflcant Difference test (HSD). In N. Salkind (Ed.), Encyclopedia of Research Design (Issue 3). Sage. https://www.researchgate.net/publication/237426041

Abràmoff, M. D., Magalhães, P. J., and Ram, S. J. (2004). Image processing with imageJ. Biophotonics Int., 11:7, 36–41. doi:10.1117/1.3589100

Adams, P. B., Butler, J. L., Baxter, C. H., Laidig, T. E., Dahlin, K. A., and Wakefield, W. W. (1995). Population estimates of Pacific coast groundfishes from video transects and swept-area trawls. Fish. Bull., 93:3, 446–455. doi:10.1016/j.simpat.2011.09.002

Aguzzi, J., Chatzievangelou, D., Marini, S., Fanelli, E., Danovaro, R., Flögel, S., Lebris, N., Juanes, F., De Leo, F. C., Del Rio, J., Thomsen, L., Costa, C., Riccobene, G., Tamburini, C., Lefevre, D., Gojak, C., Poulain, P. M., Favali, P., Griffa, A., … Company, J. B. (2019). New High-Tech Flexible Networks for the Monitoring of Deep-Sea Ecosystems. Environ. Sci. Technol., 53:12, 6616–6631. doi:10.1021/acs.est.9b00409

Ambroso, S., Dominguez-carrió, C., Grinyó, J., López-González, P. J., Gili, J.-M., Purroy, A., Requena, S., and Madurell, T. (2013). In situ observations on withdrawal behaviour of the sea pen Virgularia mirabilis. Mar. Biodivers., 43, 257–258. doi:10.1007/s12526-013-0172-5

Anderson, M. J. (2001). A new method for non-parametric multivariate analysis of variance. Austral Ecol., 26:1, 32–46. doi:10.1111/j.1442-9993.2001.tb00081.x

Anselin, L. (1995). Local Indicators of Spatial Association—LISA. Geogr. Anal., 27:2, 93–115. doi:10.1111/j.1538-4632.1995.tb00338.x

Auster, P. J., Lindholm, J., & Valentine, P. C. (2003). Variation in habitat use by juvenile Acadian redfish, Sebastes fasciatus. Environ. Biol. Fishes, 68:4, 381–389. doi:10.1023/B:EBFI.0000005751.30906.d5

Auster, P. J., Gjerde, K., Heupel, E., Watling, L., Grehan, A., and Rogers, A. D. (2011). Definition and detection of vulnerable marine ecosystems on the high seas: Problems with the “move-on” rule. ICES J. Mar. Sci., 68:2, 254–264. doi:10.1093/icesjms/fsq074

Ayma, A., Aguzzi, J., Canals, M., Lastras, G., Bahamon, N., Mecho, A., and Company, J. B. (2016). Comparison between ROV video and Agassiz trawl methods for sampling deep water fauna of submarine canyons in the Northwestern Mediterranean Sea with observations on behavioural reactions of target species. Deep. Res. Part I Oceanogr. Res. Pap., 114, 149–159. doi:10.1016/j.dsr.2016.05.013

Baco, A. R., Roark, E. B., and Morgan, N. B. (2019). Amid fields of rubble, scars, and lost gear, signs of recovery observed on seamounts on 30- To 40-year time scales. Sci. Adv., 5:8, 1–7. doi:10.1126/sciadv.aaw4513

Baillon, S., Hamel, J. F., Wareham, V. E., & Mercier, A. (2012). Deep cold-water corals as nurseries for fish larvae. Front. Ecol. Environ., 10:7, 351–356. doi:10.1890/120022

Baillon, S., Hamel, J. F., & Mercier, A. (2014a). Diversity, distribution and nature of faunal associations with deep-sea pennatulacean corals in the northwest Atlantic. PLoS One, 9:11, 14–16. doi:10.1371/journal.pone.0111519

Baillon, S., Hamel, J. F., Wareham, V. E., & Mercier, A. (2014b). Seasonality in reproduction of the deep-water pennatulacean coral Anthoptilum grandiflorum. Mar. Biol., 161:1, 29–43. doi:10.1007/s00227-013-2311-8

Bak, R. P. M., and Meesters, E. H. (1998). Coral population structure: The hidden information of colony size-frequency distributions. Mar. Ecol. Prog. Ser., 162, 301–306. doi:10.3354/meps162301

Baker, F. B., & Hubert, L. J. (1975). Measuring the power of hierarchical cluster analysis. J. Am. Stat. Assoc., 70:349, 31–38. doi:10.1080/01621459.1975.10480256

Baker, K. D., Wareham, V. E., Snelgrove, P. V. R., Haedrich, R. L., Fifield, D. A., Edinger, E. N., & Gilkinson, K. D. (2012). Distributional patterns of deep-sea coral assemblages in three submarine canyons off Newfoundland, Canada. Mar. Ecol. Prog. Ser., 445, 235–249. doi:10.3354/meps09448

Barnes, R. S. K., & Hamylton, S. M. (2019). Isometric scaling of faunal patchiness: Seagrass macrobenthic abundance across small spatial scales. Mar. Environ. Res., 146:December 2018, 89–100. doi:10.1016/j.marenvres.2019.03.011

Beazley, L. I., Kenchington, E. L., Murillo, F. J., & Sacau, M. (2013). Deep-sea sponge grounds enhance diversity and abundance of epibenthic of epibenthic megafauna in the Northwest Atlantic. ICES J. Mar. Sci., 70, 1471–1490.

Bennecke, S., Kwasnitschka, T., Metaxas, A., and Dullo, W. C. (2016). In situ growth rates of deep-water octocorals determined from 3D photogrammetric reconstructions. Coral Reefs, 35:4, 1227–1239. doi:10.1007/s00338-016-1471-7

Bennecke, S., and Metaxas, A. (2017). Effectiveness of a deep-water coral conservation area: Evaluation of its boundaries and changes in octocoral communities over 13 years. Deep. Res. Part II Top. Stud. Oceanogr., 137, 420–435. doi:10.1016/j.dsr2.2016.06.005

Ben-Said, M. (2021). Spatial point-pattern analysis as a powerful tool in identifying pattern-process relationships in plant ecology: an updated review. Ecol. Process., 10:1. doi:10.1186/s13717-021-00314-4

Benjamini, Y., & Hochberg, Y. (1995). Controlling the False Discovery Rate: A Practical and Powerful Approach to Multiple Testing. J. R. Stat. Soc. Ser. B, 57:1, 289–300.

Bjornstad, O.N. (2020). ncf: Spatial Covariance Functions. R package version 1.2-9.https://CRAN.R-project.org/package=ncf

Borcard, D., & Legendre, P. (2012). Is the Mantel correlogram powerful enough to be useful in ecological analysis? A simulation study. Ecology, 93:6, 1473–1481. doi:10.1890/11-1737.1

Boteler, B., Johnson, D. E., & Gunn, V. K. (2023). Science for the Kunming-Montreal Global Biodiversity Framework in the Atlantic Ocean region: An iAtlantic perspective. IAtlantic Policy Br., *November*. doi:10.5281/zenodo.10203890

Boulard, M., Lawton, P., Baker, K., & Edinger, E. (2023). The effect of small-scale habitat features on groundfish density in deep-sea soft-bottom ecosystems. Deep. Res. Part I Oceanogr. Res. Pap., 193:October 2022, 103891. doi:10.1016/j.dsr.2022.103891

Brown, C. J., Sameoto, J. A., & Smith, S. J. (2012). Multiple methods, maps, and management applications: Purpose made seafloor maps in support of ocean management. J. Sea Res., 72, 1–13. doi:10.1016/j.seares.2012.04.009

Bryan, T. L., & Metaxas, A. (2006). Distribution of deep-water corals along the North American continental margins: Relationships with environmental factors. Deep. Res. Part I Oceanogr. Res. Pap., 53:12, 1865–1879. doi:10.1016/j.dsr.2006.09.006

Caldas de Castro, M., & Singer, B. H. (2006). Controlling the false discovery rate: A new application to account for multiple and dependent tests in local statistics of spatial association. Geogr. Anal., 38:2, 180–208. doi:10.1111/j.0016-7363.2006.00682.x

Canadian Scientific Submersible Facility (CSSF). (1995-2020). ROPOS Technical Sheet: ROPOS Specifications Retrieved from http://www.ropos.com/index.php/ropos-rov/ropos-specifications (accessed on 01/29/2019).

Chimienti, G., Angeletti, L., and Mastrototaro, F. (2018a). Withdrawal behaviour of the red sea pen pennatula rubra (Cnidaria: Pennatulacea). Eur. Zool. J., 85:1, 64–70. doi:10.1080/24750263.2018.1438530

Chimienti G., Angeletti L., Rizzo L., Tursi A., M. F. (2018b). ROV vs trawling approaches in the study of benthic communities: the case of Pennatula rubra (Cnidaria: Pennatulacea). J. Mar. Biol. Assoc. United Kingdom, (in press), 1–11. doi:10.1017/S0025315418000851

Chimienti, G., Di Nisio, A., Lanzolla, A. M. L., Andria, G., Tursi, A., and Mastrototaro, F. (2019). Towards non-invasive methods to assess population structure and biomass in vulnerable sea pen fields. Sensors (Switzerland), 19:10, 1–12. doi:10.3390/s19102255

Chu, J. W. F., Nephin, J., Georgian, S., Knudby, A., Rooper, C., & Gale, K. S. P. (2019). Modelling the environmental niche space and distributions of cold-water corals and sponges in the Canadian northeast Pacific Ocean. Deep. Res. Part I Oceanogr. Res. Pap., 151:March, 103063. doi:10.1016/j.dsr.2019.06.009

Clark, S. H. (1979). Application of Bottom-Trawl Survey Data to Fish Stock Assessment. Fisheries, 4:3, 9–15. doi:10.1577/1548-8446(1979)004<0009:aobsdt>2.0.co;2

Clarke, K. R. (1993). Non-parametric multivariate analyses of changes in community structure. Aust. J. Ecol., 18:1, 117–143. doi:10.1111/j.1442-9993.1993.tb00438.x

Conti, L. A., Lim, A., & Wheeler, A. J. (2019). High resolution mapping of a cold water coral mound. Sci. Rep., 9:1, 1–15. doi:10.1038/s41598-018-37725-x

Couillard, C. M., Sainte-Marie, B., & Dionne, H. (2021). Late maturity and evidence for female biennial spawning in the sea pen Pennatula aculeata (Anthozoa, Pennatulacea) in eastern Canada. Invertebr. Biol., 140(4), e12351.

Dale, M. R. T., and Fortin, M.-J. (2014). Spatial analysis : a guide for ecologists (2nd ed.). Cambridge University Press. doi:10.1016/B978-0-444-53868-0.50013-7

Danovaro, R., Aguzzi, J., Fanelli, E., and Smith, C. R. (2017). An ecosystem-based deep-ocean strategy. Science (80-.)., 355:6324, 452–454.

Danovaro, R., Corinaldesi, C., Dell'Anno, A., and Snelgrove, P. V. R. (2017). The deep-sea under global change. Curr. Biol., 27:11, R461–R465. doi:10.1016/j.cub.2017.02.046

De Clippele, L. H., Buhl-Mortensen, P., & Buhl-Mortensen, L. (2015). Fauna associated with cold water gorgonians and sea pens. Cont. Shelf Res., 105, 67–78. doi:10.1016/j.csr.2015.06.007

de Mendonça, S. N., & Metaxas, A. (2021). Comparing the Performance of a Remotely Operated Vehicle, a Drop Camera, and a Trawl in Capturing Deep-Sea Epifaunal Abundance and Diversity. Front. Mar. Sci., 8:631354. doi:10.3389/fmars.2021.631354

de Mendonça, S. N., & Metaxas, A. (2024). Fine-scale spatial patterns of deep-sea epibenthic fauna in the Laurentian Channel Marine Protected area. Deep Sea Res. Part I Oceanogr. Res. Pap., 203, 104195. doi:10.1016/j.dsr.2023.104195

de Oliveira, L. M. C., Lim, A., Conti, L. A., & Wheeler, A. J. (2021). 3D Classification of Cold-Water Coral Reefs: A Comparison of Classification Techniques for 3D Reconstructions of Cold-Water Coral Reefs and Seabed. Front. Mar. Sci., 8:March, 1–19. doi:10.3389/fmars.2021.640713

DFO (Fisheries and Oceans Canada), (2012). Assessment of the Laurentian Channel Area of Interest: A Risk Characterization. https://waves-vagues.dfo-mpo.gc.ca/library-bibliotheque/40619072.pdf

DFO (Fisheries and Oceans Canada), (2015). Monitoring Indicators, Protocols and Strategies for the Proposed Laurentian Channel Marine Protected Area (MPA). DFO Can. Sci. Advis. Sec. Sci. Advis. Rep, *2014/049*.

DFO (Fisheries and Oceans Canada), (2017a). Guidance on the level of protection of significant areas of coldwater corals and sponge-dominated communities in Newfoundland and Labrador waters. DFO Can. Sci. Advis. Sec. Sci. Advis. Rep., 2017/030.

DFO. (2017b). Science Guidance on Design Strategies for a Network of Marine Protected Areas in the Newfoundland and Labrador Shelves Bioregion. DFO Can. Sci. Advis. Sec. Sci. Advis. Rep., *2017/046*.

DFO (Fisheries and Oceans Canada), (2019a). Laurentian Channel Marine Protected Area (MPA). https://www.dfo-mpo.gc.ca/oceans/mpa-zpm/laurentian-laurentien/index-eng.html (accessed on 05/14/2020 and June 23, 2022).

DFO (Fisheries and Oceans Canada), (2019b). Laurentian Channel Marine Protected Area Regulations: REGULATORY IMPACT ANALYSIS STATEMENT. Canada Gazette, Part 2, 153:9. http://www.gazette.gc.ca/rp-pr/p1/2017/2017-06-24/html/reg2-eng.html#footnote.595062

Dinn, C., Zhang, X., Edinger, E., and Leys, S. P. (2020). Sponge communities in the eastern Canadian Arctic: species richness, diversity and density determined using targeted benthic sampling and underwater video analysis. Polar Biol., 0123456789. doi:10.1007/s00300-020-02709-z

Dolan, M. F. J., Grehan, A. J., Guinan, J. C., & Brown, C. (2008). Modelling the local distribution of cold-water corals in relation to bathymetric variables: Adding spatial context to deep-sea video data. Deep. Res. Part I Oceanogr. Res. Pap., 55:11, 1564–1579. doi:10.1016/j.dsr.2008.06.010

Downie, A., Noble-James, T., Chaverra, A., & Howell, K. (2021). Predicting sea pen (Pennatulacea) distribution on the UK continental shelf: evidence of range modification by benthic trawling. Mar. Ecol. Prog. Ser., 670, 75–91. doi:10.3354/meps13744

Drazen, J. C., Leitner, A. B., Morningstar, S., Marcon, Y., Greinert, J., & Purser, A. (2019). Observations of deep-sea fishes and mobile scavengers from the abyssal DISCOL experimental mining area. Biogeosciences, 16:16, 3133–3146. doi:10.5194/bg-16-3133-2019

Durden, J., Schoening, T., Althaus, F., Friedman, A., Garcia, R., & AG Glover, J Greinert, N JacoDurden, JM, T Schoening, F Althaus, A Friedman, R Garcia, AG Glover, J Greinert, N Jacobsen Stout, DOB Jones, A Jordt, JW Kaeli, K Koser, LA Kuhnz, D Lindsay, KJ Morris, TW Nattkemper, J Osterloff, HA Ruhl, H Singh, M Tran, BJ, B. B. (2016). Perspectives in visual imaging for marine biology and ecology: from acquisition to understanding. Oceanogr. Mar. Biol. An Annu. Rev., 54, 1S72.

Eckelbarger, K. J., Tyler, P. A., & Langton, R. W. (1998). Gonadal morphology and gametogenesis in the sea pen Pennatula aculeata (Anthozoa: Pennatulacea) from the Gulf of Maine. Mar. Biol., 132:4, 677–690. doi:10.1007/s002270050432

El-Sabh, M. I. (1977). Oceanographic Features, Currents, and Transport in Cabot Strait. J. Fish. Res. Board Canada, 34:4, 516–528. doi:10.1139/f77-083

Esri (2020a). World Ocean Base Map. Available online at: https://www.arcgis.com/home/item.html?id=1e126e7520f9466c9ca28b8f28b5e500 (accessed March 8, 2021).

Esri (2020b). ArcGIS Pro (Version 2.7.3). Esri Inc. https://www.esri.com/en-us/arcgis/products/arcgis-pro/overview. (software)

Esri (2022a). Cluster and Outlier Analysis (Anselin Local Moran's I) (Spatial Statistics). https://pro.arcgis.com/en/pro-app/latest/tool-reference/spatial-statistics/cluster-and-outlier-analysis-anselin-local-moran-s.htm (accessed Aug 30 2022)

Esri (2022b). How Optimized Hot Spot Analysis works. https://pro.arcgis.com/en/pro-app/latest/tool-reference/spatial-statistics/h-how-hot-spot-analysis-getis-ord-gi-spatial-stati.htm (accessed Aug 30 2022)

Esri (2022c). How Hot Spot Analysis (Getis-Ord Gi*) works. https://pro.arcgis.com/en/pro-app/latest/tool-reference/spatial-statistics/h-how-hot-spot-analysis-getis-ord-gi-spatial-stati.htm (accessed Aug 30 2022)

Esri (2022d). Spatial Autocorrelation (Global Moran's I) (Spatial Statistics). https://pro.arcgis.com/en/pro-app/latest/tool-reference/spatial-statistics/spatial-autocorrelation.htm (accessed Aug 30 2022)

Esri (2022e). Optimized Hot Spot Analysis (Spatial Statistics). https://pro.arcgis.com/en/pro-app/latest/tool-reference/spatial-statistics/optimized-hot-spot-analysis.htm (accessed Aug 30 2022)

Fader, G. B. J. (1991). Gas-related sedimentary features from the eastern Canadian continental shelf. Cont. Shelf Res., 11:8–10, 1123–1153. doi:10.1016/0278-4343(91)90094-M

FAO (2009). Report of the Technical Consultation on International Guidelines for the Management of Deep-sea Fisheries in the High Seas. Rome, 4-8 February and 25-29 August 2008. Series number 2070-6987. https://www.fao.org/3/i0605t/i0605t.pdf

Flannery, E. and Przeslawski, R. (2015). Comparison of sampling methods to assess benthic marine biodiversity: Are spatial and ecological relationships consistent among sampling gear? Record 2015/07. Geoscience Australia, Canberra. doi:10.11636/Record.2015.007.

Fletcher, R., & Fortin, M.-J. (2018). Spatial Ecology Modeling and Conservation Modeling: Applications with R. Springer Nature. doi:10.1007%2F978-3-030-01989-1

Folkersen, M. V., Fleming, C. M., and Hasan, S. (2018). The economic value of the deep sea: A systematic review and meta-analysis. Mar. Policy, 94:May, 71–80. doi:10.1016/j.marpol.2018.05.003

Fortin, M.-J., Drapeau, P., and Legendre, P. (1989). Spatial autocorrelation and sampling design in plant ecology. Vegetatio, 83:1–2, 209–222. doi:10.1007/BF00031693

Georgian, S., Morgan, L., & Wagner, D. (2021). The modeled distribution of corals and sponges surrounding the Salas y Gómez and Nazca ridges with implications for high seas conservation. PeerJ, 9, 1–35. doi:10.7717/peerj.11972

Gerdes, K., Martínez Arbizu, P., Schwarz-Schampera, U., Schwentner, M., and Kihara, T. C. (2019). Detailed Mapping of Hydrothermal Vent Fauna: A 3D Reconstruction Approach Based on Video Imagery. Front. Mar. Sci., 6:March. doi:10.3389/fmars.2019.00096

Getis, A., & Ord, J. K. (1992). The Analysis of Spatial Association by Use of Distance Statistics. Geogr. Anal., 24:3, 189–206. doi:10.1111/j.1538-4632.1992.tb00261.x

Gilbert, D., Sundby, B., Gobeil, C., Mucci, A., & Tremblay, G. H. (2005). A seventy-two-year record of diminishing deep-water oxygen in the St. Lawrence estuary: The northwest Atlantic connection. Limnol. Oceanogr., 50:5, 1654–1666. doi:10.4319/lo.2005.50.5.1654

González-Irusta, J. M., De La Torriente, A., Punzón, A., Blanco, M., & Serrano, A. (2018). Determining and mapping species sensitivity to trawling impacts: The BEnthos Sensitivity Index to Trawling Operations (BESITO). ICES J. Mar. Sci., 75:5, 1710–1721. doi:10.1093/icesjms/fsy030

Greathead, C., Clarke, J., Boulcott, P., Blackadder, L., Weetman, A., Wright, P. J., & Gonza, J. M. (2015). Environmental requirements for three sea pen species: relevance to distribution and conservation. J. Mar. Sci., 72, 576–586.

Greeley, K. (2022). Skeletal Growth Ring Microanalysis and Growth Rates in (Issue January). Memorial University of Newfoundland January.

Grinyó, J., Gori, A., Greenacre, M., Requena, S., Canepa, A., Lo Iacono, C., Ambroso, S., Purroy, A., & Gili, J. M. (2018). Megabenthic assemblages in the continental shelf edge and upper slope of the Menorca Channel, Western Mediterranean Sea. Prog. Oceanogr., 162:February, 40–51. doi:10.1016/j.pocean.2018.02.002

Guijarro, J., Beazley, L., Lirette, C., Kenchington, E., Wareham, V., Gilkinson, K., Alonso, M. K., & Murillo, F. J. (2016). Species Distribution Modelling of Corals and Sponges from Research Vessel Survey Data in the Newfoundland and Labrador Region for Use in the Identification of Significant Benthic Areas J. In *Can. Tech. Rep. Fish. Aquat. Sci.* (Vol. 3167).

Gullage, L., Devillers, R., and Edinger, E. (2017). Predictive distribution modelling of cold-water corals in the Newfoundland and Labrador region. Mar. Ecol. Prog. Ser., 582, 57–77. doi:10.3354/meps12307

Hall-Spencer, J., Allain, V., and Fosså, J. H. (2002). Trawling damage to Northeast Atlantic ancient coral reefs. Proc. R. Soc. B Biol. Sci., 269:1490, 507–511. doi:10.1098/rspb.2001.1910

Hamylton, S. M., & Barnes, R. S. K. (2018). The effect of sampling effort on spatial autocorrelation in macrobenthic intertidal invertebrates. Hydrobiologia, 811:1, 239–250. doi:10.1007/s10750-017-3491-x

Hemery, L. G., Henkel, S. K., & Cochrane, G. R. (2018). Benthic assemblages of mega epifauna on the Oregon continental margin. Cont. Shelf Res., 159, 24–32. doi:10.1016/j.csr.2018.03.004

Hebert, D., Layton, C., Brickman, D., & Galbraith, P. S. (2023). Physical Oceanographic Conditions in the Gulf of St . Lawrence during 2022.

Heifetz, J. (2002). Coral in Alaska: Distribution, abundance, and species associations. Hydrobiologia, 471, 19–28. doi:10.1023/A:1016528631593

Hjort, N. L., Omre, H., Frisén, M., Godtliebsen, F., Helgeland, J., Møller, J., Jensen, E. B. V., Rudemo, M., & Stryhn, H. (1994). Topics in Spatial Statistics [with Discussion, Comments and Rejoinder]. Scand. J. Stat., 21:4, 289–357.

Howell, K. L., Davies, J. S., Allcock, A. L., Braga-Henriques, A., Buhl-Mortensen, P., Carreiro-Silva, M., Dominguez-Carrió, C., Durden, J. M., Foster, N. L., Game, C. A., Hitchin, B., Horton, T., Hosking, B., Jones, D. O. B., Mah, C., Marchais, C. L., Menot, L., Morato, T., Pearman, T. R. R., … Wagner, D. (2019). A framework for the development of a global standardised marine taxon reference image database (SMarTaR-ID) to support imagebased analyses. PLoS One, 14:12. doi:10.1371/journal.pone.0218904

Huetten, E., and Greinert, J. (2008). Software controlled guidance, recording and post-processing of seafloor observations by ROV and other towed devices: The software package OFOP. Geophys. Res. Abstr., 10:EGU2008-A-03088, SRef-ID: 1607-7962/gra/EGU2008-A-03088.

Huston, M. (1979). A General Hypothesis of Species Diversity. Am. Nat., 113:1, 81–101. doi:10.1086/283366

Huvenne, V. A. I., Bett, B. J., Masson, D. G., Le Bas, T. P., and Wheeler, A. J. (2016). Effectiveness of a deep-sea cold-water coral Marine Protected Area, following eight years of fisheries closure. Biol. Conserv., 200, 60–69. doi:10.1016/j.biocon.2016.05.030

ICES. (2010). Report of the ICES/NAFO Joint Working Group on Deep-water Ecology (WGDEC), 22–26 March 2010 (Issue ICES CM 2010/ACOM:26).

Jamieson, A. J., Boorman, B., and Jones, D. O. (2013). Deep-sea benthic sampling. Methods for the study of marine benthos. John Wiley and Sons, Chichester, 285-348.

Jones, D. O. B., Bett, B. J., & Tyler, P. A. (2007). Depth-related changes to density, diversity and structure of benthic megafaunal assemblages in the Fimbul ice shelf region, Weddell Sea, Antarctica. Polar Biol., 30:12, 1579–1592. doi:10.1007/s00300-007-0319-6

Jones, D. O. B., Bett, B. J., Wynn, R. B., & Masson, D. G. (2009). The use of towed camera platforms in deep-water science. Underw. Technol., 28:2, 41–50. doi:10.3723/ut.28.041

Jones, D. O. B., & Brewer, M. E. (2012). Response of megabenthic assemblages to different scales of habitat heterogeneity on the Mauritanian slope. Deep. Res. Part I Oceanogr. Res. Pap., 67, 98–110. doi:10.1016/j.dsr.2012.05.006

Katsanevakis, S., Weber, A., Pipitone, C., Leopold, M., Cronin, M., Scheidat, M., Doyle, T. K., Buhl-Mortensen, L., Buhl-Mortensen, P., D'Anna, G., de Boois, I., Dalpadado, P., Damalas, D., Fiorentino, F., Garofalo, G., Giacalone, V. M., Hawley, K. L., Issaris, Y., Jansen, J., … Vöge, S. (2012). Monitoring marine populations and communities: Methods dealing with imperfect detectability. Aquat. Biol., 16:1, 31–52. doi:10.3354/ab00426

Kenchington, E., Lirette, C., Cogswell, A., Archambault, D., Archambault, P., Benoit, H., Bernier, D., Brodie, B., Fuller, S., Gilkinson, K., Lévesque, M., Power, D., Siferd, T., Treble, M., & Wareham, V. (2010). Delineating Coral and Sponge Concentrations in the Biogeographic Regions of the East Coast of Canada Using Spatial Analyses. DFO Can. Sci. Advis. Sec. Res. D, 3848:2010/041.vi + 202 pp.

Kenchington, E., Murillo, F. J., Cogswell, A., and Lirette, C. (2011). Development of Encounter Protocols and Assessment of Significant Adverse Impact by Bottom Trawling for Sponge Grounds and Sea Pen Fields in the NAFO Regulatory Area. In Northwest Atlantic Fisheries Organization.

Kenchington, E., Murillo, F. J., Lirette, C., Sacau, M., Koen-Alonso, M., Kenny, A., Ollerhead, N., Wareham, V., and Beazley, L. (2014). Kernel density surface modelling as a means to identify significant concentrations of vulnerable marine ecosystem indicators. PLoS One, 9:10. doi:10.1371/journal.pone.0109365

Kenchington, E., Beazley, L. I., Lirette, C., Murillo, F. J., Guijarro, J., Wareham, V., Gilkinson, K., Koen-Alonso, M., Benoit, H., Bourdages, H., Sainte-Marie, B., Treble, M., and Siferd, T. (2016a). Delineation of Coral and Sponge Significant Benthic Areas in Eastern Canada Using Kernel Density Analyses and Species Distribution Models. DFO - Can. Sci. Advis. Secr., 6:November, 178.

Kenchington, E., Lirette, C., Murillo, F. J., Beazley, L., Guijarro, J., Wareham, V., Gilkinson, K., Alonso, M. K., Benoît, H., Bourdages, H., Treble, M., and Siferd, T. (2016b). Kernel Density Analyses of Coral and Sponge Catches from Research Vessel Survey Data for Use in Identification of Significant Benthic Areas Ocean and Ecosystem Sciences Division Fisheries and Oceans Canada Canadian Technical Report of Fisheries and Aquati.

Krigsman, L. M., Yoklavich, M. M., Dick, E. J., & Cochrane, G. R. (2012). Models and maps: predicting the distribution of corals and other benthic macro-invertebrates in shelf habitats. Ecosphere, 3:1, art3. doi:10.1890/es11-00295.1

Kruskal, J. B. (1964). Nonmetric multidimensional scaling: A numerical method. Psychometrika, 29:2, 115–129. doi:10.1007/BF02289694

Kwasnitschka, T., Hansteen, T. H., Devey, C. W., and Kutterolf, S. (2013). Doing fieldwork on the seafloor: Photogrammetric techniques to yield 3D visual models from ROV video. Comput. Geosci., 52, 218–226. doi:10.1016/j.cageo.2012.10.008

Lacharité, M., Metaxas, A., and Lawton, P. (2015). Using object-based image analysis to determine seafloor fine-scale features and complexity. Limnol. Oceanogr. Methods, 13:10, 553–567. doi:10.1002/lom3.10047

Lacharité, M., & Metaxas, A. (2017). Hard substrate in the deep ocean: How sediment features influence epibenthic megafauna on the eastern Canadian margin. Deep. Res. Part I Oceanogr. Res. Pap., 126:November 2016, 50–61. doi:10.1016/j.dsr.2017.05.013

Lacharité, M., Brown, C. J., Normandeau, A., and Todd, B. J. (2020). Geomorphic features and benthos in a deep glacial trough in Atlantic Canada. Seafloor Geomorphol. as Benthic Habitat, 691–704. doi:10.1016/b978-0-12-814960-7.00041-5

Langton, R. W., Langton, E. W., Theroux, R. B., and Uzmann, J. R. (1990). Distribution, behavior and abundance of sea pens, Pennatula aculeata, in the Gulf of Maine. Mar. Biol., 107:3, 463–469. doi:10.1007/BF01313430

Lauzier, L. M., & Trites, R. . (1958). The deep waters in the Laurentian Channel. J. Fish. Res. Bo. Canada, 15:6, 1247–1257. https://sci-hub.tw/10.1002/iroh.19620470121%0Ahttp://www.osti.gov/servlets/purl/4290548/

Legendre, P., & Fortin, M. J. (1989). Spatial pattern and ecological analysis. Vegetatio, 80:2, 107–138. doi:10.1007/BF00048036

Levin, S. A. (1992). The problem of pattern and scale in ecology. Ecology, 73:6, 1943–1967. doi:10.2307/1941447

Levin, L., French, S., Story, M., & Jeffery, R. (2001). Environmental Influences on Regional Deep-Sea Species Diversity. Annu. Rev. Public Health, 22:1, 309–335. papers://90f132b5-cc05-44f1-a929-d329a3498f0f/Paper/p16

Logan, J. M., Young, M. A., Harvey, E. S., Schimel, A. C. G., & Ierodiaconou, D. (2017). Combining underwater video methods improves effectiveness of demersal fish assemblage surveys across habitats. Mar. Ecol. Prog. Ser., 582, 181–200. doi:10.3354/meps12326

Lundblad, E. R., Wright, D. J., Miller, J., Larkin, E. M., Rinehart, R., Naar, D. F., Donahue, B. T., Anderson, S. M., & Battista, T. (2006). A benthic terrain classification scheme for American Samoa. Mar. Geod., 29:2, 89–111. doi:10.1080/01490410600738021

Maldonado, M., Aguilar, R., Bannister, R. J., James, J., Conway, K. W., Dayton, P. K., Cristina, D., Gutt, J., Kelly, M., Kenchington, E. L. R., Leys, S. P., Shirley, A., Tendal, O. S., Rapp, H. T., Klaus, R., & Young, C. M. (2016). Sponge grounds as key marine habitats: a synthetic review of types, structure, functional roles, and conservation concerns. In *Marine animal forests* (pp. 1–39). Springer International Publishing Switzerland. doi:10.1007/978-3-319-17001-5

McArthur, M. A., Brooke, B. P., Przeslawski, R., Ryan, D. A., Lucieer, V. L., Nichol, S., McCallum, A. W., Mellin, C., Cresswell, I. D., & Radke, L. C. (2010). On the use of abiotic surrogates to describe marine benthic biodiversity. Estuar. Coast. Shelf Sci., 88:1, 21–32. doi:10.1016/j.ecss.2010.03.003

McCallum, B. R., and Walsh, S. J. (1996). Groundfish Survey Trawls Used at the Northwest Atlantic Fisheries Centre, 1971-Present. NAFO Sci. Counc. Meet. - JUNE 1996, NAFO SCR D:Serial No. N2726.

Mcclain, C. R., & Schlacher, T. A. (2015). On some hypotheses of diversity of animal life at great depths on the sea floor. Mar. Ecol., 36:4, 849–872. doi:10.1111/maec.12288

McClintock, J. B., Amsler, C. D., Baker, B. J., & Van Soest, R. W. (2005). Ecology of Antarctic Marine Sponges : An Overview. Integr. Comp. Biol., 45, 359–368.

McIntyre, F. D., Neat, F., Collie, N., Stewart, M., and Fernandes, P. G. (2015). Visual surveys can reveal rather different "pictures" of fish densities: Comparison of trawl and video camera surveys in the Rockall Bank, NE Atlantic Ocean. Deep. Res. Part I Oceanogr. Res. Pap., 95, 67–74. doi:10.1016/j.dsr.2014.09.005

Menge, B. A., & Olson, A. M. (1990). Role of scale and environmental factors in regulation of community structure. Trends Ecol. Evol., 5:2, 52–57. doi:10.1016/0169-5347(90)90048-I

Meyer, H. K., Davies, A. J., Roberts, E. M., Xavier, J. R., Ribeiro, P. A., Glenner, H., Birkely, S. R., & Rapp, H. T. (2023). Beyond the tip of the seamount: Distinct megabenthic communities found beyond the charismatic summit sponge ground on an arctic seamount (Schulz Bank, Arctic Mid-Ocean Ridge). Deep. Res. Part I Oceanogr. Res. Pap., 191:April 2022, 103920. doi:10.1016/j.dsr.2022.103920

Miatta, M., & Snelgrove, P. V. (2021). Benthic nutrient fluxes in deep-sea sediments within the Laurentian Channel MPA (eastern Canada): The relative roles of macrofauna, environment, and sea pen octocorals. Deep. Res. Part I Oceanogr. Res. Pap., 178, 103655. doi:10.1016/j.dsr.2021.103655

Miatta, M., & Snelgrove, P. V. R. (2022). Sea pens as indicators of macrofaunal communities in deep-sea sediments: Evidence from the Laurentian Channel Marine Protected Area. Deep. Res. Part I Oceanogr. Res. Pap., 182:January, 103702. doi:10.1016/j.dsr.2022.103702

Moritz, C., Lévesque, M., Gravel, D., Vaz, S., Archambault, D., and Archambault, P. (2013). Modelling spatial distribution of epibenthic communities in the Gulf of St. Lawrence (Canada). J. Sea Res., 78, 75–84. doi:10.1016/j.seares.2012.10.009

Morris, K. J., Bett, B. J., Durden, J. M., Huvenne, V. A. I., Milligan, R., Jones, D. O. B., McPhail, S., Robert, K., Bailey, D. M., & Ruhl, H. A. (2014). A new method for ecological surveying of the abyss using autonomous underwater vehicle photography. Limnol. Oceanogr. Methods, 12:NOV, 795–809. doi:10.4319/lom.2014.12.795

Mortensen, P. B., Buhl-Mortensen, L., Dolan, M., Dannheim, J., & Kröger, K. (2009). Megafaunal diversity associated with marine landscapes of northern Norway: A preliminary assessment. Nor. Geol. Tidsskr., 89:1–2, 163–171.

Muntoni, M., Devillers, R., & Koen-Alonso, M. (2019). Science should not be left behind during the design of a marine protected area: Meeting conservation priorities while integrating stakeholder interests. Facets, 2019:4, 472–492. doi:10.1139/facets-2018-0033

Murillo, F. J., Kenchington, E., Beazley, L., Lirette, C., Knudby, A., Guijarro, J., Benoit, H., Bourdages, H., & Sainte-Marie, B. (2016). Distribution modelling of sea pens, sponges, stalked tunicates and soft corals from research vessel survey data in the Gulf of St. Lawrence for use in the identification of significant benthic areas. Can. Tech. Rep. Fish. Aquat. Sci., 3170, vi + 132 p.

Murillo, F. J., MacDonald, B. W., Kenchington, E., Campana, S. E., Sainte-Marie, B., & Sacau, M. (2018). Morphometry and growth of sea pen species from dense habitats in the Gulf of St. Lawrence, eastern Canada. Mar. Biol. Res., 1000, 1–17. doi:10.1080/17451000.2017.1417604

Murillo, F. J., Kenchington, E., Koen-Alonso, M., Guijarro, J., Kenchington, T. J., Sacau, M., Beazley, L., and Rapp, H. T. (2020). Mapping benthic ecological diversity and interactions with bottom-contact fishing on the Flemish Cap (northwest Atlantic). Ecol. Indic., 112:February, 106135. doi:10.1016/j.ecolind.2020.106135

Neves, B. M., Du Preez, C., & Edinger, E. (2014). Mapping coral and sponge habitats on a shelf-depth environment using multibeam sonar and ROV video observations: Learmonth Bank, northern British Columbia, Canada. Deep. Res. Part II Top. Stud. Oceanogr., 99, 169–183. doi:10.1016/j.dsr2.2013.05.026

Neves, B. M., Edinger, E., Layne, G. D., and Wareham, V. E. (2015). Decadal longevity and slow growth rates in the deep-water sea pen Halipteris finmarchica (Sars, 1851) (Octocorallia: Pennatulacea): implications for vulnerability and recovery from anthropogenic disturbance. Hydrobiologia, 759:1, 147–170. doi:10.1007/s10750-015-2229-x

Neves, B., Edinger, E., Hayes, V. W., Devine, B., Wheeland, L., & Layne, G. (2018). Size metrics, longevity, and growth rates in Umbellula encrinus (Cnidaria: Pennatulacea) from the eastern Canadian Arctic. Arct. Sci., 4:4, 722–749. doi:10.1139/as-2018-0009

Neves, B. M., Faille, G., Murillo, F., Dinn, C., Pućko, M., Dudas, S., Devanney, A., & Allen, P. (2021). A National Monitoring Framework for Coral and Sponge Areas Identified as Other Effective Area-Based Conservation Measures. DFO Can. Sci. Advis. Sec. Sci. Advis. Rep., 2021/048:November, 1–23.

Neves, B. M., Auger, V., Edinger, E., Lockhart, P., & Morrissey, C. (2023). Preparing for remotely operated vehicle (ROV) seafloor surveys : a descriptive checklist for ocean scientists and managers Canadian Technical Report of Fisheries and Aquatic Sciences 3578 (Issue November).

Nybakken, J., Craig, S., Smith-Beasley, L., Moreno, G., Summers, A., & Weetman, L. (1998). Distribution density and relative abundance of benthic invertebrate megafauna from three sites at the base of the continental slope off central California as determined by camera sled and beam trawl. Deep. Res. Part II Top. Stud. Oceanogr., 45:8–9, 1753–1780. doi:10.1016/S0967-0645(98)80016-7

Oksanen, J., Simpson, G. L., Blanchet, F. G., Kindt, R., Legendre, P., Minchin, P. R., O'Hara, R. B., Solymos, P., Stevens, M. H. H., Szoecs, E., Wagner, H., Barbour, M., Bedward, M., Bolker, B., Borcard, D., Carvalho, G., Chirico, M., De Caceres, M., Durand, S., … Weedon, J. (2022). Package "Vegan" Title Community Ecology Package. Cran, 1–297.

Ord, J. K., & Getis, A. (1995). Local Spatial Autocorrelation Statistics: Distributional Issues and an Application. Geogr. Anal., 27:4, 286–306. doi:10.1111/j.1538-4632.1995.tb00912.x

Pacunski, R., Lowry, D., Hillier, L., and Blaine, J. (2016). A comparison of groundfish species composition, abundance, and density estimates derived from a scientific bottom-trawl and a small remotely-operated vehicle for trawlable habitats (Issue March).

Pearman, T. R. R., Brewin, P. E., Baylis, A. M. M., & Brickle, P. (2022). Deep-Sea Epibenthic Megafaunal Assemblages of the Falkland Islands, Southwest Atlantic. Diversity, 14:8. doi:10.3390/d14080637

Piepenburg, D., & Schmid, M. K. (1996). Brittle star fauna (Echinodermata: Ophiuroidea) of the Arctic northwestern Barents Sea: composition, abundance, biomass and spatial distribution. Polar Biol., 16:6, 383–392. doi:10.1007/s003000050069

Pierdomenico, M., Gori, A., Guida, V. G., & Gili, J. M. (2017). Megabenthic assemblages at the Hudson Canyon head (NW Atlantic margin): Habitat-faunal relationships. Prog. Oceanogr., 157, 12–26. doi:10.1016/j.pocean.2017.08.001

Pielou, E. C. (1966). Shannon's formula as a measure of specific diversity: its use and misuse. Am. Nat., 100:914, 463–465.

Pierdomenico, M., Russo, T., Ambroso, S., Gori, A., Martorelli, E., D'Andrea, L., Gili, J. M., & Chiocci, F. L. (2018). Effects of trawling activity on the bamboo-coral *Isidella elongata* and the sea pen *Funiculina quadrangularis* along the Gioia Canyon (Western Mediterranean, southern Tyrrhenian Sea). Prog. Oceanogr., 169, 214–226. doi:10.1016/j.pocean.2018.02.019

Pitcher, C. R., Doherty, P., Arnold, P., Hooper, J., Gribble, N., Bartlett, C., Browne, M., Campbell, N., Cannard, T., Cappo, M., Carini, G., Chalmers, S., Cheers, S., Chetwynd, D., Colefax, A., Coles, R., Cook, S., Davie, P., De'ath, G., … Yearsley, G. (2007). Seabed Biodiversity on the Continental Shelf of the Great Barrier Reef World Heritage Area. In Final Report (Issue July). http://www.reef.crc.org.au/resprogram/programC/seabed/final-report.htm

Proudfoot, B., Devillers, R., Brown, C. J., Edinger, E., & Copeland, A. (2020). Seafloor mapping to support conservation planning in an ecologically unique fjord in Newfoundland and Labrador, Canada. J. Coast. Conserv., 24:3. doi:10.1007/s11852-020-00746-8

Price, D. M., Lim, A., Callaway, A., Eichhorn, M. P., Wheeler, A. J., Lo Iacono, C., & Huvenne, V. A. I. (2021). Fine-Scale Heterogeneity of a Cold-Water Coral Reef and Its Influence on the Distribution of Associated Taxa. Front. Mar. Sci., 8:556313. doi:10.3389/fmars.2021.556313

R Core Team (2021). R: A language and environment for statistical computing. R Foundation for Statistical Computing, Vienna, Austria. URL https://www.R-project.org/.

Ramirez-Llodra, E., Brandt, A., Danovaro, R., De Mol, B., Escobar, E., German, C. R., Levin, L. A., Martinez Arbizu, P., Menot, L., Buhl-Mortensen, P., Narayanaswamy, B. E., Smith, C. R., Tittensor, D. P., Tyler, P. A., Vanreusel, A., & Vecchione, M. (2010). Deep, diverse and definitely different: Unique attributes of the world's largest ecosystem. Biogeosciences, 7:9, 2851–2899. doi:10.5194/bg-7-2851-2010

Ramirez-Llodra, E., Tyler, P. A., Baker, M. C., Bergstad, O. A., Clark, M. R., Escobar, E., Levin, L. A., Menot, L., Rowden, A. A., Smith, C. R., and van Dover, C. L. (2011). Man and the last great wilderness: Human impact on the deep sea. PLoS One, 6:8. doi:10.1371/journal.pone.0022588

Ramos, R. B., dos Santos, R. F., Schattner, U., Figueira, R. C. L., Bícego, M. C., Lobo, F. J., & de Mahiques, M. M. (2020). Deep pockmarks as natural sediment traps: a case study from southern Santos Basin (SW Atlantic upper slope). Geo-Marine Lett., 40:6, 989–999. doi:10.1007/s00367-019-00617-8

Robert, K., Jones, D. O. B., Tyler, P. A., Van Rooij, D., & Huvenne, V. A. I. (2015). Finding the hotspots within a biodiversity hotspot: Fine-scale biological predictions within a submarine canyon using high-resolution acoustic mapping techniques. Mar. Ecol., 36:4, 1256–1276. doi:10.1111/maec.12228

Roberts, J. M., Wheeler, A., Freiwald, A., & Cairns, S. (2009). Cold-water corals: the biology and geology of deep-sea coral habitats. Cambridge University Press.

Robinson, T. P. (2000). Spatial statistics and geographical information systems in epidemiology and public health. Adv. Parasitol., 47, 81–128. doi:10.1016/s0065-308x(00)47007-7

Ross, R. E., Gonzalez-Mirelis, G., Lozano, P., & Buhl-Mortensen, P. (2021). Discerning the Management-Relevant Ecology and Distribution of Sea Pens (Cnidaria: Pennatulacea) in Norway and Beyond. Front. Mar. Sci., 8:November, 1–20. doi:10.3389/fmars.2021.652540

Rex, M. A. (1981). Community Structure in the Deep-Sea Benthos. Annu. Rev. Ecol. Syst., 12:1, 331–353. doi:10.1146/annurev.es.12.110181.001555

Ruiz-Pico, S., Serrano, A., Punzón, A., Altuna, Á., Fernández-Zapico, O., & Velasco, F. (2017). Sea pen (Pennatulacea) aggregations on the northern Spanish shelf: Distribution and faunal assemblages | Agregaciones de pennatuláceos en la plataforma del norte de España: Distribución y agrupaciones faunísticas. Sci. Mar., 81:3, 413–423. doi:10.3989/scimar.04359.06A

Schoening, T., Purser, A., Langenkämper, D., Suck, I., Taylor, J., Cuvelier, D., Lins, L., Simon-Lledó, E., Marcon, Y., Jones, D. O. B., Nattkemper, T., Köser, K., Zurowietz, M., Greinert, J., & Gomes-Pereira, J. (2020). Megafauna community assessment of polymetallic-nodule fields with cameras: platform and methodology comparison. Biogeosciences, 17:12, 3115–3133. doi:10.5194/bg-17-3115-2020

Scientific Abyss Mapping Services. (2009). OFOP documentation: Version 3.2.0k. 1–42. http://www.ofop-by-sams.eu/ (7/11/17), also see https://www.emma-technologies.com/products/software/ofop/.

Sigler, M., Rooper, C., Goddard, P., Wilborn, R., & Williams, K. (2023). Alaska deep-sea coral and sponge assemblages are well-defined and mostly predictable from local environmental conditions. Mar. Ecol. Prog. Ser., 712, 67–85. doi:10.3354/meps14317

Simon-Lledó, E., Bett, B. J., Huvenne, V. A. I., Köser, K., Schoening, T., Greinert, J., and Jones, D. O. B. (2019). Biological effects 26 years after simulated deep-sea mining. Sci. Rep., 9:1, 1–13. doi:10.1038/s41598-019-44492-w

Somoza, L., Rueda, J. L., Sánchez-Guillamón, O., Medialdea, T., Rincón-Tomás, B., González, F. J., Palomino, D., Madureira, P., López-Pamo, E., Fernández-Salas, L. M., Santofimia, E., León, R., Marino, E., Fernández-Puga, M. del C., & Vázquez, J. T. (2021). The Interactive Role of Hydrocarbon Seeps, Hydrothermal Vents and Intermediate Antarctic/Mediterranean Water Masses on the Distribution of Some Vulnerable Deep-Sea Habitats in Mid Latitude NE Atlantic Ocean. Oceans, 2:2, 351–385. doi:10.3390/oceans2020021

Stanley, R., Belley, R., Snelgrove, P., Morris, C., Pepin, P., & Metaxas, A. (2015). Strategies for Marine Protected Areas and Areas of Interest in Newfoundland and Labrador. In Ecosystems Management Publication Series, Newfoundland and Labrador Region, 0011: 192 p.

Sumida, P. Y. G., Yoshinaga, M. Y., Madureira, L. A. S. P., & Hovland, M. (2004). Seabed pockmarks associated with deepwater corals off SE Brazilian continental slope, Santos Basin. Mar. Geol., 207:1–4, 159–167. doi:10.1016/j.margeo.2004.03.006

Swanborn, D. J. B., Huvenne, V. A. I., Malpas, T., Pittman, S. J., Rogers, A. D., Taylor, M. L., & Woodall, L. C. (2023). Seamount seascape composition and configuration shape Southwest Indian Ridge fish assemblages. Deep. Res. Part I Oceanogr. Res. Pap., 191:November 2022, 103921. doi:10.1016/j.dsr.2022.103921

Sward, D., Monk, J., and Barrett, N. (2019). A systematic review of remotely operated vehicle surveys for visually assessing fish assemblages. Front. Mar. Sci., 6:APR, 1–19. doi:10.3389/fmars.2019.00134

Taylor, J., Krumpen, T., Soltwedel, T., Gutt, J., & Bergmann, M. (2016). Regional- and local-scale variations in benthic megafaunal composition at the Arctic deep-sea observatory HAUSGARTEN. Deep. Res. Part I Oceanogr. Res. Pap., 108, 58–72. doi:10.1016/j.dsr.2015.12.009

Terribile, K., Evans, J., Knittweis, L., & Schembri, P. J. (2016). Maximising MEDITS: Using data collected from trawl surveys to characterise the benthic and demersal assemblages of the circalittoral and deeper waters around the Maltese Islands (Central Mediterranean). Reg. Stud. Mar. Sci., 3, 163–175. doi:10.1016/j.rsma.2015.07.006

Tissot, B. N., Yoklavich, M. M., Love, M. S., York, K., & Amend, M. (2006). Benthic invertebrates that form habitat on deep banks off southern California, with special reference to deep sea coral. Fish. Bull., 104:2, 167–181.

Todd, B. J. (2016). The Laurentian Channel: A major cross-shelf trough in Atlantic Canada. Geol. Soc. Mem., 46:1, 161–162. doi:10.1144/M46.124

Trenkel, V. M., Francis, R. I. C. C., Lorance, P., Mahévas, S., Rochet, M. J., and Tracey, D. M. (2004). Availability of deep-water fish to trawling and visual observation from a remotely operated vehicle (ROV). Mar. Ecol. Prog. Ser., 284:Muntz 1983, 293–303. doi:10.3354/meps284293

Underwood, A.J. (1997). Experiments in ecology: their logical design and interpretation using analysis of variance. New York: Cambridge University Press. 504p.

Uzmann, J. R., Cooper, R. a, Theroux, R. B., & Wigley, R. L. (1977). Synoptic comparison of three sampling techniques for estimating abundance and distribution of selected megafauna: submersible vs. camera sled vs. otter trawl. Mar. Fish. Rev, 39:12, 11–19.

Vad, J., Kazanidis, G., Henry, L. A., Jones, D. O. B., Gates, A. R., & Roberts, J. M. (2020). Environmental controls and anthropogenic impacts on deep-sea sponge grounds in the Faroe-Shetland Channel, NE Atlantic: The importance of considering spatial scale to distinguish drivers of change. ICES J. Mar. Sci., 77:1, 451–461. doi:10.1093/icesjms/fsz185

Vázquez, A. (2010). Catchability Comparison Between Lofoten and Campelen Gears. Reprod. Biol., NAFO SCR Doc. 02/74.

Walbridge, S., Slocum, N., Pobuda, M., & Wright, D. J. (2018). Unified geomorphological analysis workflows with benthic terrain modeler. Geosci., 8:3. doi:10.3390/geosciences8030094

Walsh, S. J. (1992). Size-Dependent Selection at the Footgear of a Groundfish Survey Trawl. North Am. J. Fish. Manag., 12:3, 625–633. doi:10.1577/1548-8675(1992)012<0625:sdsatf>2.3.co;2

Walsh, S. J., Hickey, W. H., Porter, J., Delouche, H., and MacCallum, B. R. (2009). NAFC survey trawl operations manual: Version 1.0. Fish. Ocean. Canada, Northwest Atl. Fish. Centre, Newfoundl. Reg. St. John's., June, 190 pp.

Warren, W. G. (1997). Report on the comparative fishing trial between the Gadus Atlantica and Teleost. NAFO Sci. Counc. Stud., 29, 81–92.

Wassenberg, T. J., Dews, G., and Cook, S. D. (2002). The impact of fish trawls on megabenthos (sponges) on the north-west shelf of Australia. Fish. Res., 58:2, 141–151. doi:10.1016/S0165-7836(01)00382-4

Watters, D. L., Laidig, T. E., & Yoklavich, M. M. (2022). A biogeographical assessment of deep-sea coral assemblages from coastwide visual surveys off California. Deep. Res. Part I Oceanogr. Res. Pap., 185:April, 103773. doi:10.1016/j.dsr.2022.103773

Webb, K. E., Barnes, D. K. A., & Planke, S. (2009). Pockmarks: Refuges for marine benthic biodiversity. Limnol. Oceanogr., 54:5, 1776–1788. doi:10.4319/lo.2009.54.5.1776

Wickham et al., (2019). Welcome to the tidyverse. Journal of Open Source Software, 4(43), 1686, https://doi.org/10.21105/joss.01686

Wigand, L. A., Klinger, T., & Logsdon, M. G. (2013). Patterns in groundfish abundance along the Eastern Bering Sea outer continental margin. ICES, 70:6, 1181–1197. doi:10.1093/icesjms/fst054

Williams, G. (1999). Index Pennatulacea Annotated Bibliography and Indexes of the Sea Pens (Coelenterata: Octocorallia) of the World 1469-1999. Proc. Calif. Acad. Sci., 51:2, 19–103. http://biostor.org/reference/78405

Williams, G., and Alderslade, P. (2011). Three new species of pennatulacean octocorals with the ability to attach to rocky substrata (Cnidaria: Anthozoa: Pennatulacea). Zootaxa, 3001, 33–48. doi:10.11646/zootaxa.3001.1.2

Wilson, M. T., Andrews, A. H., Brown, A. L., & Cordes, E. E. (2002). Axial rod growth and age estimation of the sea pen, Halipteris willemoesi K??lliker. Hydrobiologia, 471, 133–142. doi:10.1023/A:1016509506094

Zajac, R. N. (2008). Challenges in marine, soft-sediment benthoscape ecology. Landsc. Ecol., 23:SUPPL. 1, 7–18. doi:10.1007/s10980-007-9140-4

Zhulay, I., Iken, K., Renaud, P. E., and Bluhm, B. A. (2019). Epifaunal communities across marine landscapes of the deep Chukchi Borderland (Pacific Arctic). Deep. Res. Part I Oceanogr. Res. Pap., 151:June. doi:10.1016/j.dsr.2019.06.011

APPENDIX I: CHAPTER 3 (REGIONAL DIVERSITY AND SPATIAL PATTERNS OF EPIBENTHIC COMMUNITIES IN THE LAURENTIAN CHANNEL MARINE PROTECTED AREA)

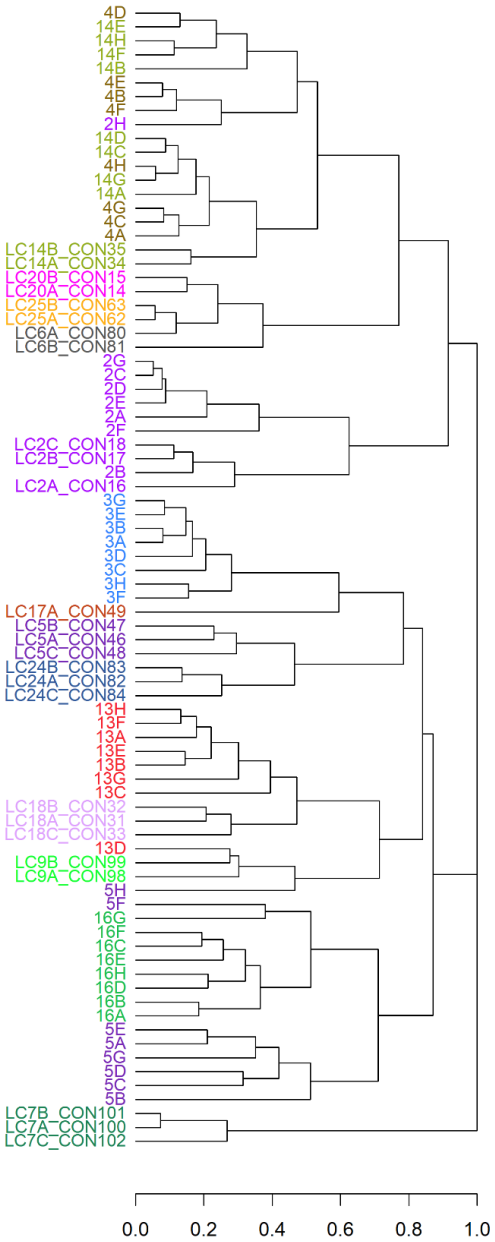

Figure AI.1 Hierarchical clustering dendrogram for all 82 transects (ROPOS and Campod), using the complete linkage method and based on total abundance of each taxon per transect (m^{-2}; summed counts by 63 taxa, divided by summed area per transect). All Campod transect labels include "CON". Unique colours used for each station.

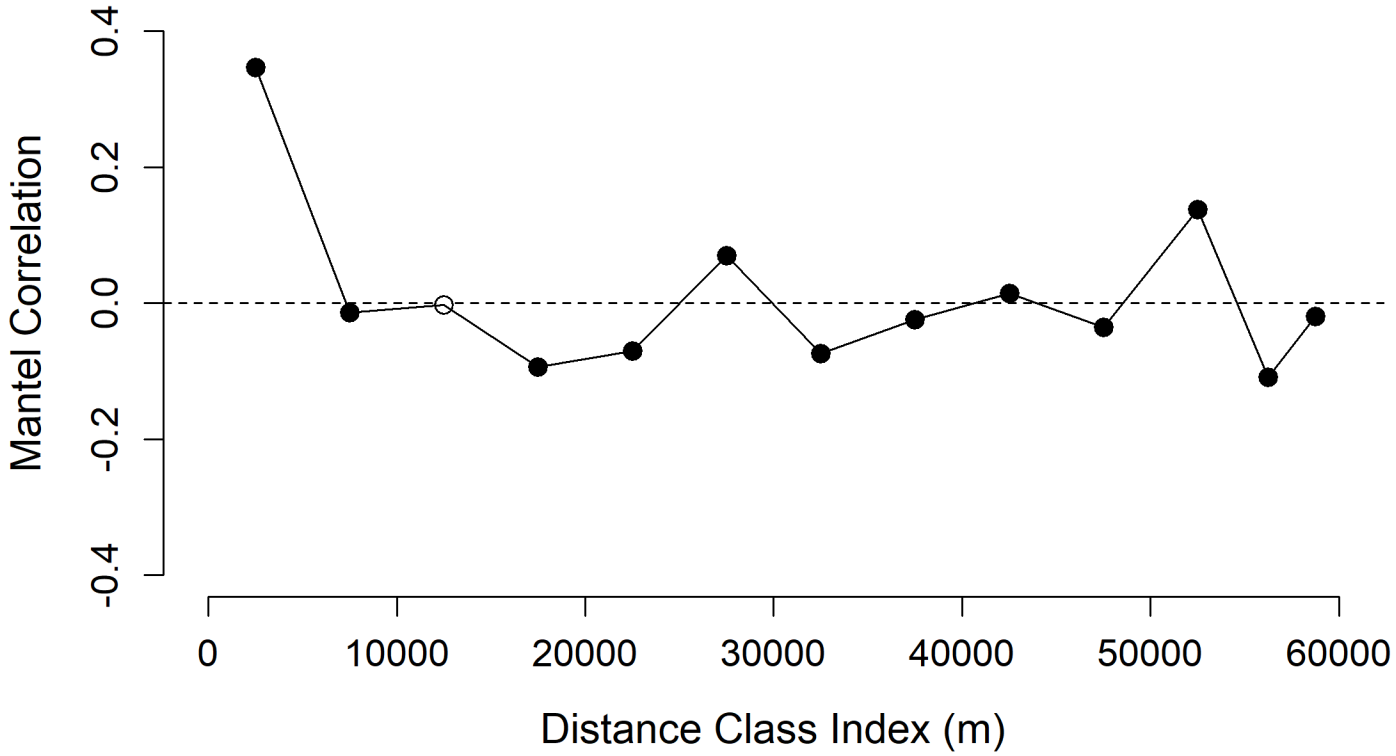

Figure AI.2 Mantel correlogram based on a Brays-Curtis dissimilarity distance matrix and Euclidean distance matrix throughout the Laurentian Channel MPA, includes 2976 images (ROPOS and Campod combined but excluding images with zero taxon abundance). Computed using the Spearman's *r*, 999 permutations, with the cutoff option to limit the distance classes to include all points, and the Holm method for dealing with multiple testing problems. For each distance class index in meters, the median distance value is used to represent distance classes increments of ~5 km (e.g., distance class 1 includes distances 0-5 km, distance class 2 includes 5-10 km, etc.). Spatial range is ~10 km.

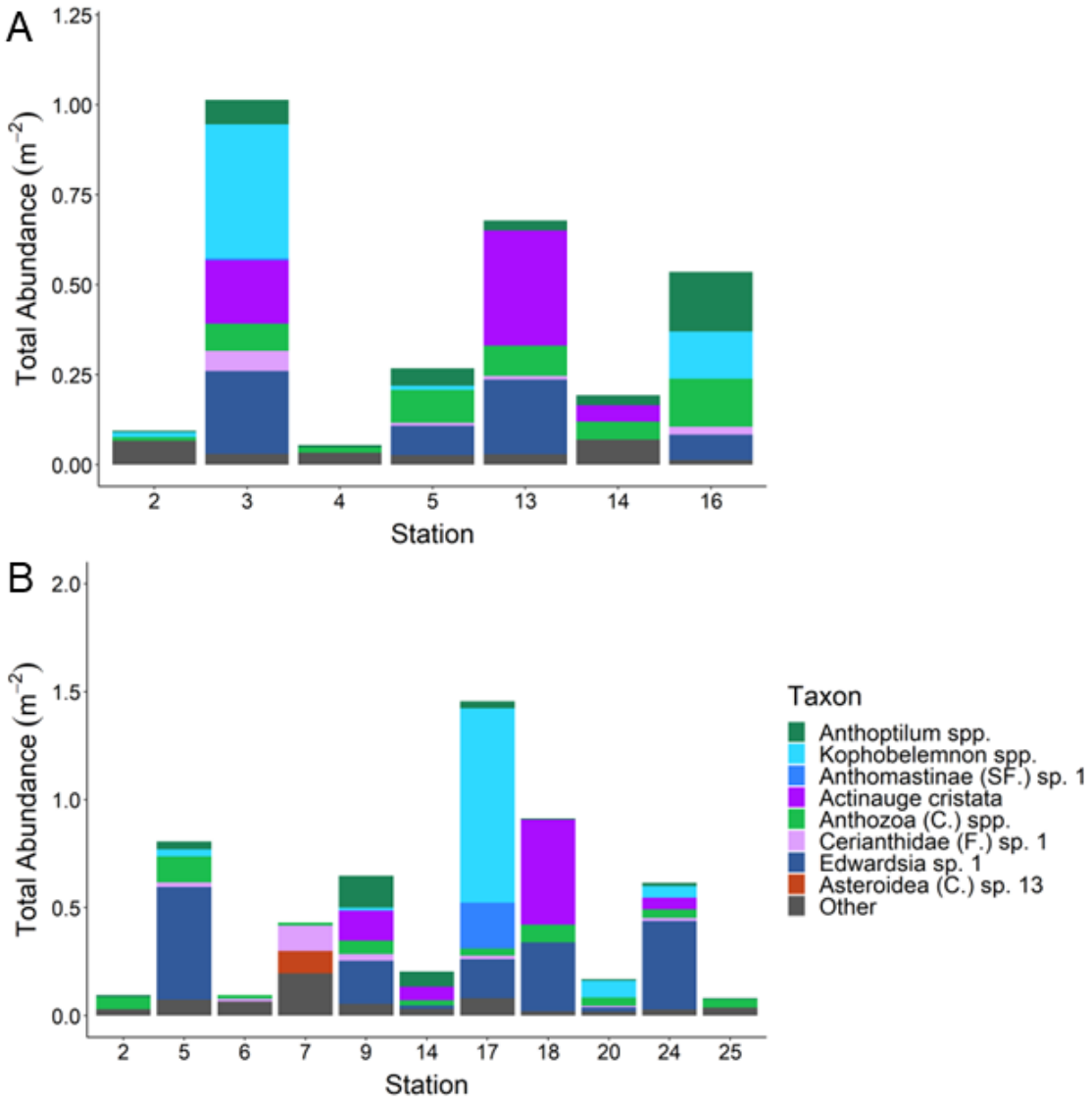

Figure AI.3 Overall abundance and composition of aggregated taxa, excluding the three most abundant taxa *Pennatula* sp. 2, Porifera (P.) sp. 21, and Hexacorallia (SC.) spp. that skew scale (see Figure 3), throughout the 15 Laurentian Channel MPA stations for A) ROPOS and B) Campod. Total abundance calculated for each station as summed taxon counts divided by summed area analyzed.

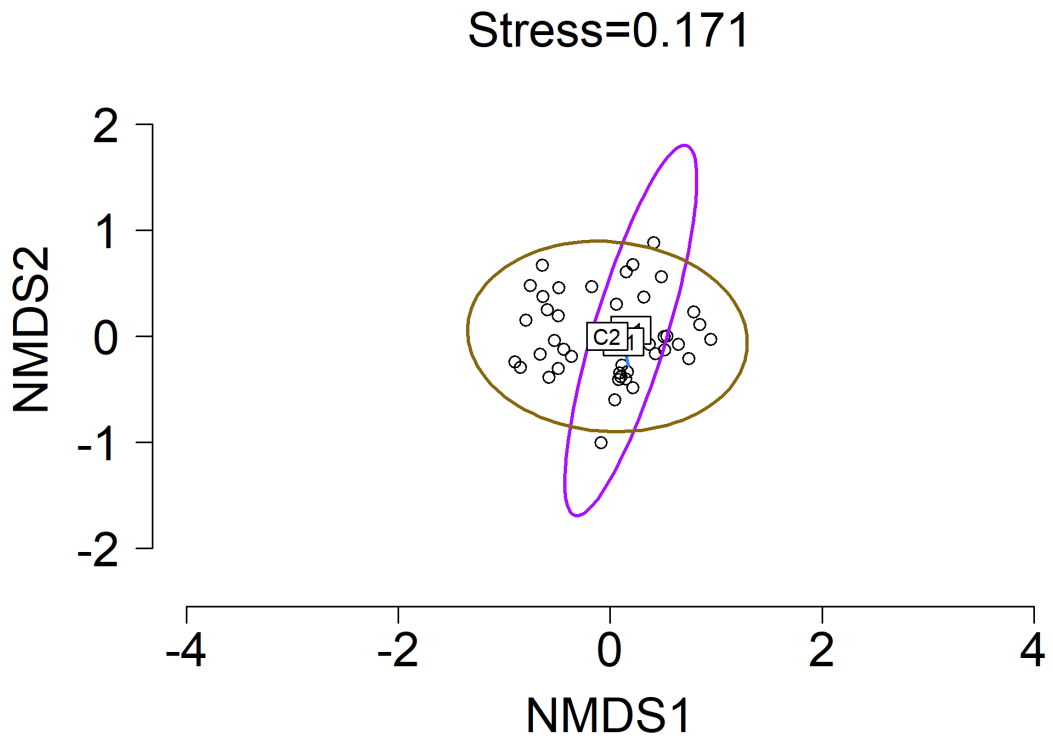

Figure AI.4 Non-metric multi-dimensional scaling (NMDS) for Assemblage 2, with stress of 0.171, Bray-Curtis dissimilarity, using total abundance of each taxon per transect (m^{-2}; summed counts, divided by summed area per transect). Different coloured ellipses outline the 95% confidence intervals for the groupings based on primary benthoscapes. See Figure 6, for all three assemblages. Note: Despite the overlap in confidence intervals, PERMANOVA was significant for both the benthoscape and station factors. At least 3 data points are needed to draw ellipses with 95% confidence intervals. For benthoscape class C1, there were 2 transects, resulting in a warning. While the ordination is valid, the "ellipse" appeared as a line (blue).

Table AI.1 Characteristics of benthoscape classes derived in the Laurentian Channel in the area surrounding the Area of Interest for the establishment of a Marine Protected Area.9

Class	Surface area (km^2; % of study area	# Infauna samples	Depth[a]	Slope[b]	Scours[c]	Pockmarks/ pits[d]	Surficial sediment
A1	3178 (23%)	14	Deep	Flat	Sparse	Very abundant	Fine sediment (predominantly mud)
A2	1564 (11%)	7	Mid-depth	Low relief	Sparse	Very abundant	Mixed sediment (presence of gravel)
B1	66 (0.5%)	0	Shallow	Very steep	Absent	Sparse	Gravel/Sandy Gravel
B2	745 (5%)	2	Shallow	Steep	Absent	Sparse	Muddy/gravelly Sand
C1	1274 (9%)	2	Deep	Low relief	Very abundant	Sparse	Bioturbated mud
C2	4654 (34%)	7	Deep	Low relief	Abundant	Sparse	Sandy mud (gravel traces)
TZ1	1595 (12%)	7	Mid-depth	Low relief	Sparse	Intermediate	Mixed sediment (presence of gravel)
TZ2	589 (4%)	5	Deep	Flat	Sparse	Intermediate	Fine sediment (predominantly mud)

For each characteristic, distinct groupings reflect average values in each class.
[a]Shallow (<200 m); Mid-depth (200–400 m); Deep (>400 m).
[b]Flat (<0.5 degree); Low relief (0.5–1 degree); Steep (>1 degree); Very steep (>3 degree).
[c]Absent (close to 0 km^{-2}); Sparse (<1 km^{-2}); Abundant/Very abundant (>2 km^{-2}).
[d]Sparse (<1 km^{-2}); Intermediate (1–2 km^{-2}); Very abundant (>5 km^{-2}).

9 Reprinted from Seafloor Geomorphology as Benthic Habitat, Lacharité, M., Brown, C. J., Normandeau, A., and Todd, B. J, *Geomorphic features and benthos in a deep glacial trough in Atlantic Canada*, Pages No. 691–704, Copyright (2020), with permission from Elsevier. [Table 41.1, caption, and notes]

Table AI.2 Summary of transect metadata in the Laurentian Channel MPA, including number, area, depth, altitude relative to seafloor or each image, as well as the start and end points (total of 82 transects: 8 transects per ROPOS station A, B, C, D, E, F, G, and H, 1-3 transects per Campod station). Altitude refers to the height of the altimeter attached to the ROV relative to the seabed.

Transect	Number of Images Analyzed	Total sum of area analyzed (m^2)	Mean Depth (m)	Standard Deviation of Depth (m)	Mean altitude above seafloor (m)	Standard deviation altitude (m)	Mean analyzed area per image (m^2)	Standard deviation area per image (m^2)	Start Longitude (Decimal Degrees)	Start Latitude (Decimal Degrees)	End Longitude (Decimal Degrees)	End Latitude (Decimal Degrees)
ROPOS												
2A	62	141.9	348.15	0.68	1.23	0.33	2.29	0.56	-56.67042	45.53298	-56.66594	45.53123
2B	54	120.49	348.74	0.70	1.04	0.28	2.23	0.55	-56.66649	45.53134	-56.67034	45.53284
2C	63	124.87	349.82	0.52	0.92	0.17	1.98	0.28	-56.66719	45.52954	-56.67163	45.53128
2D	64	132.88	349.79	0.50	1.06	0.25	2.08	0.50	-56.67175	45.53124	-56.66736	45.52950
2E	62	117.86	351.25	0.75	0.83	0.10	1.90	0.16	-56.66848	45.52790	-56.67281	45.52957
2F	58	133.72	351.23	0.83	1.20	0.36	2.31	0.55	-56.67298	45.52954	-56.66854	45.52782
2G	62	114.94	353.58	0.76	0.88	0.13	1.85	0.17	-56.66980	45.52625	-56.67415	45.52796
2H	61	146.52	353.77	0.95	1.22	0.38	2.40	0.63	-56.67426	45.52791	-56.66982	45.52615
3A	65	93.31	445.92	0.35	0.99	0.16	1.44	0.20	-57.37146	45.94323	-57.36749	45.94554
3B	64	91.01	445.78	0.35	0.94	0.13	1.42	0.18	-57.36737	45.94548	-57.37137	45.94314
3C	63	83.22	445.80	0.83	1.07	0.31	1.32	0.21	-57.36950	45.94191	-57.36556	45.94421
3D	56	83.01	445.84	0.79	1.00	0.29	1.48	0.25	-57.36550	45.94412	-57.36943	45.94183
3E	65	104.36	445.87	0.42	1.04	0.20	1.61	0.25	-57.36767	45.94066	-57.36371	45.94294
3F	58	87.91	446.09	0.42	0.90	0.09	1.52	0.11	-57.36378	45.94281	-57.36759	45.94060
3G	65	97.56	446.29	0.51	1.00	0.16	1.50	0.22	-57.36586	45.93942	-57.36183	45.94169
3H	63	99.49	446.35	0.56	0.97	0.15	1.58	0.20	-57.36181	45.94158	-57.36573	45.93933
4A	64	114.31	333.00	0.68	1.15	0.20	1.79	0.29	-57.24532	46.09556	-57.24032	46.09642
4B	60	85.64	333.09	0.74	1.16	0.24	1.43	0.33	-57.24038	46.09634	-57.24540	46.09548
4C	65	115.34	335.66	0.81	1.10	0.23	1.77	0.28	-57.24472	46.09372	-57.23965	46.09460
4D	64	117.8	335.85	1.04	0.96	0.13	1.84	0.27	-57.23962	46.09453	-57.24472	46.09366

Table AI.2 *(Continued)*

Transect	Number of Images Analyzed	Total sum of area analyzed (m^2)	Mean Depth (m)	Standard Deviation of Depth (m)	Mean altitude above seafloor (m)	Standard deviation altitude (m)	Mean analyzed area per image (m^2)	Standard deviation area per image (m^2)	Start Longitude (Decimal Degrees)	Start Latitude (Decimal Degrees)	End Longitude (Decimal Degrees)	End Latitude (Decimal Degrees)
4E	63	75.12	337.10	1.43	1.19	0.34	1.19	0.30	-57.24401	46.09189	-57.23896	46.09279
4F	65	87.58	337.18	1.52	1.17	0.30	1.35	0.34	-57.23889	46.09270	-57.24398	46.09180
4G	65	135.63	337.67	1.20	1.19	0.28	2.09	0.41	-57.24332	46.09007	-57.23826	46.09094
4H	65	131.11	337.66	1.21	1.10	0.29	2.02	0.41	-57.23823	46.09085	-57.24329	46.09000
5A	55	109.94	438.52	0.63	0.93	0.10	2.00	0.28	-57.52767	46.21098	-57.53005	46.21384
5B	40	74.74	438.08	0.56	1.34	0.40	1.87	0.44	-57.53016	46.21380	-57.52765	46.21069
5C	63	97.18	440.47	0.22	0.91	0.02	1.54	0.17	-57.52980	46.20974	-57.53241	46.21284
5D	44	70.66	440.37	0.37	1.36	0.35	1.61	0.42	-57.53240	46.21263	-57.52996	46.20969
5E	62	101.6	439.78	0.41	1.13	0.34	1.64	0.45	-57.53216	46.20877	-57.53468	46.21186
5F	38	40.49	440.24	0.22	1.07	0.22	1.07	0.24	-57.53492	46.21189	-57.53246	46.20894
5G	46	59.31	440.03	0.23	1.00	0.18	1.29	0.28	-57.53446	46.20778	-57.53702	46.21084
5H	32	38.74	439.83	0.32	1.14	0.27	1.21	0.28	-57.53648	46.20998	-57.53464	46.20777
13A	63	87.86	433.64	0.64	1.12	0.24	1.39	0.31	-57.20464	45.86164	-57.20946	45.86288
13B	63	91.18	433.80	0.77	1.19	0.28	1.45	0.34	-57.20943	45.86296	-57.20461	45.86173
13C	61	76.8	433.23	0.81	0.97	0.23	1.26	0.22	-57.20366	45.86334	-57.20842	45.86462
13D	64	55.23	432.59	0.72	1.00	0.15	0.86	0.18	-57.20839	45.86472	-57.20366	45.86345
13E	64	90.54	431.19	0.38	0.96	0.13	1.41	0.27	-57.20262	45.86504	-57.20744	45.86627
13F	39	56.26	431.39	0.27	0.98	0.19	1.44	0.23	-57.20746	45.86639	-57.20309	45.86527
13G	33	45.03	430.92	0.35	0.89	0.02	1.36	0.13	-57.20325	45.86719	-57.20609	45.86789
13H	56	71.72	430.94	0.42	1.01	0.21	1.28	0.28	-57.20649	45.86808	-57.20167	45.86687
14A	65	60.78	343.18	1.60	0.98	0.18	0.94	0.16	-56.85260	45.73767	-56.84814	45.73952
14B	63	65.38	342.95	1.51	1.03	0.20	1.04	0.24	-56.84811	45.73941	-56.85237	45.73765
14C	64	71.84	343.34	1.77	1.24	0.34	1.12	0.37	-56.85119	45.73603	-56.84671	45.73790

Table AI.2 *(Continued)*

Transect	Number of Images Analyzed	Total sum of area analyzed (m^2)	Mean Depth (m)	Standard Deviation of Depth (m)	Mean altitude above seafloor (m)	Standard deviation altitude (m)	Mean analyzed area per image (m^2)	Standard deviation area per image (m^2)	Start Longitude (Decimal Degrees)	Start Latitude (Decimal Degrees)	End Longitude (Decimal Degrees)	End Latitude (Decimal Degrees)
14D	65	99.25	343.35	1.65	1.22	0.35	1.53	0.47	-56.84662	45.73781	-56.85112	45.73595
14E	62	70.21	343.96	1.52	1.24	0.31	1.13	0.31	-56.84999	45.73446	-56.84569	45.73629
14F	60	59.02	344.35	1.47	1.12	0.29	0.98	0.22	-56.84565	45.73619	-56.84986	45.73438
14G	54	90.52	344.32	1.41	1.36	0.36	1.68	0.31	-56.84874	45.73287	-56.84440	45.73473
14H	62	99.94	344.51	1.30	0.97	0.18	1.61	0.22	-56.84443	45.73462	-56.84864	45.73281
16A	63	87.3	444.26	1.09	1.03	0.21	1.39	0.16	-57.51709	46.14507	-57.51707	46.14150
16B	61	85.63	444.36	1.10	1.03	0.17	1.40	0.19	-57.51721	46.14165	-57.51719	46.14506
16C	48	42.89	444.58	0.67	1.12	0.24	0.89	0.15	-57.51976	46.14507	-57.51979	46.14146
16D	61	55.17	444.53	0.65	0.99	0.15	0.90	0.14	-57.51994	46.14146	-57.51992	46.14504
16E	46	47.94	444.41	0.90	1.41	0.32	1.04	0.18	-57.52253	46.14507	-57.52252	46.14146
16F	62	45.28	444.95	1.00	0.97	0.08	0.73	0.09	-57.52267	46.14147	-57.52267	46.14507
16G	58	52.18	445.77	1.71	1.41	0.29	0.90	0.14	-57.52525	46.14505	-57.52526	46.14148
16H	58	48.28	446.13	1.66	0.96	0.13	0.83	0.12	-57.52538	46.14146	-57.52539	46.14504
Campod												
LC2A_CON16	29	55.8	340.43	1.37	1.81	0.58	1.92	0.82	-56.65879	45.53846	-56.66221	45.53608
LC2B_CON17	32	73.39	341.69	1.95	1.72	0.53	2.29	1.08	-56.65979	45.53925	-56.66370	45.53701
LC2C_CON18	36	70.33	342.82	1.39	1.61	0.52	1.95	0.87	-56.66184	45.54047	-56.66548	45.53813
LC5A_CON46	31	59.93	439.79	0.84	1.76	0.40	1.93	0.65	-57.52393	46.22137	-57.52665	46.21836
LC5B_CON47	31*	71.64	439.09	1.01	1.63	0.33	2.31	0.67	-57.52566	46.22215	-57.52842	46.21914
LC5C_CON48	28	58.21	440.50	1.22	1.41	0.30	2.08	0.56	-57.52809	46.22326	-57.53082	46.22028
LC6A_CON80	26	73.28	319.09	0.56	1.64	0.30	2.82	0.83	-57.68201	46.69580	-57.68422	46.69888
LC6B_CON81	33	93.48	318.42	0.42	1.61	0.28	2.83	1.00	-57.67905	46.69616	-57.68142	46.69933

Note: * Metadata were missing for some images, mean and standard deviation for depth and altitude calculated for N=18 images.

Table AI.2 *(Continued)*

Transect	Number of Images Analyzed	Total sum of area analyzed (m^2)	Mean Depth (m)	Standard Deviation of Depth (m)	Mean altitude above seafloor (m)	Standard deviation altitude (m)	Mean analyzed area per image (m^2)	Standard deviation area per image (m^2)	Start Longitude (Decimal Degrees)	Start Latitude (Decimal Degrees)	End Longitude (Decimal Degrees)	End Latitude (Decimal Degrees)
LC7A_CON100	31	105.32	219.06	15.84	1.74	0.31	3.40	1.01	-58.04335	46.98517	-58.04728	46.98286
LC7B_CON101	27	75.83	216.48	15.09	1.51	0.31	2.81	0.98	-58.04514	46.98686	-58.04842	46.98413
LC7C_CON102	32	89.87	227.18	16.52	1.72	0.34	2.81	0.99	-58.05041	46.98499	-58.04681	46.98749
LC9A_CON98	30	69.28	421.43	1.95	1.56	0.26	2.31	0.74	-58.63610	46.86871	-58.63129	46.87015
LC9B_CON99	25	60.38	422.33	1.35	1.51	0.20	2.42	0.64	-58.63477	46.86764	-58.63001	46.86890
LC14A_CON34	33	72.02	353.81	0.95	1.78	0.38	2.18	0.71	-56.85527	45.73157	-56.85808	45.72862
LC14B_CON35	30	55.37	355.06	1.18	1.74	0.47	1.85	0.78	-56.85777	45.73252	-56.86049	45.72951
LC17A_CON49	29	61.16	467.47	0.82	1.61	0.32	2.11	0.84	-57.73437	46.28095	-57.73533	46.27748
LC18A_CON31	32	73.16	406.02	0.97	1.61	0.42	2.29	0.79	-56.94063	45.60503	-56.94396	45.60232
LC18B_CON32	31	68.19	405.18	0.60	1.57	0.35	2.20	0.76	-56.94261	45.60623	-56.94576	45.60338
LC18C_CON33	30	62.48	404.54	0.57	1.56	0.29	2.08	0.52	-56.94450	45.60740	-56.94761	45.60451
LC20A_CON14	31	81.91	388.23	1.05	2.44	0.83	2.64	0.81	-56.68143	45.35706	-56.68485	45.35460
LC20B_CON15	27	71.87	388.18	1.30	2.21	0.89	2.66	0.75	-56.68826	45.35706	-56.68560	45.35966
LC24A_CON82	30	63.47	454.49	0.35	1.46	0.25	2.12	0.57	-57.92200	46.63570	-57.92454	46.63882
LC24B_CON83	37	80.68	453.27	0.43	1.43	0.28	2.18	0.72	-57.91986	46.63652	-57.92238	46.63965
LC24C_CON84	29	59.17	452.67	0.47	1.45	0.31	2.04	0.68	-57.91764	46.63742	-57.92009	46.64052
LC25A_CON62	28	65.63	332.61	1.23	1.51	0.34	2.34	0.86	-57.63362	46.63062	-57.63701	46.62792
LC25B_CON63	32	94.19	332.72	1.18	1.62	0.21	2.94	0.76	-57.63561	46.63201	-57.63893	46.62931

Table AI.3 Detailed results for the Mantel correlogram. The median distance value is given for each distance class, and each class represents increments of ~9.42 km. In total, we used 2976 non-zero images. The R function mantel.correlog uses Sturges equation to select break points and to cut off distance classes that do not include all points, here distance classes 13-24. Spearman's R method was used to calculate Mantel correlation values with 999 permutations, and p values were adjusted for multiple testing using the holm method. Distance classes 1 – 12 had ≥ 39000 pairs of images, included in the analysis.

Distance Class	Class Index (m)	Mantel value (using spearman's r)	P values (corrected using holm)
1	4709.47	0.33	0.001
2	14126.23	-0.01	0.079
3	23542.99	-0.03	0.003
4	32959.75	-0.06	0.004
5	42376.50	-0.11	0.005
6	51793.26	0.06	0.006
7	61210.02	-0.03	0.007
8	70626.78	-0.15	0.008
9	80043.53	0.17	0.009
10	89460.29	-0.01	0.014
11	98877.05	-0.13	0.011
12	108293.81	-0.01	0.012
13	117710.56	-	-
14	127127.32	-	-
15	136544.08	-	-
16	145960.84	-	-
17	155377.59	-	-
18	164794.35	-	-
19	174211.11	-	-
20	183627.87	-	-
21	193044.62	-	-
22	202461.38	-	-
23	211878.14	-	-
24	221294.90	-	-

APPENDIX II: CHAPTER 4 (FINE-SCALE SPATIAL PATTERNS OF DEEP-SEA EPIBENTHIC FAUNA IN THE LAURENTIAN CHANNEL MARINE PROTECTED AREA)[10]

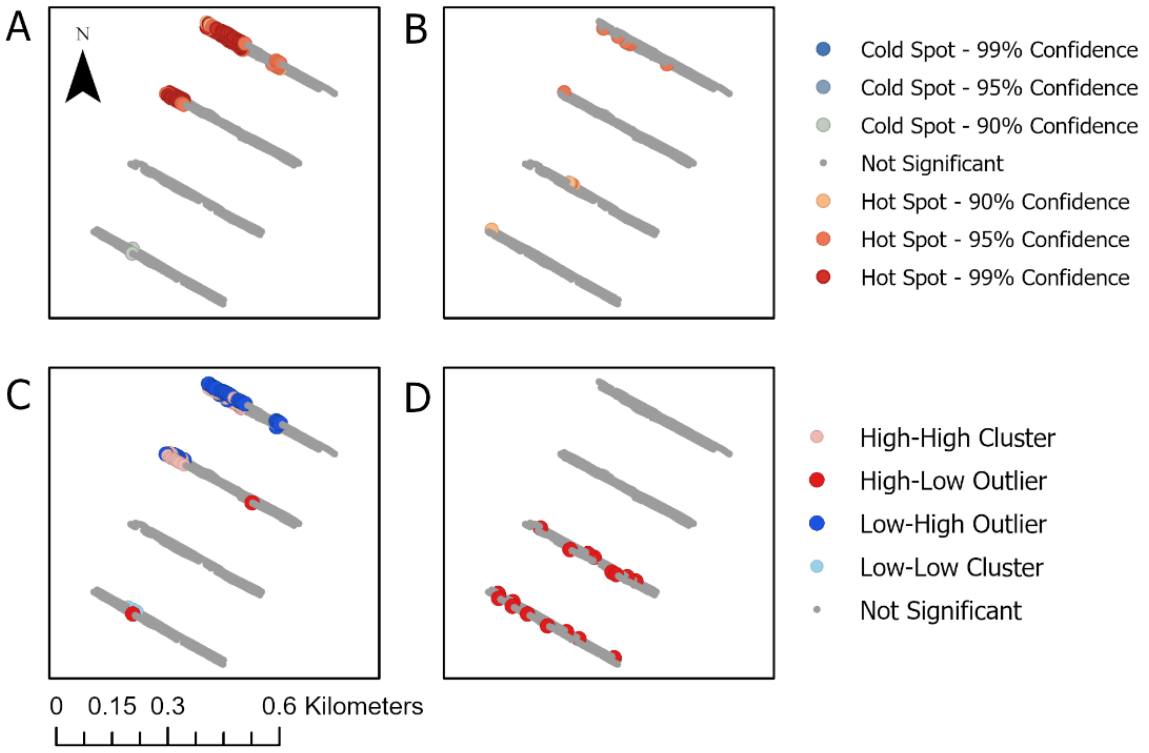

Figure AII.1 Local spatial statistical output for Hexacorallia (SC.) spp. at station 2 in the LC MPA; A&C: station-level patterns using neighbourhood of ~39 m including all 8 transects in calculations; B&D: transect-level patterns using 10 m neighbourhood distance for each transect pair (AB, CD, EF, GH) separately. A&B are results from *Gi** hotspot analysis using upper legend; C&D are results from local Moran's *I* analysis using lower legend (see explanation of legend in Figure 4.2 caption).[11]

---

[10] Part of supplementary file for the article published in *Deep Sea Research Part I: Oceanographic Research Papers*, *203*, 104195. de Mendonça, S. N., & Metaxas, A. Fine-scale spatial patterns of deep-sea epibenthic fauna in the Laurentian Channel Marine Protected area. Copyright Elsevier (2024). DOI: 10.1016/j.dsr.2023.104195

[11] Excerpt from Figure 4.2 caption: "For local Moran's *I*, a positive statistic results in clusters of similar abundance values: value of observation high and value of the neighbourhood also high (High-High; HH) or low observation-low neighbourhood (Low-Low; LL), whereas negative values of the statistic result from an

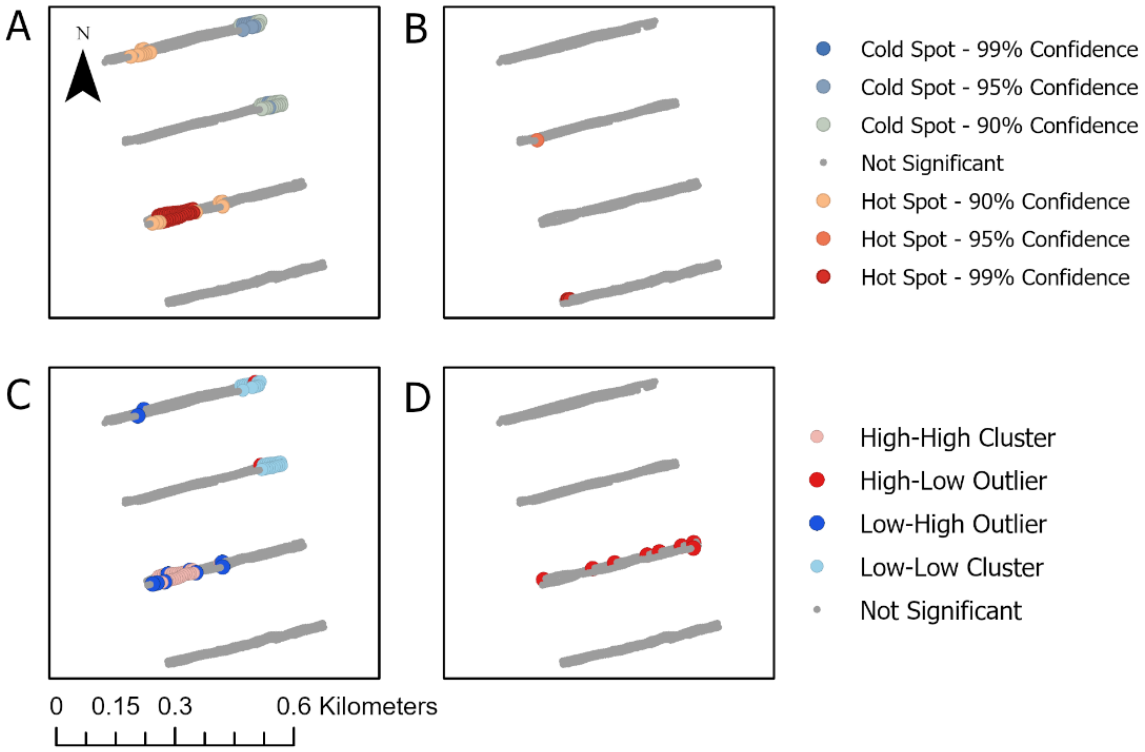

Figure AII.2 Local spatial statistical output for *Pennatula* sp. 2 at station 4 in the LC MPA; A&C: station-level patterns using neighbourhood of ~46 m neighbourhood distance with 25 neighbours including all 8 transects in calculations; B&D: transect-level patterns using 10 m neighbourhood distance for each transect pair (AB, CD, EF, GH) separately. A&B are results from *Gi** hotspot analysis using upper legend; C&D are results from local Moran's *I* analysis using lower legend (see explanation of legend in Figure 4.2 caption).

observation and its neighbourhood having dissimilar abundances, thus outliers, high observation-low neighbourhood (High-Low; HL) or low observation-high neighbourhood (Low-High; LH)."

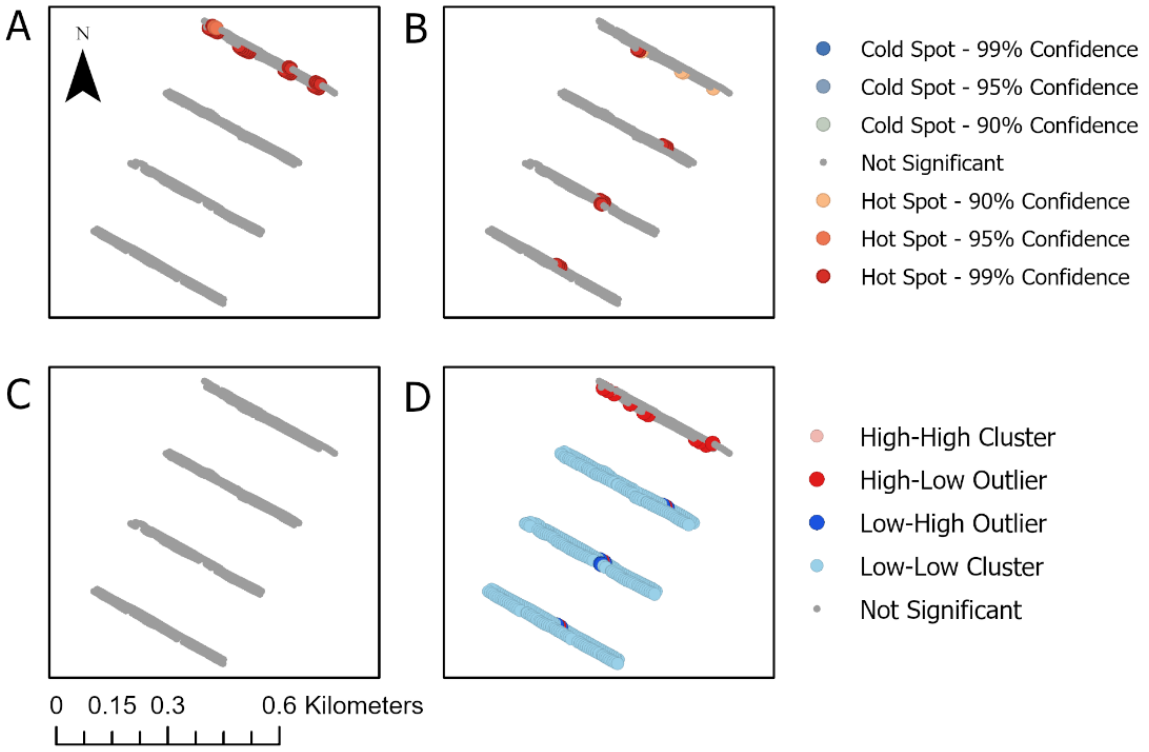

Figure AII.3 Local spatial statistical output for Pennatuloidea (SF.) sp. 9 at station 2 in the LC MPA; A&C: station-level patterns using neighbourhood of ~15 m including all 8 transects in calculations; B&D: transect-level patterns using 10 m neighbourhood distance for each transect pair (AB, CD, EF, GH) separately. A&B are results from *Gi** hotspot analysis using upper legend; C&D are results from local Moran's *I* analysis using lower legend (see explanation of legend in Figure 4.2 caption).

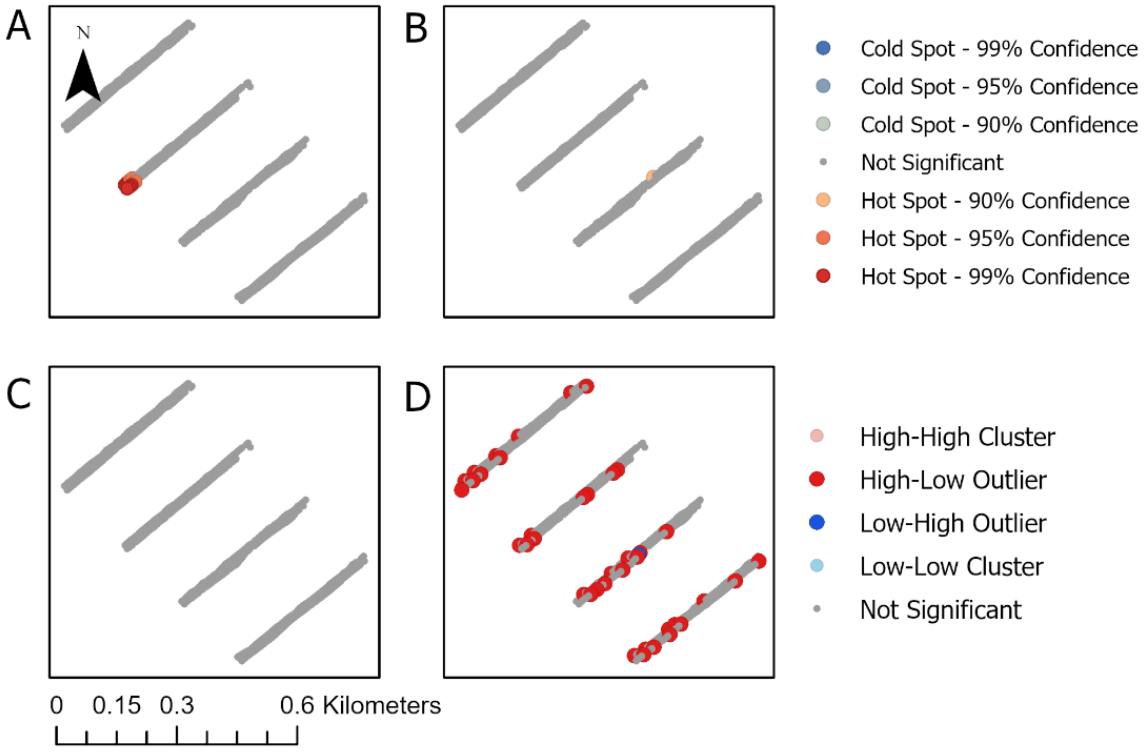

Figure AII.4 Local spatial statistical output for *Anthoptilum* spp. at station 3 in the LC MPA; A&C: station-level patterns using neighbourhood of ~44 m including all 8 transects in calculations; B&D: transect-level patterns using 10 m neighbourhood distance for each transect pair (AB, CD, EF, GH) separately. A&B are results from *Gi** hotspot analysis using upper legend; C&D are results from local Moran's *I* analysis using lower legend (see explanation of legend in Figure 4.2 caption).

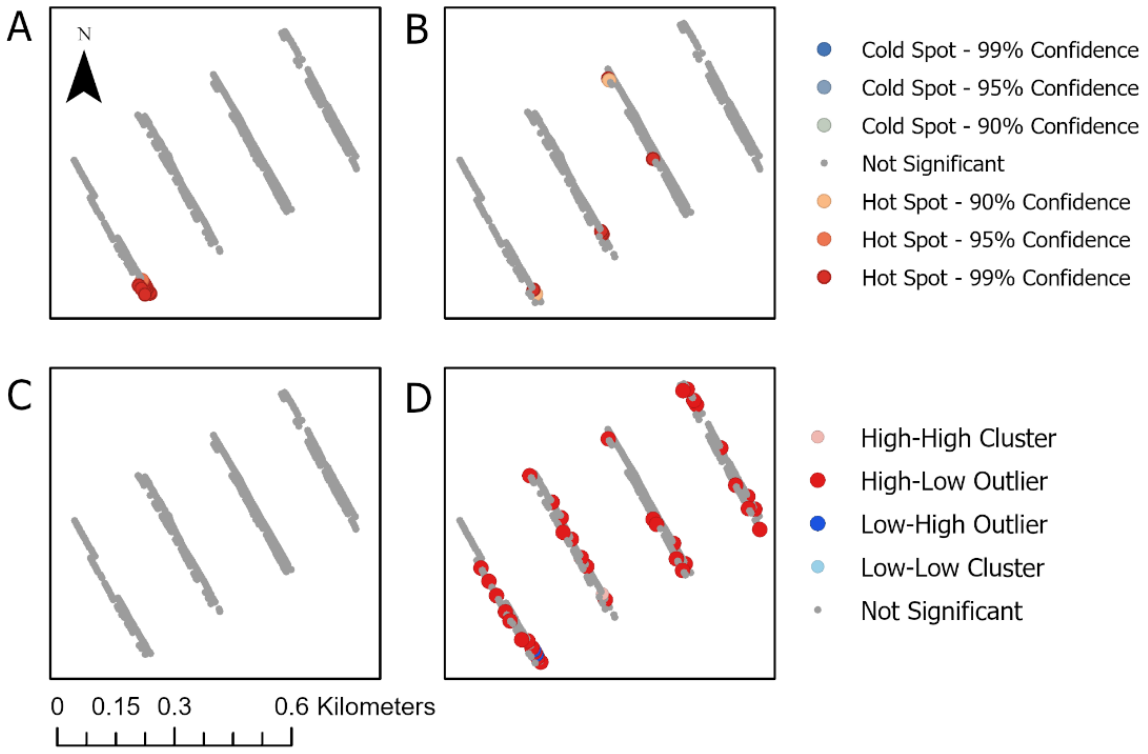

Figure AII.5 Local spatial statistical output for *Edwardsia* sp. 1 at station 5 in the LC MPA; A&C: station-level patterns using neighbourhood of ~47 m neighbourhood distance with 19 neighbours including all 8 transects in calculations; B&D: transect-level patterns using 10 m neighbourhood distance for each transect pair (AB, CD, EF, GH) separately. A&B are results from *Gi** hotspot analysis using upper legend; C&D are results from local Moran's *I* analysis using lower legend (see explanation of legend in Figure 4.2 caption).

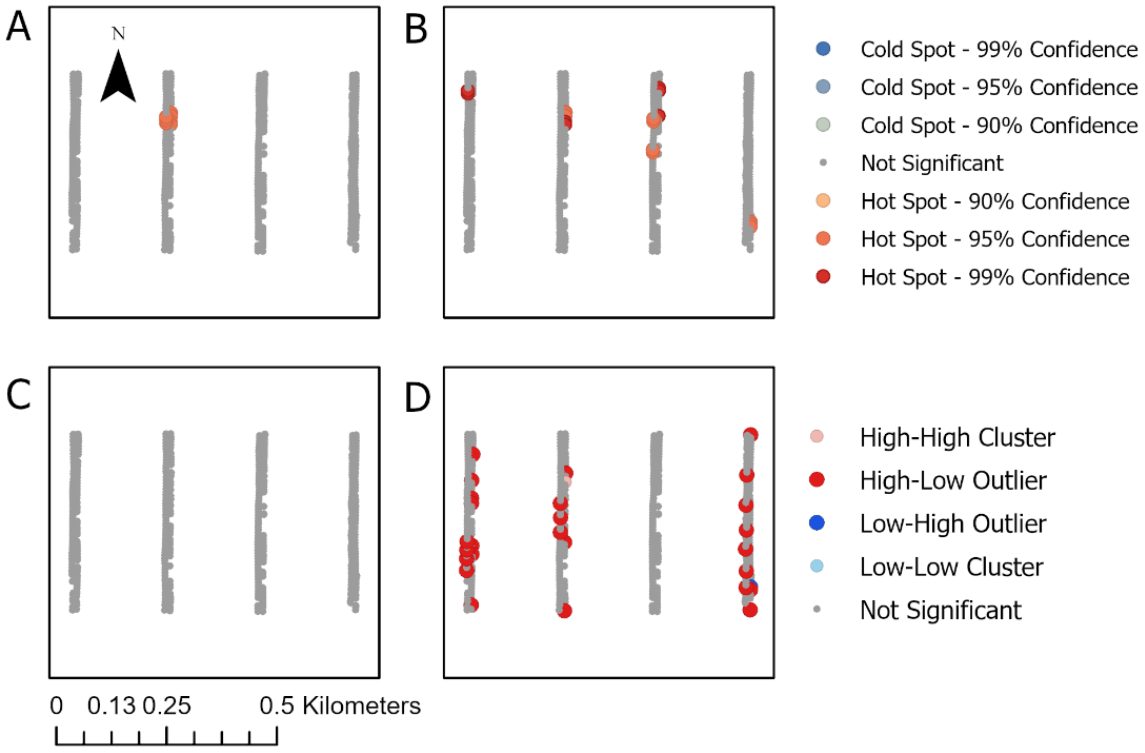

Figure AII.6 Local spatial statistical output for Anthozoa (C.) spp. at station 16 in the LC MPA; A&C: station-level patterns using neighbourhood of ~27 m including all 8 transects in calculations; B&D: transect-level patterns using 10 m neighbourhood distance for each transect pair (AB, CD, EF, GH) separately. A&B are results from *Gi** hotspot analysis using upper legend; C&D are results from local Moran's *I* analysis using lower legend (see explanation of legend in Figure 4.2 caption).

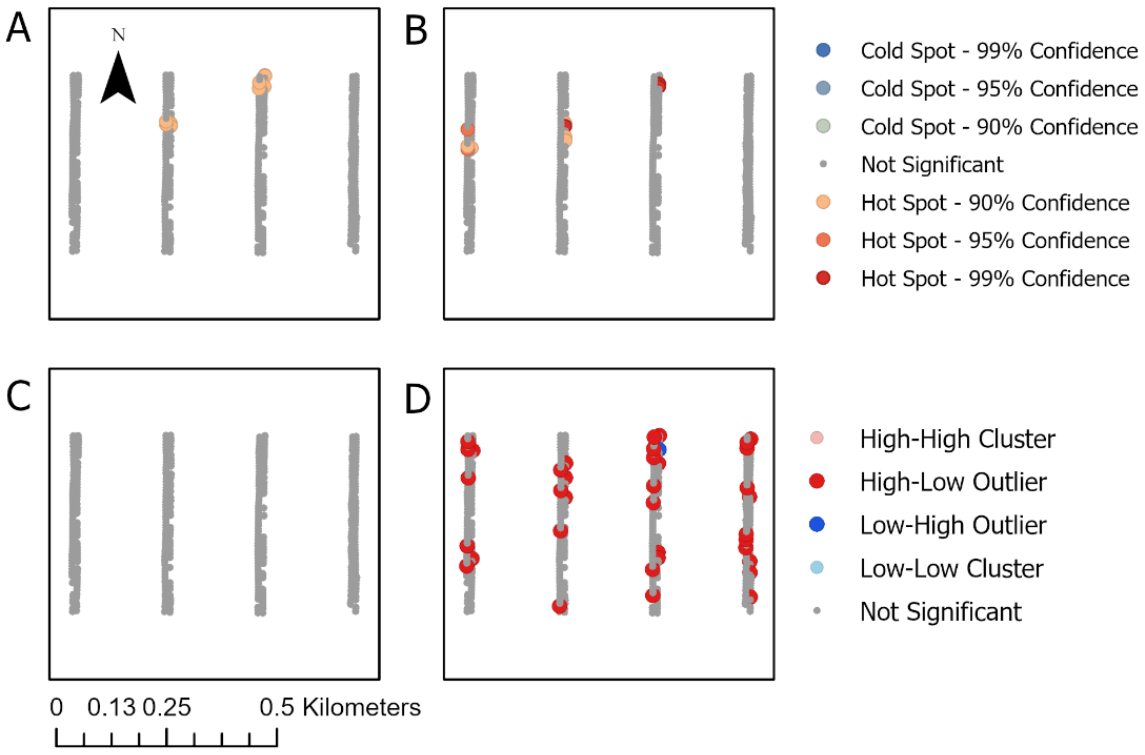

Figure AII.7 Local spatial statistical output for *Anthoptilum* spp. at station 16 in the LC MPA; A&C: station-level patterns using neighbourhood of ~38 m including all 8 transects in calculations; B&D: transect-level patterns using 10 m neighbourhood distance for each transect pair (AB, CD, EF, GH) separately. A&B are results from *Gi** hotspot analysis using upper legend; C&D are results from local Moran's *I* analysis using lower legend (see explanation of legend in Figure 4.2 caption).

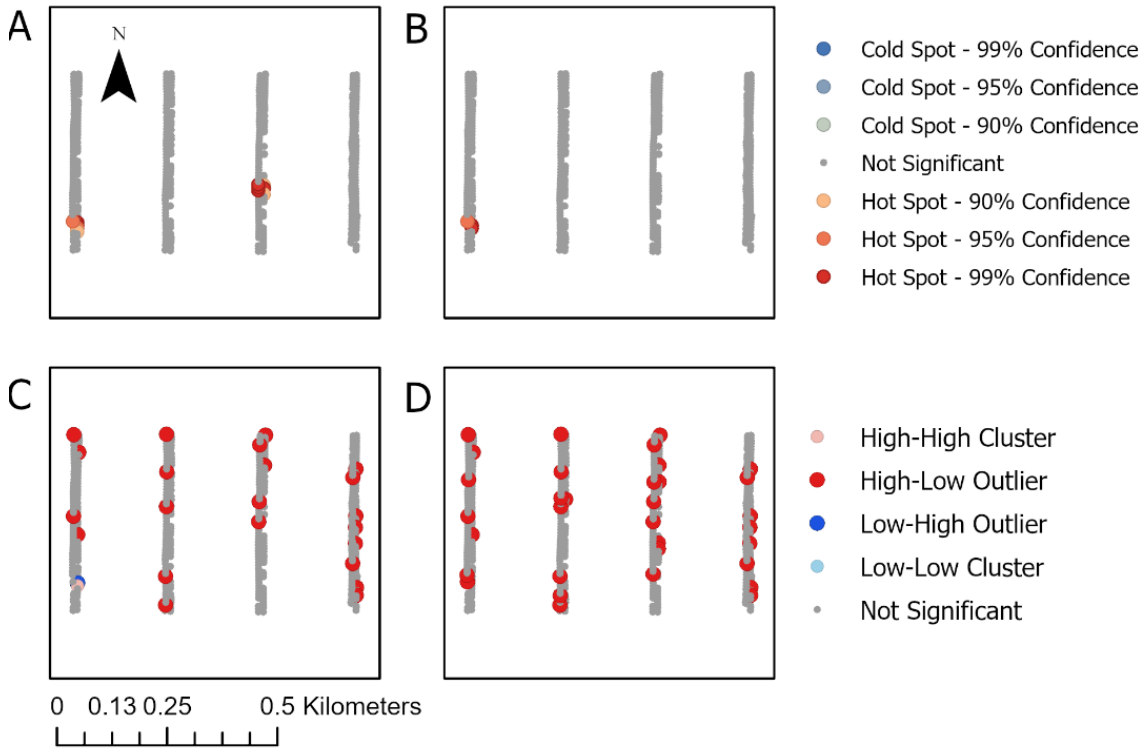

Figure AII.8 Local spatial statistical output for *Kophobelemnon* spp. at station 16 in the LC MPA; A&C: station-level patterns using neighbourhood of ~16 m including all 8 transects in calculations; B&D: transect-level patterns using 10 m neighbourhood distance for each transect pair (AB, CD, EF, GH) separately. A&B are results from *Gi** hotspot analysis using upper legend; C&D are results from local Moran's *I* analysis using lower legend (see explanation of legend in Figure 4.2 caption).

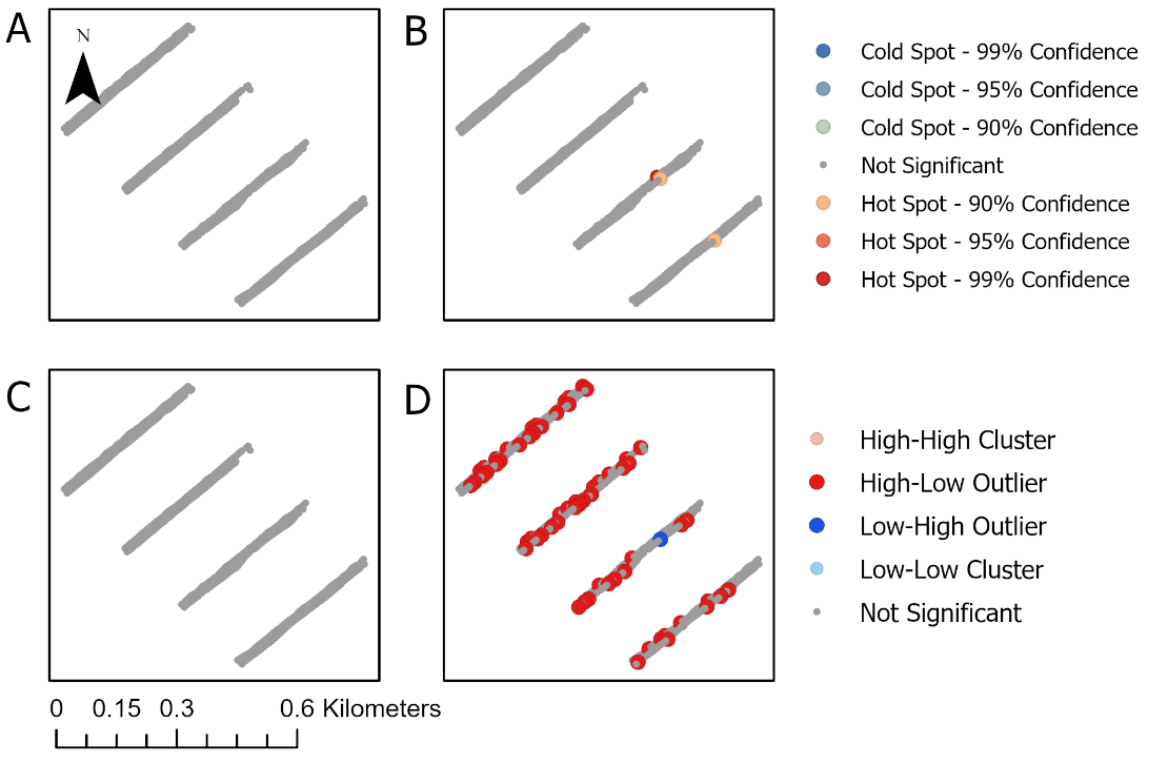

Figure AII.9 Example of station-level pattern that is not significantly different than random (A&C) but has some transect-level pattern (B&D). Local spatial statistical output for *Edwardsia* sp. 1 at Station 3 in the LC MPA; A&C: station-level patterns using neighbourhood of ~44 m including all 8 transects in calculations; B&D: transect-level patterns using 10 m neighbourhood distance for each transect pair (AB, CD, EF, GH) separately. A&B are results from *Gi** hotspot analysis using upper legend; C&D are results from local Moran's *I* analysis using lower legend (see explanation of legend in Figure 4.2 caption). Note: Nine other taxa-stations were random at the station level, but those figures are not included in this appendix.

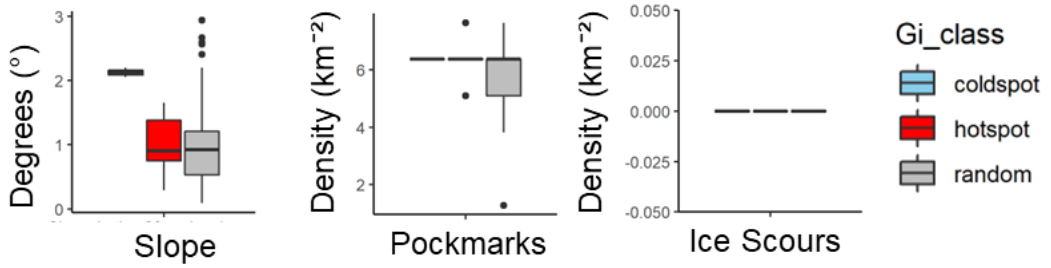

Figure AII.10 Boxplots of environmental variables for station 2 Hexacorallia (SC.) spp. station-level *Gi** hotspots, coldspots, and random locations, ~39m neighbourhood. Hotspots n=63 (including 17 with zero-abundance), coldspots n=2, random n= 421. Based on geomorphic features and 20 m bathymetry provided by Lacharité et al., (2020).

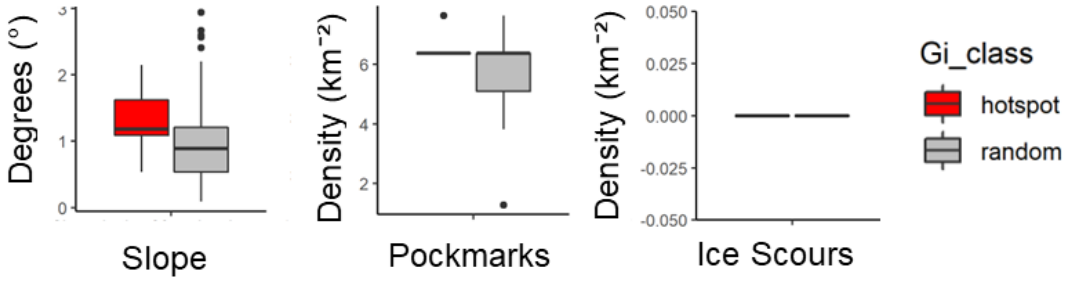

Figure AII.11 Boxplots of environmental variables for station 2 Pennatuloidea (SF.) sp. 9 station-level *Gi** hotspots and random locations, ~15m neighbourhood. Hotspots n=26 (including 16 with zero-abundance), coldspots n=0, random n=460. Note: Not showing the environmental boxplots for 6 other taxa-stations with small station-level hotspots (less than 12 images in their hotspots) and no coldspots, therefore the small sample size makes associations with environmental variables indeterminate. Based on geomorphic features and 20 m bathymetry provided by Lacharité et al., (2020).

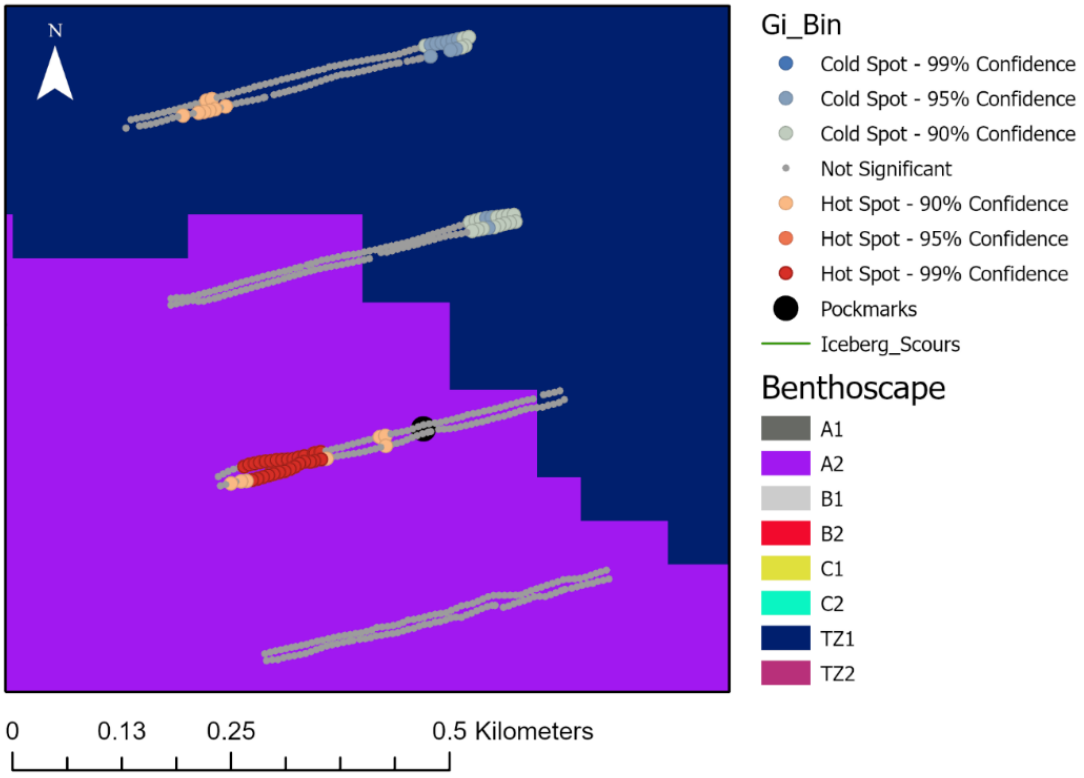

Figure AII.12 Two different benthoscapes present at station 4, with *Pennatula* sp. 2 station-level hotspots and coldspots overlaid (46 m fixed distance for 25 neighbours) and a single pockmark/pit center location (unknown size). Benthoscape classes layer and geomorphic features provided by Lacharité et al., (2020).

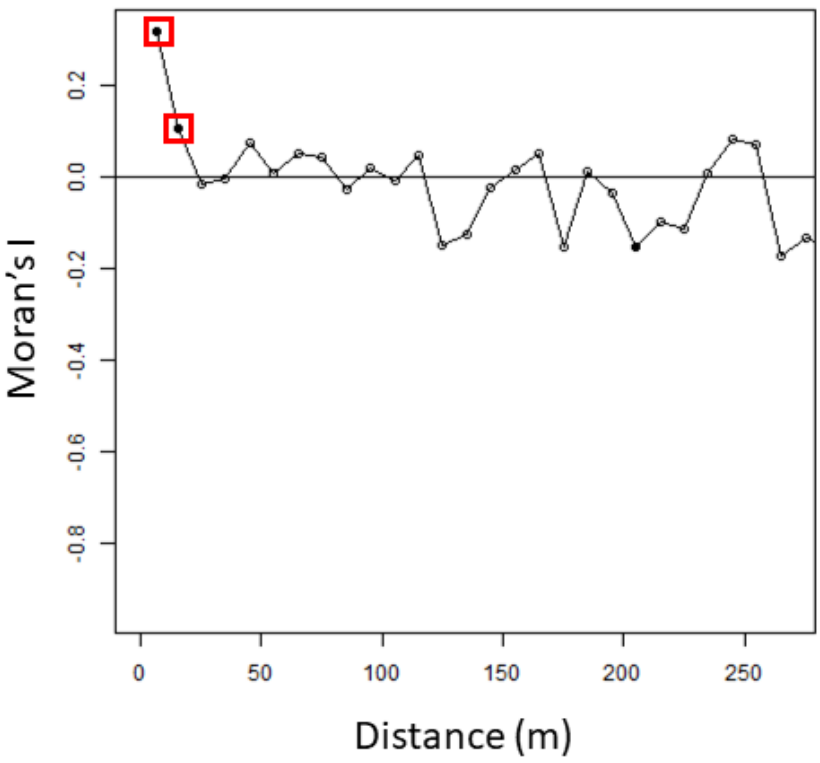

Figure AII.13 Example of spatial correlograms performed for taxa in the Laurentian Channel Marine Protected Area (LC MPA) using Moran's *I*, for *Pennatula* sp. 2 on transect pair CD at station 2. Open circles are not significant, filled circles are significant, using alpha 0.05, and red boxes are still significant after progressive Bonferroni correction (Dale & Fortin, 2014).

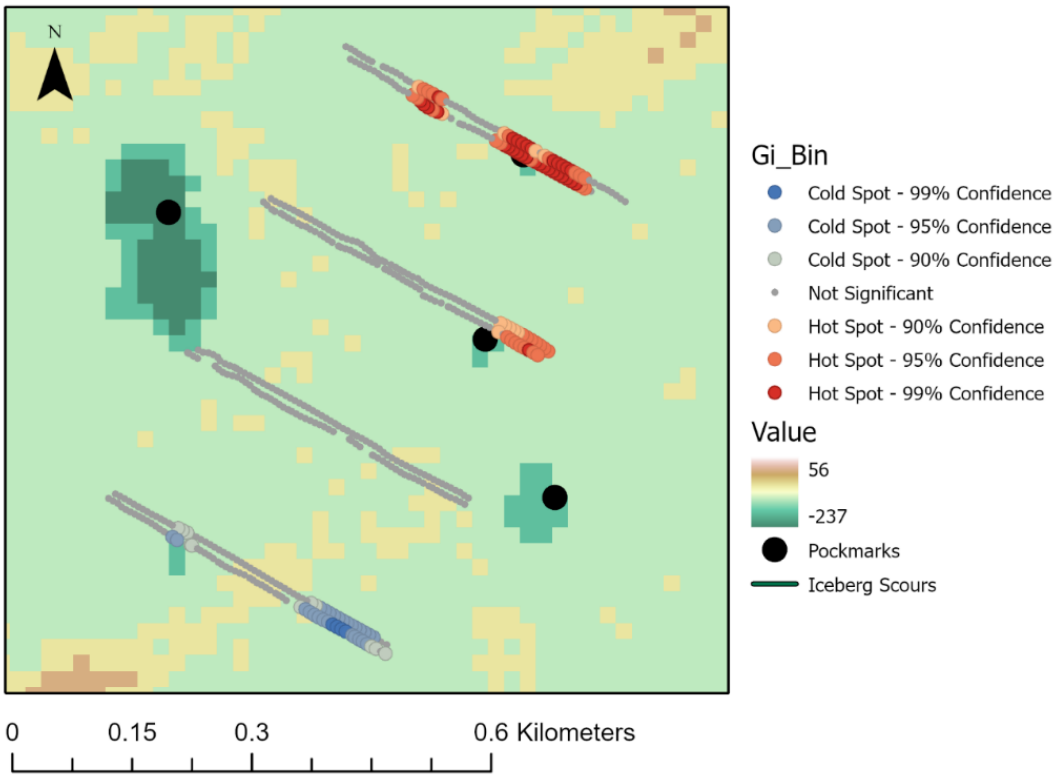

Figure AII.14 Bathymetry position index showing fine-scale features, with inner radius 1 cells and outer radius 25, scale factor 500 m, at station 2 with *Pennatula* sp. 2 station-level hotspots and coldspots overlaid (27 m neighbourhood distance), with pockmark/pit center locations (unknown size) but without ice scours. Based on geomorphic features and 20 m bathymetry provided by Lacharité et al., (2020).

Table AII.1 Morphospecies groupings renamed from de Mendonça & Metaxas (2021).

Taxa from Publication 2021	Taxa Renamed	Comment
Gersemia sp. 1	Malacalcyonacea (O.) spp.	Precaution: may contain several genera with similar morphology
Pteraster sp. 1	Asteroidea (C.) sp. 20	Precaution: may be another genus
Actiniaria (O.) sp. 23	*Edwardsia* sp. 1	Reidentified: has short and long rows of tentacles
Actiniaria (O.) spp.	Anthozoa (C.) spp.	Precaution: some individuals may be cerianthids rather than anemones
Actinoscyphia spp.	*Actinauge cristata*	Reidentified
Scleractinia (O.) spp.	Hexacorallia (SC.) spp.	Precaution: small size and orientation can make it difficult to identify with complete certainty, while some could be small anemones, most are high likely cup corals (undetermined genus).
Unidentified sp. 216*	Pennatuloidea (SF.) sp. 9	A sea pen, possibly *Funiculina* sp. or *Virgularia* sp., but image quality obscured view of polyps (small and colour similar to sediment).
Pennatulacea (O.) sp. 5	Pennatuloidea (SF.) sp. 5	Taxonomy changed
Pennatulacea (O.) spp.	Pennatuloidea (SF.) spp.	Taxonomy changed
Cerianthidae (F.) spp.	Cerianthidae (F.) sp. 1	Renamed

Table AII.2 Range of environmental variables at each station in the LC MPA, minimum to maximum values.

Station	Depth (m)	Oxygen (mL/L)	Salinity (PSU)	Temperature (° C)	pH	Pockmark density (#/km²)	Ice scour density (#/km²)	Slope (°)
2	347–357	3.11–4.24	35–35.01	6.22–6.42	7.9–7.93	1.27–7.64	0–0	0.09–2.94
3	445–450	3.99–4.16	34.99–35	5.94–6.04	7.92–7.94	0–0	1.06–3.44	0.1–2.45
4	331–342	2.2–3.99	31.29–35.02	6.51–6.93	7.92–7.93	1.27–6.37	0–0.15	0.05–2.88
5	427–441	3.83–3.99	34.99–34.99	5.78–5.98	7.88–7.93	0–2.55	1.13–3.11	0.17–2.28
13	430–436	4.06–4.16	34.99–35	5.92–6.08	7.92–7.95	0–1.27	0–2.43	0.13–2.86
14	340–347	2.38–4.62	35.01–35.02	6.52–6.64	7.9–7.93	0–5.09	0–0	0.17–3.08
16	442–449	3.96–4.07	35–35	6.01–6.04	7.94–7.95	0–0	2.79–4.02	0.16–4.97

Table AII.3 All taxon-station combinations (present on >10% on any transect pair) with significant positive autocorrelation using Global Moran *I* at the station-level (α=0.05); distance threshold default ArcGIS Pro ensures that each feature had at least one neighbour.

Station	Taxa	Global Moran *I*	P Value	Distance threshold (m)
2	*Pennatula* sp. 2	0.50	0.00	8.32
2	Pennatuloidea (SF.) sp. 9	0.21	0.00	8.32
2	Hexacorallia (SC.) spp.	0.38	0.00	8.32
3	*Pennatula* sp. 2*	0.24	0.00	11.51
4	*Pennatula* sp. 2	0.09	0.01	11.47
16	Anthozoa (C.) spp.	0.08	0.02	12.17
16	*Kophobelemnon spp.*	0.07	0.04	12.17

Note: Global Moran *I* less than 0.2, are considered weaker patterns but still significant.
* Not one of the 20 focal taxon-station combinations.

Table AII.4 Summary of spatial correlograms, including significant positive or negative autocorrelation using Global Moran *I* on the transect level for all distance classes (10 m bins) and excluding significant positive autocorrelation in the first distance (see Table AII.3). Progressive Bonferroni adjusted significance level where α= 0.05/distance class. Spatial range is the distance of the interpolated *x*-intercept using the *ncf* r package where Global Moran *I* is 0 and there is the absence of spatial autocorrelation. It can be interpreted as patch size if it is the first distance class in significantly positive autocorrelation. For additional results for taxon-station combinations not included in the focal taxa see Table AII.5.

Station	Pair	Taxon	Mean of Distance Class (m)	Global Moran *I*	Probability value	Spatial Range (m)
13	CD	Anthozoa (C.) spp.	34.92	0.11	0.01	8.43
16	EF	Anthozoa (C.) spp.	24.84	0.19	0.01	8.83
16	EF	*Anthoptilum* spp.	14.79	0.14	0.02	50.26
2	CD	*Pennatula* sp. 2	15.25	0.10	0.01	16.43
4	EF	*Pennatula* sp. 2	15.32	0.12	0.01	26.30
2	CD	Pennatuloidea (SF.) sp. 9	15.25	-0.01	0.02	-
2	GH	Pennatuloidea (SF.) sp. 9	15.09	-0.01	0.02	-
2	EF	Pennatuloidea (SF.) sp. 9	6.74	-0.02	0.03	-
2	CD	Hexacorallia (SC.) spp.	24.93	0.14	0.01	155.05

Table AII.5 Additional results for taxon-station combinations not included in the focal taxa (extension of Table AII.4). Spatial correlograms performed separately for each taxon-station combination and transect pair. Shown are for taxon-station combinations with significant positive spatial autocorrelation for the first distance class (mean distance presented in meters), associated Global Moran *I* and probability values using α=0.05. Patch size, also known as spatial range, is the distance of the interpolated *x*-intercept from the spatial correlograms using the *ncf* r package. Note: * Patch size ~10 m, can be interpreted as a patch that includes immediate neighbouring images; if > 10 m, patch extends farther.

Station	Transect Pair	Taxon	Mean of Distance Class (m)	Global Moran I	Probability value	Patch Size* (m)
3	CD	Actiniaria (O.) sp. 1	15.09	-0.01	0.02	-
3	GH	Actiniaria (O.) sp. 1	6.90	-0.02	0.02	-
2	AB	Anthozoa (C.) spp.	15.55	0.10	0.02	-
2	GH	Anthozoa (C.) spp.	6.46	-0.02	0.02	-
4	AB	Anthozoa (C.) spp.	25.24	0.14	0.01	-
4	GH	*Anthoptilum* spp.	7.28	-0.01	0.02	-
5	CD	*Anthoptilum* spp.	14.99	0.15	0.02	-
2	AB	Asteroidea (C.) sp. 4	6.50	-0.02	0.02	-
3	CD	Asteroidea (C.) sp. 4	15.09	-0.01	0.02	-
3	CD	Asteroidea (C.) sp. 4	6.51	-0.01	0.04	-
13	AB	Asteroidea (C.) sp. 4	6.97	-0.03	0.02	-
2	GH	Asteroidea (C.) spp.	6.46	-0.03	0.03	-
4	GH	Asteroidea (C.) spp.	7.28	-0.01	0.02	-
5	EF	Asteroidea (C.) spp.	6.52	-0.03	0.02	-
16	GH	Cerianthidae (F.) sp. 1	7.17	0.21	0.02	27.41
16	GH	Cerianthidae (F.) sp. 1	15.14	0.16	0.01	27.41
16	GH	Cerianthidae (F.) sp. 1	25.11	0.22	0.01	27.41
16	AB	*Edwardsia* sp. 1	7.13	-0.07	0.04	-
2	AB	*Flabellum alabastrum*	15.55	-0.02	0.02	-
2	AB	*Kophobelemnon spp.*	15.55	-0.01	0.02	-
5	EF	*Kophobelemnon spp.*	24.84	0.26	0.01	-
5	AB	*Kophobelemnon spp.*	6.43	-0.02	0.02	-
4	GH	Ophiuroidea (C.) spp.	15.10	0.00	0.02	-
4	GH	Pennatuloidea (SF.) sp. 5	7.28	-0.01	0.02	-
5	CD	Pennatuloidea (SF.) sp. 9	14.99	-0.01	0.02	-
2	AB	*Protoptilum* sp. 1	15.55	-0.01	0.02	-
2	CD	*Protoptilum* sp. 1	6.80	-0.02	0.03	-
3	CD	*Protoptilum* sp. 1	15.09	-0.01	0.02	-
4	CD	*Protoptilum* sp. 1	7.40	-0.01	0.02	-
4	EF	*Protoptilum* sp. 1	6.83	-0.02	0.02	-
3	EF	Hexacorallia (SC.) spp.	6.93	-0.02	0.02	-
5	GH	Hexacorallia (SC.) spp.	6.23	0.01	0.03	10.85
16	GH	Hexacorallia (SC.) spp.	7.17	0.24	0.02	8.21
16	GH	Hexacorallia (SC.) spp.	34.98	0.19	0.01	8.21

APPENDIX III: COPYRIGHT PERMISSIONS

Re: Permission to include journal article in PhD thesis [231221-009088]

Permissions Helpdesk <permissionshelpdesk@elsevier.com>
Fri 12/22/2023 2:07 AM
To:Sarah De Mendonca <sarah.de.mendonca@dal.ca>

Dear Sarah N. de Mendonça

We hereby grant you permission to reprint the material below at no charge in your thesis subject to the following conditions:

RE: Fine-scale spatial patterns of deep-sea epibenthic fauna in the Laurentian Channel Marine Protected area, Deep Sea Research Part I: Oceanographic Research Papers, Volume 203, January 2024, Mendonça et al.

1. If any part of the material to be used (for example, figures) has appeared in our publication with credit or acknowledgment to another source, permission must also be sought from that source. If such permission is not obtained then that material may not be included in your publication/copies.

2. Suitable acknowledgment to the source must be made, either as a footnote or in a reference list at the end of your publication, as follows:

"This article was published in Publication title, Vol number, Author(s), Title of article, Page Nos, Copyright Elsevier (or appropriate Society name) (Year)."

3. Your thesis may be submitted to your institution in either print or electronic form.

4. Reproduction of this material is confined to the purpose for which permission is hereby given.

5. This permission is granted for non-exclusive world English rights only. For other languages please reapply separately for each one required. Permission excludes use in an electronic form other than submission. Should you have a specific electronic project in mind please reapply for permission.

6. As long as the article is embedded in your thesis, you can post/share your thesis in the University repository.

7. Should your thesis be published commercially, please reapply for permission.

8. Posting of the full article/ chapter online is not permitted. You may post an abstract with a link to the Elsevier website [http://www.elsevier.com,]www.elsevier.com, or to the article on ScienceDirect if it is available on that platform.

Kind regards,

Roopa Lingayath
Senior Copyrights Specialist
ELSEVIER | HCM - Health Content Management

Visit Elsevier Permissions

From: Sarah de Mendonca
Date: Thursday, December 21, 2023 01:39 AM GMT

Elsevier and Deep-Sea Research Part I,

I am preparing my PhD thesis for submission to the Faculty of Graduate Studies at Dalhousie University, Halifax, Nova Scotia, Canada. I am seeking your permission to include a manuscript version of the following paper(s) as a chapter in the thesis:

de Mendonça, S. N., & Metaxas, A. (2024). Fine-scale spatial patterns of deep-sea epibenthic fauna in the Laurentian Channel Marine Protected area. Deep Sea Research Part I: Oceanographic Research Papers, 104195.

Dalhousie graduate theses are collected and stored online by Dalhousie University and Library and Archives of Canada. I am seeking your permission for the material described above to be stored online in **Dalhousie University's institutional repository and in Library and Archives of Canada (LAC)'s Theses Canada Collection.**

Full publication details and a copy of this permission letter will be included in the thesis.

Yours sincerely,

Sarah Natasha de Mendonça

Permission is granted for:

a) the inclusion of the material described above in your thesis.

b) for the material described above to be included in the copy of your thesis that is sent to the Library and Archives of Canada inclusion in Theses Canada.

c) For the material described above to be included in the copy of your thesis that is sent to Dalhousie University's institutional repository.

Additional note:

General permissions are also outlined at https://www.elsevier.com/about/policies-and-standards/copyright, including "Theses and dissertations which contain embedded final published articles as part of the formal submission can be posted publicly by the awarding institution with DOI links back to the formal publication on ScienceDirect" (Elsevier 2024; accessed January 11 2024).

ELSEVIER LICENSE
TERMS AND CONDITIONS

Mar 19, 2024

This Agreement between Sarah de Mendonça ("You") and Elsevier ("Elsevier") consists of your license details and the terms and conditions provided by Elsevier and Copyright Clearance Center.

License Number	5752580730936
License date	Mar 19, 2024
Licensed Content Publisher	Elsevier
Licensed Content Publication	Elsevier Books
Licensed Content Title	Seafloor Geomorphology as Benthic Habitat
Licensed Content Author	Myriam Lacharité,Craig J. Brown,Alexandre Normandeau,Brian J. Todd
Licensed Content Date	Jan 1, 2020
Licensed Content Pages	14
Start Page	691
End Page	704
Type of Use	reuse in a thesis/dissertation
Portion	figures/tables/illustrations
Number of figures/tables/illustrations	1
Format	both print and electronic
Are you the author of this Elsevier chapter?	No
Will you be translating?	No
Title of new work	SPATIAL ECOLOGY OF DEEP-SEA BENTHOS FOR MANAGEMENT OF MARINE PROTECTED AREAS
Institution name	Dalhousie University
Expected presentation date	Mar 2024
Portions	Table 41.1
Requestor Location	Sarah de Mendonça [redacted] [redacted] Attn: Sarah de Mendonça
Publisher Tax ID	[redacted]
Total	**0.00 USD**

Reprinted from Seafloor Geomorphology as Benthic Habitat, Lacharité, M., Brown, C. J., Normandeau, A., and Todd, B. J, *Geomorphic features and benthos in a deep glacial trough in Atlantic Canada*, Pages No. 691–704, Copyright (2020), with permission from Elsevier.